GEOTECHNICAL AND GEOPHYSICAL INVESTIGATIONS WITH PGA

ESTIMATION OF THE KATHMANDU FUN PARK PROJECT,

THANKOT, KATHMANDU, NEPAL

A Dissertation Submitted to the

TRIBHUVAN UNIVERSITY

CENTRAL DEPARTMENT OF GEOLOGY

Kirtipur, Kathmandu

In Partial Fulfillment of the Requirement for the Award of Degree of

Master of Science in Geology

By

ASHIM RIJAL

2014

©Tribhuvan University

GEOTECHNICAL AND GEOPHYSICAL INVESTIGATIONS WITH PGA

ESTIMATION OF THE KATHMANDU FUN PARK PROJECT,

THANKOT, KATHMANDU, NEPAL

TRIBHUVAN UNIVERSITY

CENTRAL DEPARTMENT OF GEOLOGY
OFFICE OF THE HEAD OF DEPARTMENT

Kirtipur, Kathmandu,
Nepal

Ref No.

Date: 2071.05.13 BS.
29th Aug 2012 AD

RECOMMENDATION

This is to certify that **ASHIM RIJAL** has completed this dissertation work entitled **"GEOTECHNICAL AND GEOPHYSICAL INVESTIGATIONS WITH PGA ESTIMATION OF THE KATHMANDU FUN PARK PROJECT, THANKOT, KATHMANDU, NEPAL"** as a partial fulfillment of the requirements of M.Sc. degree in Geology under my supervision. To my knowledge this work has not been submitted for any other degree.

Dr. SUBESH GHIMIRE

Assistant Professor

Central Department of Geology

Tribhuvan University

iii

iii

TRIBHUVAN UNIVERSITY
CENTRAL DEPARTMENT OF GEOLOGY
OFFICE OF THE HEAD OF DEPARTMENT
Kirtipur, Kathmandu,
Nepal

Ref No.

071-05-29 BS
Date: 14.09.2014 AD

CERTIFICATE OF APPROVAL

On the recommendation of **SUBESH GHIMIRE** this dissertation work of **ASHIM RIJAL** is approved for the examination and is submitted to the Tribhuvan University in partial fulfillment of the requirements of M.Sc. degree in Geology.

Prof. Dr. Lalu Prasad Paudel

Head of the Department

Central Department of Geology

Tribhuvan University

iv

BOARD OF THE EXAMINERS

Recommended by:

Dr. SUBESH GHIMIRE

(Supervisor)

Approved by:

Prof. Dr. LALU PRASAD PAUDEL

(Head of the Department)

Examined by:

(Internal Examiner)

Examined by:

(External Examiner)

071-05- 29 BS

Date: 14. 09. 2014 A D

v

ACKNOWLEDGEMENTS

ABSTRACT

This work focuses on the study of the foundation characteristics by geotechnical and geophysical investigations with PGA estimation of the Kathmandu Fun Park Project (KFPP) located in Thankot area, Kathmandu.

To obtain information on subsurface material, velocity distribution and soil thickness seismic refraction survey was conducted using a 24 channel seismograph system by Oyo. Other soil properties were studied by in-situ Direct Cone Penetration Test (DCPT) and laboratory test of samples. The problem of ground shaking in the case of large earthquake near the Kathmandu valley is assessed in terms of synthetic peak ground acceleration (PGA) due to the lack of observed data. The present study provides tools for estimating geotechnical parameters from seismic wave velocity in the area where soil test are difficult to conduct. Fewer amounts of observed data and unavailability of instruments for undisturbed sampling have somehow affected this research work. Manual picking of travel time data from waveforms has affected the subsequent processing and interpretation of seismic refraction data.

The study area comprises of colluvium deposits, mainly washout with high clay content. The high moisture content, low unconfined compressive strength and low bearing capacity of the soil are noteworthy. A modeled equation relating the P-wave velocity and porosity for the Lesser Himalayan colluvium soil has been established together with the material velocity. Similarly, the PGA distribution due to 1934 Taplejung, 1988 Udayapur and other two hypothetical earthquakes shows the PGA may exceed 150 gal for earthquakes greater than magnitude 8. However, the result shows the PGA hardly reach 15 gal for small but strong earthquakes. Moreover, the geotechnical parameters, specially moisture content, unconfined compressive strength, friction angle and porosity, show reasonably good correlation with seismic P-wave velocity. The single field measurement (i.e. seismic P-wave velocity) can serve the best for estimating other geotechnical parameters.

Keywords: seismic refraction, PGA, DCPT, colluvium, Fun-park, Chandragiri, Thankot.

Contents

ANNEXES

ANNEX A: In-situ DCP Tests.

ANNEX B: Soil Profiles.

ANNEX C: Laboratory Tests of Samples.

ANNEX D: Seismic Refraction Waveform Data and Travel-time Curves.

ANNEX E: Synthetic accelerogram obtained by simulating 1934 Taplejung earthquake.

List of Tables

List of Figures

Abbreviations

ASTM	American Society for Testing and Materials
CBR	California Bearing Ratio
CCT	Central Churia Thrust
DCP	Direct Cone Penetrometer
DCPT	Direct Cone Penetration Test
ERMC	Environment and Resource Management Consultancy
GRF	Ground Response Function
HFT	Himalaya Frontal Thrust
KFPP	Kathmandu Fun Park Project
MCT	Main Central Thrust
MBT	Main Boundary Thrust
MFT	Main Frontal Thrust
Ma	Million years
NESS	Nepal Environmental and Scientific Services
P-wave	Primary wave
PCA	Portland Cement Association
PGA	Peak Ground Acceleration
SRT	Seismic Refraction Tomography
S-wave	Secondary wave
STDS	South Tibetan Detachment System

UCS	Unconfined Compressive Strength
UTM	Universal Transverse Mercator
cm	centimeter
km	kilometer
m	meter
mm	millimeter
cm/s^2	centimeter per square second
m/s	meter per second
mm/y	millimeter per year
μm	micro meter
Hz	Hertz
°C	degree Celsius

CHAPTER I

INTRODUCTION AND OBJECTIVES

1.1 Background

The country of Nepal occupies 800 km long segment of central Himalaya which is tectonically active consisting of fragile geology. However, the small as well as large entrepreneurs from Nepal are being interested in founding high rise buildings, fun parks, cable cars and other civil structures targeting the highly dense settlement, i.e., Kathmandu valley. The Kathmandu Fun Park Project is one of such ambitious project with many components of civil structures. The purpose of the project is to promote the eco-tourism activities in the area focusing to both domestic and foreign tourist thereby contributing to both local and national economy. For the sustainability of such civil engineering projects proper design should be recommended addressing the natural hazards such as earthquake and landslides, which frequently hit Nepal and are one of the major development obstacles. For this, proper geotechnical investigation of foundation and quantification of risk in the area are the most challenging issues. Therefore, this work intends to contribute towards the geotechnical investigations, seismic refraction survey for the velocity distribution in the subsurface and peak ground acceleration analysis of the Kathmandu Fun Park Project.

However, Kathmandu valley is said to be at very high seismic risk, there is no proper measure in terms of ground shaking, liquefaction etc. in the case of a large earthquake near the valley. In this study the problem of ground shaking in terms of peak ground acceleration map in the project area by the most inevitable earthquake are studied. Estimations of soil thickness are other major issues of this study. These problems are resolved by geophysical investigation, particularly seismic refraction survey in the study area. Furthermore, soil properties serve basis for foundation design hence, their characteristics are studied in detail.

This research work aims to recommend the proper measure for the sustainability of large projects addressing the high seismic risk in the perspective of the Nepal Himalaya. This thesis could be the best example for estimating geotechnical parameters from seismic velocity measurements in the area where other test are difficult to conduct. Similarly, peak ground

acceleration analysis could serve as an ideal example which can be followed in geotechnical & geophysical investigations and seismic hazard analysis of large projects.

1.2 Location

The Kathmandu Fun Park Project (KFPP) is situated at the northern slope of Chandragiri Hills in the western part of capital city Kathmandu (Fig. 1.1) between Easting 619000 and 620500 and Northing 3064000 and 3061000 (Fig. 1.2). KFPP is aimed to develop a fun park and resorts in the eastern part of Bhaleshwor Temple and about 2.5 km long cable car linking Chunikhel (Ward No. 1) at the bottom station to Bhaleshwor Temple (Ward No. 9) at the topstation of the Thankot Village Development Committee, Kathmandu. Geologically, the study area lies in the Phulchoki Group of the Kathmandu Complex (Stöcklin and Bhattarai, 1977). The main landforms observed in the project area are fan deposits and washout colluvium deposits. Rock outcrops in the study area are very few and mostly covered by the colluvium soil. The geological study is carried out to assess the geotechnical and geophysical parameters, and peak ground acceleration estimation required for the project.To investigate geotechnical parameters for different towers altogether seven pits were dug at the base station and along the cable car alignment and their locations are shown in Fig. 1.2.

1.3 Topography

The study area is dissected by a few numbers of streams and gullies. The relief varies along the cable car alignment from base station to top station. For example, along the cable car alignment northern part (downhill) of the pit no. 6 is steep colluvium slope but the uphill side is relatively flat, the downhill side and uphill side of the pit no. 4 is also steep colluvium slope, and so on. The top and bottom stations are relatively flat compared to the cable car alignment. Although the slope is covered by colluvium, the relief is still controlled by the subsurface lithology and structures.

1.4 Objectives

The general objective of present study is to carry out geotechnical and geophysical studies of the project specially the foundation characteristics of tower locations of cable car ropeway.

Out of 12 tower locations, 7 locations were selected for the detailed geotechnical investigation in this study. The specific objectives of the study are:

- To obtain information on the geology of the study area.
- To obtain foundation characteristics for the selected tower locations.
- To explore sub-surface geology using seismic refraction survey along the major engineering structures.
- To correlate various geotechnical parameters with seismic wave velocity.
- To estimate peak ground acceleration (PGA) during major earthquakes in the Himalaya and prepare PGA map.
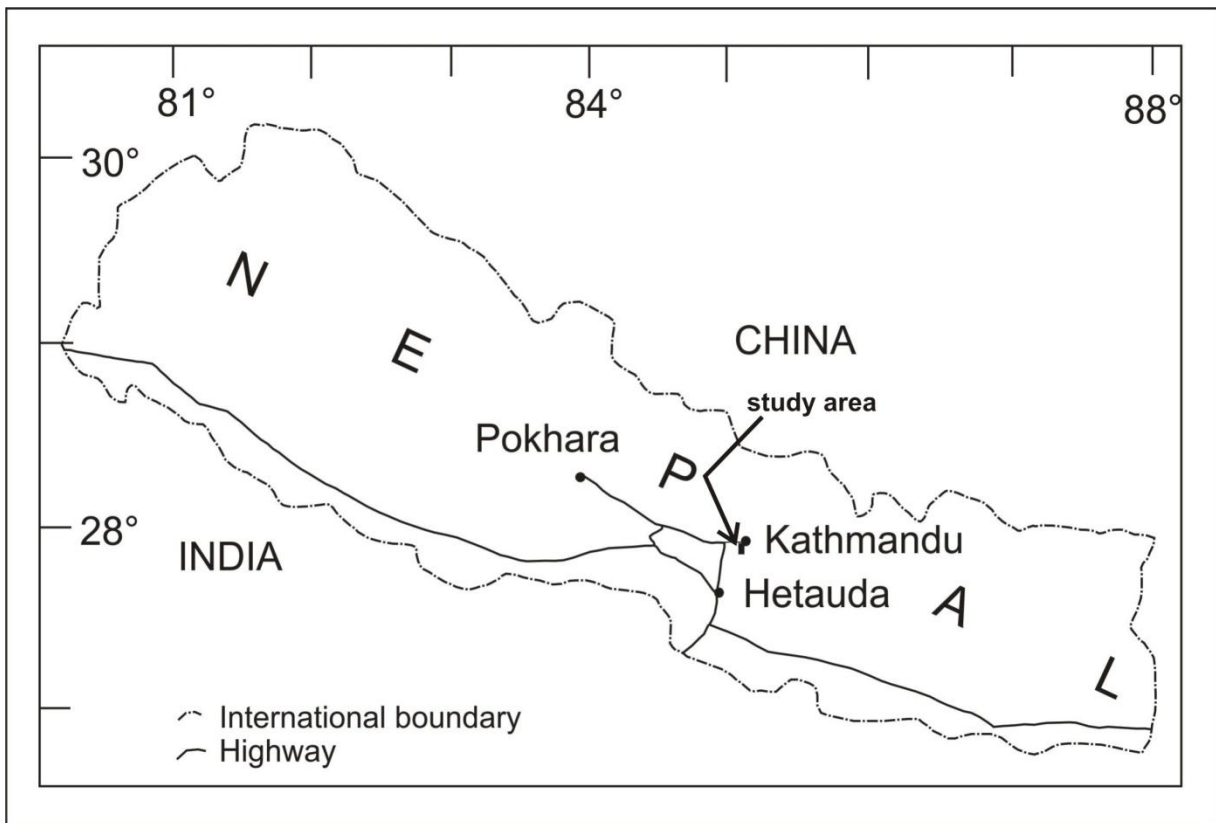
Fig. 1.1: Location map of the study area.
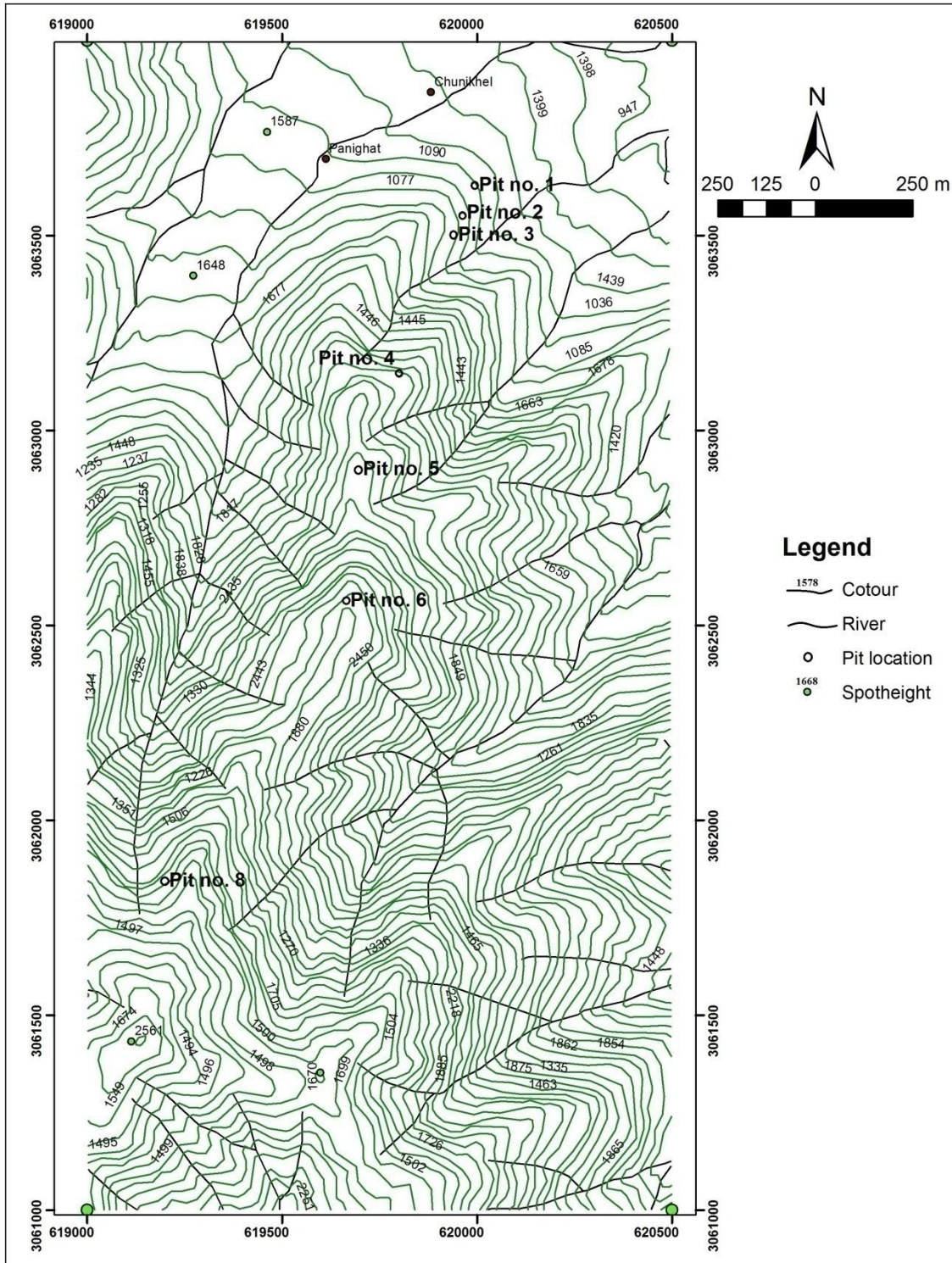
Fig. 1.2: Location of pits in the study area. Open circles labeled as Pit no.1, Pit no.2, etc represents pit holes dug for geotechnical investigations.

1.5 Limitations of the study

The seismic measurements were carried out using seismograph McSEIS 170f. Although the in-built function of the machine was capable of giving digital data, we could only print out the hard copies of data due to machine's defect. This had limited the further digital processing of the data and subsequent interpretation specially in terms Seismic Refraction Tomography (SRT). Similarly, the interpretation of seismic data by travel time-distance curve method is also affected by manual picking of data from hard copies of waveforms. Moreover, manual picking of data was time consuming.

Seismic signals were generated using the sledge hammer of 10kg weight. For the use of explosives one should follow the hectic process imposed by the government which was time consuming and expensive. Signals generations by hammer were not always reliable in terms of resolution and signal to noise ratio which was the serious limitation of the study.

Dynamic Cone Penetration (DCP) was used in in-situ test. The use of Standard Penetration Test (SPT) would be more reliable but the unavailability of instrument, specially at Central Department of Geology, during the field work program posed problems to the research work. Using DCP has high variability of data in case of large, well graded granular materials. Although, fewer materials with a maximum aggregate size of larger than 2 inches were encountered in this study, the use of DCP in such case has always been questionable.

Though the study area is located near the Kathmandu valley, the site specific accessibility problem like the unavailability of foot trails along cable car alignment or to a specific tower was one problem that had limited the in-situ test to some extent.

The field work was carried in June and July which is monsoon periods in Nepal and monsoon had affected the moisture content in every test procedures.

Peak ground acceleration (PGA) calculation was synthetic, instead of real. Hence, absence of real data for any earthquake is still to be tested.

CHAPTER II

LITERATURE REVIEW

2.1 Regional Geology

Himalaya is an active orogenic system created by continental-continental collision. It is created by collision between northward moving Indian Plate and the Eurassian Plate. The present day continuation of the orogeny in the Himalaya belt is evident by the occurrence of intense seismic activities in the Himalaya and continued northward movement of the Indian Plate at a rate of about 5 cm per year (Seeber and Armbruster, 1981; Jakson and Bilham, 1994; Pandey et al., 1995). This leads to the large crustal shortening. Most of the convergence is accommodated within Himalaya by movement on various thrusts and folds (Upreti, 1999).

Tectono-morphologically, the whole Himalaya can be divided into different longitudinal units, each having unique stratigraphic and evolutionary characters (Gansser, 1964). Moving towards north from south these units are the Terai, Sub-Himalaya (Siwalik), Lower or Lesser Himalaya, Higher Himalaya and the Tethys Himalaya (Fig. 2.1). The Terai zone, which is the southernmost tectonic unit of the Himalaya, is covered by alluvium deposit of Pleistocene to recent age. Its northern margin is the Himalayan Frontal Thrust (HFT) which separates it from the Sub-Himalayan zone. The mollassic deposits of the Siwalik or Sub-Himalaya zone is of middle Miocene to early Pleistocene age and it is separated by Main Boundary Thrust (MBT) from Lesser or Lower Himalaya in the north. Meta-sediments of the Lesser or Lower Himalaya extends up to Main Central Thrust (MCT) in the north. The geology of the Lesser Himalaya is complicated due to intense folding and thrusting and is largely unfossiliferous. The entire Lesser Himalaya consists of allochthonous and autochthonous settings with various nappes, klippes and tectonic windows. The Higher Himalayan Crystalline rocks of Precambrian age overlie the Lesser Himalaya along the MCT. The South Tibetan Detachment System (STDS) separates the medium to high grade metamorphic Higher Himalayan rocks from the overlying low-grade sedimentary rocks of the Tethys Himalaya. Except Cambrian, all systems of Paleozoic and Mesozoic Erathems have been well established by fossil contents (Sah, 1999) in the Tethys Himalaya zone.
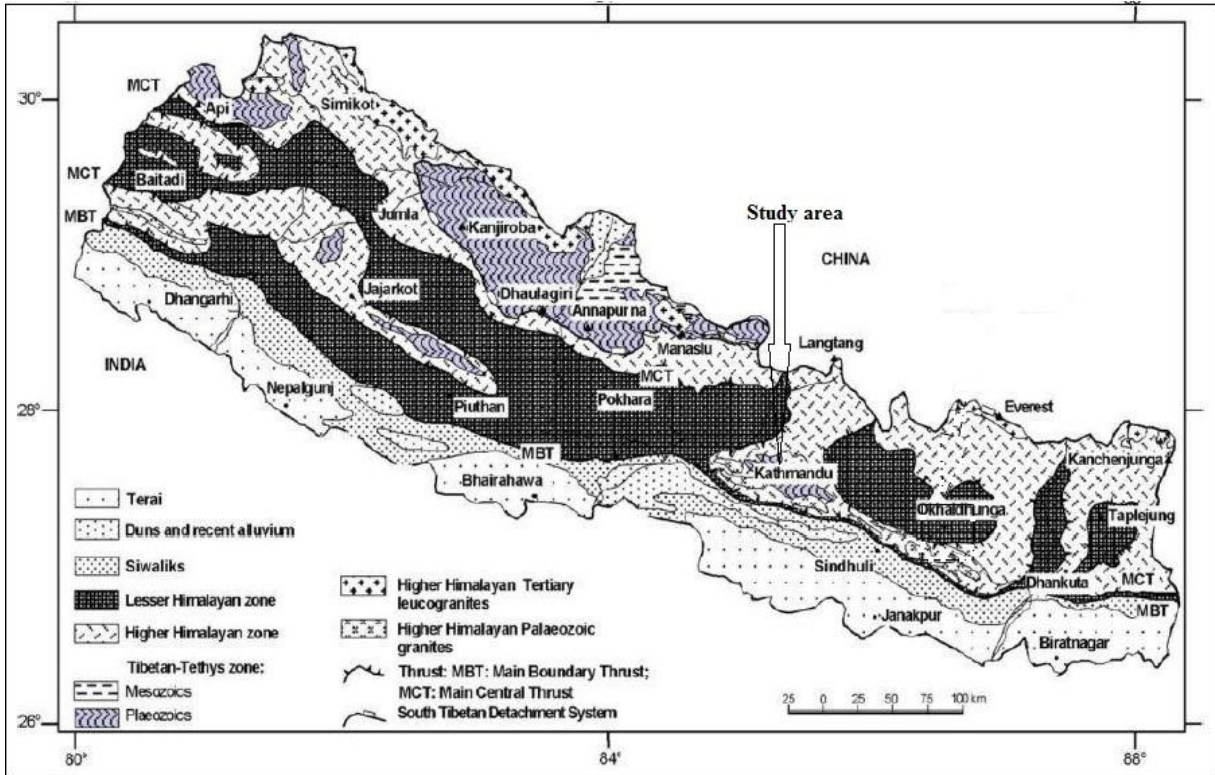
Fig. 2.1: Generalised geological map of Nepal showing the present study area (source: Amatya and Jnawali, 1994).

2.2 Geology of the Study Area

Geology has always been an important part for any studies related to geotechnical, geophysical and peak ground acceleration analysis. Despite long research history of the Himalayan Geology, to date a few geological investigations have been carried out related to the bedrock geology of the Kathmandu Valley. The main literature on the geology of the Kathmandu Valley is attributed to Stöcklin and Bhattarai (1977), based on their study of aerial photography. According to them the study area lies on the northern flank of the Mahabharat Synclinorium with rocks of the Phulchauki Group dipping south.

Similarly, Acharya and Dhital (2006) studied the geology and structure of Raniban-Champadevi area, Kathmandu Valley and their detailed geological study is confined to the lower four formations of the Phulchauki Group, namely Tistung Formation, Sopyang Formation, Chandragiri Limestone and Chitlang Formation. Based on Acharya and Dhital

(2006), the study area consist rocks of Sopyang Formation, Chandragiri Limestone and Chitlang Formation. The Sopyang Formation consists of intercalation of grey merasandstone, grey-green calcareous phyllite, and dolomite (Fig. 2.2). The Sopyang Formation is 200m thick and the age is Cambrian. The rocks of the Chandragiri Limestone are mainly grey limestone with grey-green slate partings and interbeds (Fig. 2.2). The age belongs to Ordovician and the thickness is 2000m. Similarly, the Chitlang Formation is composed of interbedded grey-green slate and white quartzite in the lower part and argillaceous limestone in the upper part (Fig. 2.2). The thickness of this formation is 1000m and belongs to Silurian age.

On the other hand, Sakai et al. (2006) suggested that the Kathmandu basin in the southern rim is separated from the Mahabharat Range by the active Chandragiri thrust fault. They suggested that simultaneous deposition of the fanglomerate in the northern slope of the Mahabharat Range and boulder conglomerate in the Siwalik Basin indicates that the both frontal range of the Himalaya and intra-basinal high in the Siwalik belt started rapid uplift at about 1 Ma (Fig. 2.3).

Stöcklin and Bhattarai (1977) and Acharya and Dhital (2006) in their work did not indicate the Chandragiri thrust. But, the presence of Chandragiri thrust fault has been described by Sakai et al. (2006) in their work on soft sediments of Kathmandu valley. During this research work no direct evidence of this thrust in the field was found because it has always been difficult to locate the fault in contact zone between basement rock and soft sediments. However, the abrupt change in altitude and the extensive fan deposits in the southernmost rim of the Kathmandu valley as compared to the northernmost rim where fan deposited by rivers are low, suggests the presence of fault. Thus, the modified (after Acharya and Dhital, 2006) geological map of the basement rock of the study area is shown in Fig. 2.4.
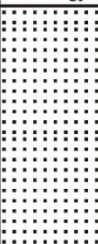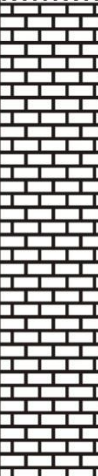
Group	Formation	Lithology	Thickness (m)	Age	Description
Phulchauki Group	Chitlang Formation		1000	Silurian	Interbedded grey-green slate and white quartzite in the lower part and argillaceous limestone in the upper part
	Chandragiri Formation		2000	Ordovician	Mainly grey limestone with grey-green slate and interbeds
	Sopyang Formation		200	Cambrian	Intercalation of grey meta-sandstone, grey-green calcareous phyllite, and dolomite

Fig. 2.2: Stratigraphic column of the Raniban-Champadevi area (modified after Acharya and Dhital, 2006).
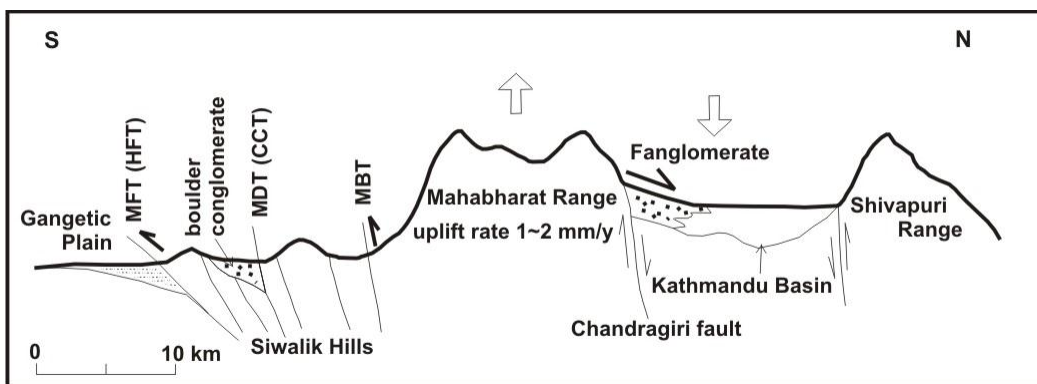
Fig. 2.3: A schematic cross section of the Lesser Himalaya and the Sub-Himalaya in Central Nepal (modified after Sakai et al., 2006). MFT= Main Frontal Thrust, CCT= Central Churia Thrust, MBT= Main Boundary Thrust.
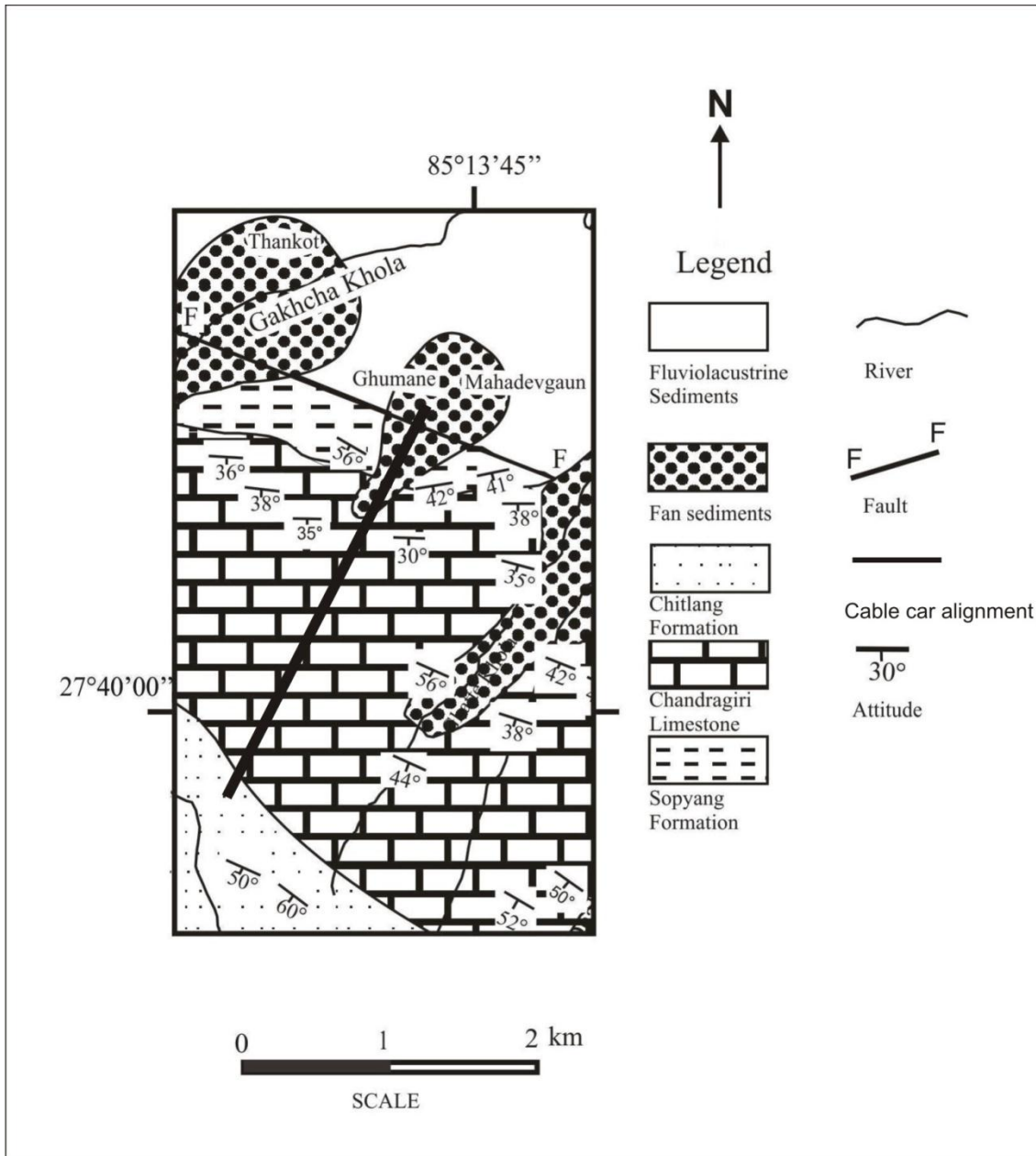
Fig. 2.4: Geological map of the study area (modified after Acharya and Dhital, 2006).

2.3 Geotechnical Studies

In-situ test and laboratory analysis of samples both were parts of the geotechnical studies in this study. Literatures relevant to both analyses are listed and described briefly in the

following sections. Detail methodologies adopted after reviewing such literatures will be discussed in chapter III under methods and materials.

2.3.1 In-situ Direct Cone Penetration Test

Standard test method for use of the Dynamic Cone Penetrometer, designation: D 6951-03, as described by American Society of Testing and Materials (ASTM International) covers the measurement of the penetration rate of the Dynamic Cone Penetrometer (DCP) through undisturbed soil and/or compacted materials. The penetration rate may be related to in-situ strength such as an estimated in-situ California Bearing Ratio (CBR). The penetration per blow is used to estimate in-situ CBR or strength using the appropriate correlation.

The ASTM D 6951-03 suggests the use of correlation equation recommended by the United States Army Corps of Engineers. Classification of soil prior to correlation is needed in this equation, because there are different correlation equations for different soil types. For example the correlation equation for low plastic clay with CBR less than 10 and high plastic clay are different. However, this paper also suggests that selection of the appropriate correlation is a matter of professional judgment. Kleyn and Van (1983) after their extensive work in DCP soundings proposed a correlation equation for shallow ground investigation. This research work tempted to follow the correlation proposed by them. The CBR thus calculated was used for the bearing capacity calculation suggested by PCA (1995). This relationship between bearing capacity and CBR is also adopted by United States Army Corps of Engineers.

2.3.2 Laboratory Studies

Proper evaluation of the various soils is frequently required for its use as foundation material. Some properties used in determination of soil classes can be determined selectively quite quickly and easily and which will have role in important aspect of engineering behavior of soils such as strength. Following properties were tested in present studies and the methodologies followed were adopted mainly from ASTM International.

2.3.2.1Sieve and Hydrometer Analysis for Soil Classification

This test was performed to classify the soils by determining the percentage of different grain sizes contained within a soil sample. Arthur Casagrande developed a new engineering soil classification system during World War II. Since then, it has been updated and now is standardized by ASTM International in its ASTM D2487-06 as Unified Soil Classification (USCS). Similarly, the standard test method for particle size analysis of soil has been published in ASTM D 422-63. This test method covers the quantitative determination of the distribution of particle sizes in soils. The distribution of particle sizes larger than 75 μm is determined by sieving, while the distribution of particle sizes smaller than 75 μm is determined by a sedimentation process, using a hydrometer to secure the necessary data (ASTM D 422-63).

2.3.2.2Moisture Content

Moisture or water content of a soil has direct effect on its strength and stability. Standard test method for laboratory determination of water (moisture) content of soil is described in ASTM D2216-98. In this method the loss of mass due to oven drying is considered to be water.

2.3.2.3 Atterberg Limits Test

Liquid and plastic limits together with shrinkage limit are often collectively known as Atterberg limits. ASTM D4318-10 describes the standard methods for liquid limit, plastic limit, and plasticity index of the soils. Wet preparation method was followed in this research work for the sample preparation.

2.3.2.4 Specific Gravity of Soils

The standard test method for specific gravity of soils is described by ASTM International in its ASTM D854-10. This test method covers the determination of the specific gravity of soil solids that pass the 4.75 mm (No. 4) sieve by means of a water pycnometer.

2.3.2.5 Direct Shear Test

Standard direct shear test of soil samples has been described by ASTM D 3080-98. The test is performed by deforming a specimen at a controlled strain rate on or near a single shear plane determined by configuration of the apparatus. The shear strength parameters cohesion (c) and Phi (ϕ) were determined by this test.

2.4 Seismic Refraction Survey

The equipment, field procedures, and interpretation methods for the determination of the depth, thickness and seismic velocity of subsurface soil and rock or engineered materials using seismic refraction method has been described in ASTM D5777-00. The seismic refraction method is used to map geologic conditions including depth to bedrock, or to water table, stratigraphy, lithology, structure, and fractures or all of these. The calculated seismic wave velocity is related to mechanical material properties. Therefore, characterization of the material (type of rock, degree of weathering, and rippability) is made on the basis of seismic velocity and other geologic information (ASTM, D5777-00). Refraction field methods have been described by Telford (1981). Similarly, the interpretation techniques of seismic refraction data have been described by Telford et al. (1981), and Raynolds (1997).

2.5 Peak Ground Acceleration

Generally, PGA is estimated from observed accelerograms. In the case of present study area no observed data is available. For the modeling of accelerograms (PGA) synthetic earthquakes are generated from finite fault source (Honda and Yomogida, 2003b). Methods developed by Honda and Yomogida (2003a, 2003b and 2003c) uses wavenumbers to calculate accelerograms. For the source velocity model given by Ghimire and Kasahara (2007) was used. Similarly, a computer program in C+ language written by Honda (2003) was used in PGA calculation. Details are discussed in section 3.4. Earlier works in PGA distribution has been conducted by Bhattarai et al. (2011) using 1934 Taplejung and 1988 Udayapur earthquakes as point source. However, their preliminary probabilistic seismic hazard analysis is concentrated in Eastern Nepal.

CHAPTER III

METHODS AND MATERIALS

Methodologies adopted during this study can be categorize into three parts viz. desk study of the literatures relevant to thesis work (see chapter II, Literature Review); field work including geological study, geotechnical investigations & seismic refraction survey; and laboratory analysis of data & interpretation of data.

Geological maps and earlier works of the study area conducted by various researchers were studied prior to the field work between 25th and 28th April 2013. This was followed by a reconnaissance survey with a team of experts including geotechnical engineer, engineering geologist and geophysicist from Nepal Environmental and Scientific Services Private Limited (NESS), which was responsible for this Kathmandu Fun Park Project (KFPP). Reconnaissance survey was conducted between 1st and 7th June 2013 for the geological, geotechnical assessment of the project area. This reconnaissance survey team planned the methodologies to be adopted for the in-situ and laboratory test and analysis of data, and accordingly further studies were conducted. Geological survey was performed between 8th and 12th June 2013. This includes identification of bedrock geology of the project site and nearby places. In succession the geotechnical investigations were carried out which included the digging of test pits (size 2mx2mx2m) at seven selected tower locations between 19th and 25th July 2013. Similarly, for the strength and bearing capacity calculations in the field the Direct Cone Penetration Test (DCPT) was conducted at each tower locations between 26th and 29th July 2013. Furthermore, laboratory tests for soil classification, liquid limit—plastic limit and strength parameters (c and ø) of soil were performed from 27th to 31st July 2013. At last of the field work the seismic refraction survey was carried out in early August 2013. Similarly, interpretation of data from laboratory analysis and from field test, and gathering and interpretation of data of past earthquakes for the seismic hazard analysis were conducted in the successive months of 2013.

Materials, equipments, software etc. needed for the field studies, laboratory analysis and data interpretations are described below in the separate sections like geotechnical investigations,

seismic refraction survey, and peak ground acceleration calculation to access the seismic hazard.

3.1 Geotechnical Studies

3.1.1 In-situ Test

The general direction of proposed tower alignment for cable car is NE-SW (Fig. 1.2). The proposed tower alignment of the cable car lay mostly on loosely deposited colluvium. To investigate geotechnical parameters for different towers altogether seven pits of dimension 2mx2mx2m were dug (Fig. 3.1). For the field test DCPT was performed and soil profiles were also prepared (from surface up to 2m).
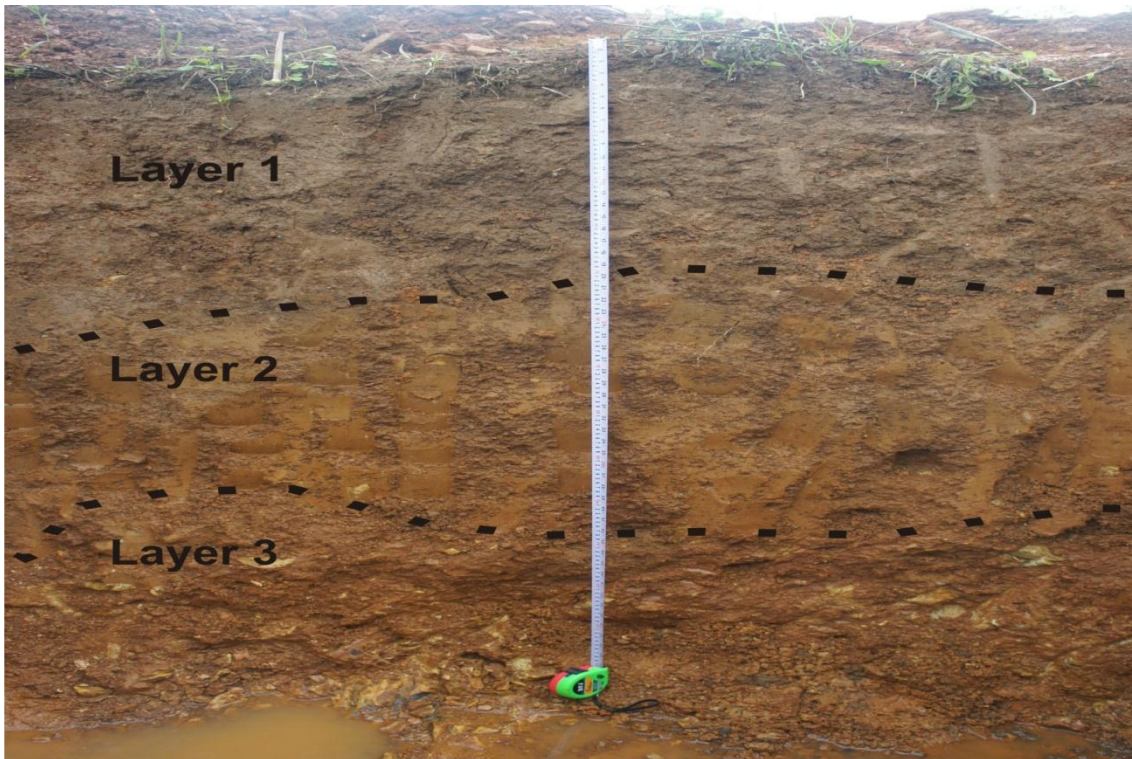
Fig. 3.1: Pit hole dug for geotechnical investigations, pit no. 1 (for detail description of pit profile see section 4.2).

3.1.1.1Direct Cone Penetration Test

ASTM D6951-03 suggests that the Dynamic Cone Penetration (DCP) test is used to access in-situ strength of undisturbed soil and/or compacted materials. The penetration rate of the 8 kg DCP can be used to estimate in-situ CBR, to identify strata thickness, shear strength of strata, and other material characteristics. This instrument is typically used to access material properties to a depth of 1000 mm below the surface. The 8 kg DCP is shown schematically in Fig. 3.2. It consists of following components: a 15.8 mm diameter steel drive rod with a replaceable point or disposable cone tip (tip angle 60 degree and diameter at the base of 20 mm), an 8 kg hammer which is dropped a fixed height of 575 mm, a coupler assembly, and a handle. The procedure was the operator derived the DCP tip into soil by lifting the sliding hammer to the handle then releasing it (Fig. 3.3). The total penetration for a given number of blows was measured and recorded in mm/blow, which was then used to describe stiffness, estimate an in-situ CBR strength from an appropriate correlation chart, or other material characteristics.

Normally readings were taken after a fixed number of blows, that is, 1 blow for soft material, 5 blows for "normal" materials and 10 blows for very resistive materials. The penetration to the nearest 1 mm corresponding to a specific number of blows was recorded. A reading was taken immediately when the material properties or penetration rate changed significantly. Using DCP has high variability of data in case of large, well graded granular materials. Although fewer materials with a maximum aggregate size of larger than 2 inches were encountered in this study, the use of DCP in such case has always been questionable.
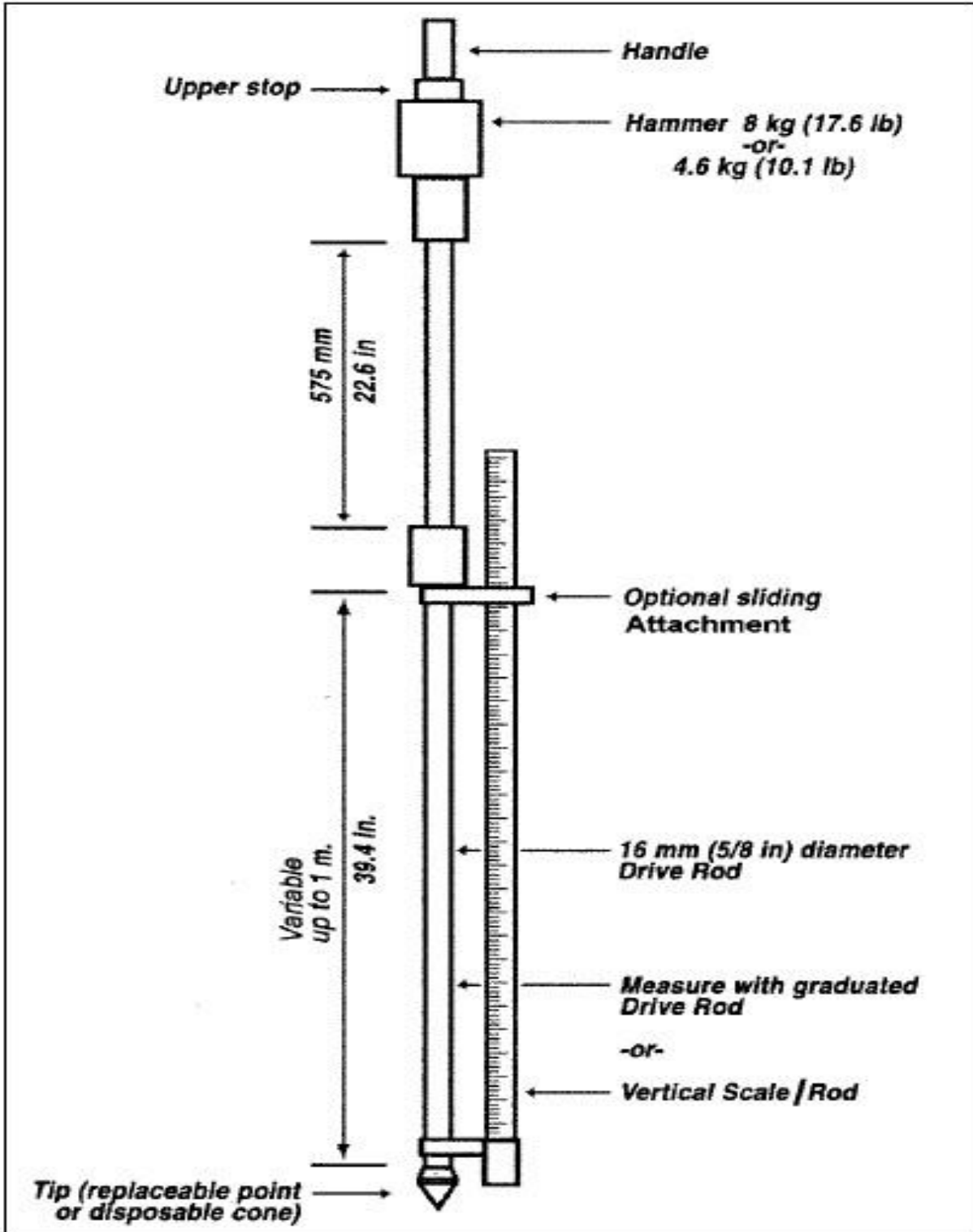
Fig. 3.2: Schematic of DCP device (source: ASTM D6951-03).

Fig. 3.3: Conducting DCP test in the field.

Kleyn and Van (1983) after their extensive work in DCP soundings proposed a correlation equation between DCP strength and for shallow ground investigation which is given as;

$$\log_{10}(CBR) = 2.632 - 1.28 * \log_{10}(Strength) \dots\dots\dots\dots\dots\dots (1)$$

Similarly, Unconfined Compressive Strength (UCS) can also be calculated Kleyn and Van (1983) equation and is given as;

$$UCS = 15 * CBR^{0.88} \dots\dots\dots\dots\dots\dots\dots\dots (2)$$

Thus calculated CBR was used to calculate the bearing capacity which is suggested by PCA (1995) as;

$$Bearing\ Capacity = 16 * (CBR)^{0.66} \dots\dots\dots\dots\dots\dots (3)$$

3.1.1.2 Soil Profiles

The test pits of size 2mx2mx2m for geotechnical studies were used for profiling the soils up to 2m depth from the surface. Profiles were made at field by using field identification and description of soils given by Anon (1981).

3.1.2 Laboratory Studies

Since the geotechnical studies are only concerned with the tower location, base station and top station no particular sampling method was followed during this study. Hence, the samples were taken from the bottom (i.e. 2 m below the surface) of each seven pits for the laboratory analysis. Similarly, the samples taken were disturbed samples. Five different tests were performed in the laboratory of Environment and Resource Management Consultancy (ERMC) Private Limited, Baneshwor, Kathmandu. They are described as follows.

3.1.2.1 Classification of Soils

Quantitative determination of the distribution of particle sizes in soils has been described by ASTM in ASTM D422-63. The distribution of particle sizes larger than 75 μm (retained on the No. 200 Sieve) was determined by sieving, while the distribution of particle sizes smaller than 75 μm was determined by a sedimentation process, using a hydrometer to secure the necessary data. Similarly, the standard practice for classification of soils for engineering purposes has been describe by ASTM as unified soil classification system in ASTM D2487-06. This practice describes a system for classifying mineral and organo-mineral soils for engineering purposes based on laboratory determination of particle-size characteristics, liquid limit, and plasticity index and shall be used when precise classification is required. Apparatus used in the soil classification were balance, set of sieves, cleaning brush, sieve shaker, mixer, hydrometer, sedimentation cylinder, control cylinder, thermometer, beaker, timing device, etc.

Sieving was used in the particle size analysis of sands and gravels. The sample was placed on a nest of standard sieves (prescribed by ASTM standard), of decreasing size from top to bottom, and shaken by a ro-tap vibrator. At the end of the test the soil fractions retained on each sieve were weighed. However, if a significant amount of fine-grained material is present in the sample, it may have to be washed through the sieves, after treating with a deflocculating

agent. The dry fractions retained on each sieve were then weighed. In hydrometer method, the sample was treated with sodium hexametaphosphate to complex Ca^{++}, Al^{3+}, Fe^{3+}, and other cations that bind clay and silt particles into aggregates. The sample was then mixed with distilled water and was placed in a cylinder. The relative density of the suspension was measured at the same given times. The size of the soil particles in the suspension, and consequently its density, decreases with time as the larger particles settle out. Corrections were made for the density and temperature of the dispersing solution. The results of particle size analysis were given in the fractions, by weight, of different size grades. These fractions were expressed as a percentage of the whole sample and were generally summed to obtain a cumulative percentage. Cumulative curves were then plotted in semi-log paper and soil was classified.

3.1.2.2 Moisture Content Determination

For many materials, the water content is one of the most significant properties used in establishing a correlation between soil behavior and its index properties. The water content of a material is used in expressing the phase relationships of water, air, and solids in a given volume of material. The standard test method for laboratory determination of water (moisture) content of soil and rock by mass has been standardized in ASTM D2216-98. Apparatus used were based on standard as prescribed by this standard and were drying oven, balances, specimen containers, desiccators, holder, knives, spatulas, scoops, sample splitters, etc. The procedure was that a test specimen was dried in an oven at a temperature of $110° \pm 5°C$ to a constant mass. The loss of mass due to drying was considered to be water. The water content was calculated using the mass of water (M_w) and the mass of the solids (M_s).

Water content (w) = (M_w/M_s)*100 ……………………………………………………..... (4)

3.1.2.3 Atterberg LimitsTest

Atterberg limit test are used as an integral part of several engineering classification systems to characterize the fine-grained fractions of soils and to specify the fine-grained fraction of construction materials. The liquid limit, plastic limit, and plasticity index of soils are also widely used extensively, either individually or together, with other soil properties to correlate

with engineering behavior such as compressibility, hydraulic conductivity, compactibility, shrink-swell, and shear strength (ASTM D4318-10).

Procedure was followed as suggested in ASTM D4318-10. The specimen was processed to remove any material retained on a 425 μm (No.40) sieve. The liquid limit was determined by performing trials in which a portion of the specimen was spread in a brass cup, divided in two by a grooving tool, and then allowed to flow together from the shocks caused by repeatedly dropping the cup in a standard mechanical device. The three trials plotted or calculated to make a relationship from which the liquid limit was determined. The plastic limit was determine by alternately pressing together and rolling into a 3.2 mm diameter thread a small portion of plastic soil until its water content was reduced to a point at which the thread crumbles and can no longer be pressed together and re-rolled. The water content of the soil at this point was reported as the plastic limit. The Fig. 3.4 shows the essential features and critical dimensions of the hand operated liquid limit device.
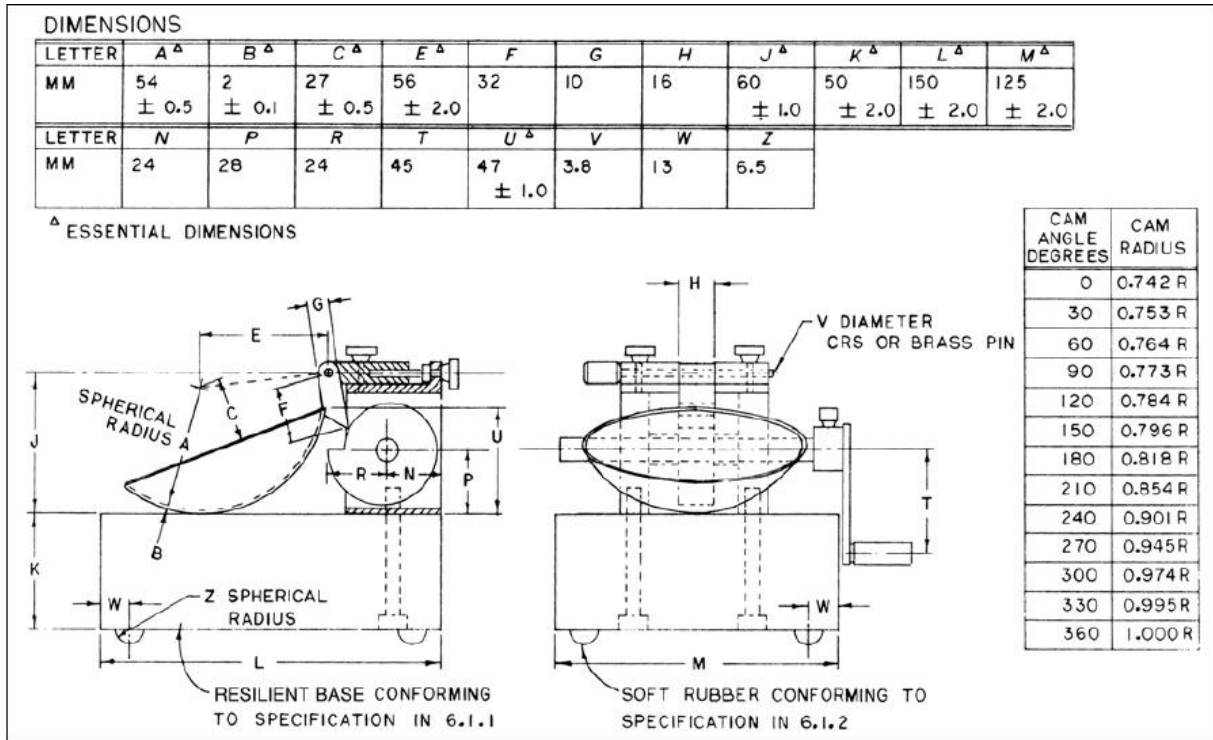
Fig. 3.4: Hand operated liquid limit device (source: ASTM D438-10).

3.1.2.4 Specific Gravity of Soils

The specific gravity of soil is used in calculating the phase relationships of soils, such as void ratio and degree of saturation. Similarly, it is also used to calculate the density of soils. Standard method for this test has been described by ASTM International in ASTM D854-10. This method covers the determination of the specific gravity of soil solids that pass the 4.75 mm (No. 4) sieve, by means of a water pycnometer. Apparatus required in this test are pycnometer, balance, vacuum pump, funnel, spoon, etc.

Specific Gravity $G_s = W_o/(W_o+(W_a-W_b))$ …………………………………………………. (5)

Where, W_o= weight of sample of oven-dry soil. W_a= weight of pycnometer filled with water.

W_b= weight of pycnometer filled with water and soil.

3.1.2.5 Direct Shear Test

ASTM D3080-98 covers the test method for determination of the shear strength of a soil material in direct shear. Apparatus required are shear device, shear box, porous insert, device for applying and measuring the normal force, device for shearing the specimen, shear force measurement device, shear box bowl, deformation indicators, balances, etc. The procedure is to place the specimen in the direct shear device, applying a predetermined normal stress, providing for wetting or draining of the test specimen, or both, consolidating the specimen under normal stress, unlocking the frames that hold the specimen, and displacing one frame horizontally with respect to the another at a constant rate of shearing deformation and measuring the shearing force and horizontal displacements as the specimen is sheared.

Nominal shear stress, acting on the specimen is;

$\tau = F/A$ .... (6)

Where, τ is nominal shear stress, F= shear force, and A is initial area of the specimen.

Normal stress acting on the specimen is;

$$n = N/A \quad\text{..} \quad (7)$$

Where n= normal stress, and N= normal vertical force acting on the specimen.

$$\text{Displacement rate } (d_r) = d_h/t_e \quad\text{..} \quad (8)$$

Where, d_h= relative lateral displacement, and t_e= elapsed time of test.

3.2 Seismic Refraction Method

3.2.1 Introduction to Basic Theory of Seismic Waves

A seismic disturbance is transmitted by periodic elastic displacement of the particles of materials. The progress of the seismic wave through a medium is determined by the advancement of the wave fronts. Seismic waves, which consist of tiny packets of elastic strain energy, travel away from any seismic source at speeds determined by the elastic moduli and the densities of the media which they pass. There are mainly two types of seismic waves. One which passes through the bulk of a medium known as body waves and another that confined to the interfaces between media with contrasting elastic properties, particularly the ground-air surface, known as surface waves. Two types of body waves can travel through an elastic medium. Material particles oscillate about fix points in the direction of wave propagation by compressional and dilational strain in P-wave or compressional waves or primary waves. While in S-waves or secondary waves or shear waves, particle motion is at right angles to the direction of wave propagation and occurs by pure shear strain. Velocity of P-wave (Reynolds, 1997) is given as;

$$V_p = (E/\rho)^{1/2} \quad\text{……………………………………………………………………...} \quad (9)$$

$$V_p = [(K+4\mu/3)/\rho]^{1/2} \quad\text{……………………………………………………...……...…} \quad (10)$$

Where, V_p= P-wave velocity. E = Young's modulus.

ρ = density of medium. K = bulk modulus and

μ = shear modulus.

Velocity of the S-wave is given by;

$$V_s = (\mu/\rho)^{1/2} \dots\dots\dots\dots\dots\dots\dots\dots\dots\dots\dots\dots\dots\dots\dots\dots\dots\dots\dots\dots\dots\dots\dots \ (11)$$

The only elastic property that determines the velocity of the shear wave is the rigidity modulus μ. In liquids and gases μ is zero and hence, shear waves cannot propagate. Comparing equations (10) and (11), we get;

$$V_p{}^2 - 4/3(V_s{}^2) = K/\rho \dots\dots\dots\dots\dots\dots\dots\dots\dots\dots\dots\dots\dots\dots\dots\dots\dots\dots\dots\dots \ (12)$$

By definition, the bulk modulus, K, is positive (if it were negative, an increase in confining pressure would cause an increase in volume). Shear waves from an earthquake travel more slowly than primary waves and are recorded as latter arrivals. Velocity ratio of seismic body waves in terms of Poisson's ratio (υ) is very useful parameter and is given by following equation.

$$(V_p/V_s)^2 = (1-\upsilon)/(0.5-\upsilon) \dots\dots\dots\dots\dots\dots\dots\dots\dots\dots\dots\dots\dots\dots\dots\dots\dots \ (13)$$

P-wave velocity for different materials is shown in Table 3.1. Similarly, typical values of Poisson's ratio are given in Table 3.2. For most consolidated rock material, V_p/V_s is between 1.5 and 2.0. Poisson's ratio can be calculated from equation (13). It can vary between the theoretical limits of 0 (a hard, rigid medium) and 0.5 (fluid). Earth material exhibit values for Poisson's ratio from about 0.05 for very hard rock to 0.45 for water-bearing unconsolidated materials (Sheriff and Geldart, 1982).

3.2.2 Factors Affecting P- and S- waves

Seismic velocity depends mainly on porosity, pressure and water saturation. Different sediment types are characterized by different velocity values and velocity dependencies of controlling parameters. These are controlled by differences in the mineralogical composition, grain size distribution and grain shape, etc. In consolidated sediments P-wave velocity depends on the porosity and on the material filling the pores. The velocity generally increases as the porosity decreases. The relationship given by Wyllie et al. (1958) is given below.

$$1/V_p = \phi/V_f + (1-\phi)/V_m \dots\dots\dots\dots\dots\dots\dots\dots\dots\dots\dots\dots\dots\dots\dots\dots\dots\dots\dots \ (14)$$

Where, V_p and ϕ are velocity of P-wave and porosity respectively, while V_f and V_m are acoustic velocities in the pore fluid and the matrix respectively. Typical values for the V_f and V_m are 1450 m/s and 2800 m/s for water and consolidated materials respectively. In this study area most of the area is covered by unconsolidated materials, first the models of P-wave velocity and porosity were prepared using Wyllie's equation (equation 14). The model was then used to fit the observed data.

Table 3.1: P-wave velocities through some materials (source: Reynolds, 1997).

Material	Velocity (m/s)	Material	Velocity (m/s)
Air	330	Dolomites	2500-6500
Water	1450-1530	Anhydrite	3500-6500
Loess	200-600	Rock salt	4000-5500
Soil	100-150	Gypsum	3000-3500
Shale	2000-4100	Granites	4600-6200
Sand (loose)	200-2000	Basalts	5500-6500
Sand (dry, loose)	2000-1000	Gabbro	6400-7000
Sand (water saturated, loose)	1500-2000	Peridotite	7800-8400
Glacial moraine	1500-2700	Serpentinite	5500-6500
Sand and gravels (near surface)	400-2300	Gneiss	3500-7600
Sand and gravels (at 2km depth)	3000-3500	Marbles	3780-7000
Clay	1000-2500	Sulphide ores	3950-6700
Flood plain alluvium	1800-2200	Made ground (rubble, etc.)	160-600
Permafrost (Quaternary sediment)	1500-4900	Landfill refuse	400-750
Sandstone	1400-4500	Clay landfill cap (compacted)	335-380
Limestone (soft)	1700-4200	Disturbed soil	180-335
Limestone (hard)	2800-7000		

Table 3.2: Typical Values of Poisson's ratio (Source: Arora, 2000).

S. N.	Types of soil	Poisson's ratio
1.	Saturated clay	0.4-0.5
2.	Unsaturated clay	0.1-0.3
3.	Silt	0.3-0.35
4.	Loose sand	0.3-0.5
5.	Dense sand	0.2-0.3

P-wave velocity is higher for denser rocks. An empirical relationship given by Gardner et al., 1974 shows an increase in velocity with the density (ρ in g/cm^3);

$$\rho = 0.31 \, V_p^{1/4} \dots\dots\dots\dots\dots\dots\dots\dots\dots\dots\dots\dots\dots\dots\dots\dots\dots\dots\dots\dots\dots\dots\dots\dots \quad (15)$$

There exist significant correlation between velocity and porosity for unconsolidated sediments (Schon, 1983). Velocity values in unconsolidated sediments are distinctly lower than in consolidated sediments. The differences between the velocities in dry and water saturated state increase with increasing porosity and decreases with increasing pressure (Klimentos, 1991). The influence is generally much stronger for P-waves due to the distinct difference of the compressibility of fluids and gases than for S-waves where only the change of the density and boundary effects play a role. At low pressure range, there is a marked increase of velocity with depth. Similarly, with increasing amount of clay content the velocity generally decreases in unconsolidated sediments.

3.2.3 Loss of Seismic Energy

The loss of amplitude of seismic wave with distance occurs mainly in three ways as spherical divergence or geometrical spreading, intrinsic attenuation and scattering.

Seismic wave propagates radially away from the source and decreases in amplitude with increasing distance. The total energy (E) generated at the shot instant is spread out over a hemi-spherical shell with a radius (r) that increase with time. The energy is spread out over the surface of the half sphere such that the energy density or intensity for body wave is at distance, r, from source (Lowrie, 2007);

$$I_b = E_b/2\pi r^2 \dots\dots\dots\dots\dots\dots\dots\dots\dots\dots\dots\dots\dots\dots\dots\dots\dots\dots\dots\dots\dots\dots\dots\dots \quad (16)$$

Where, I_b, E_b, and r are the intensity of body wave, total energy of body wave at source, and distance from the source respectively. The surface wave is constrained to spread out laterally. The disturbance affects not only the free surface but extends into the medium to a depth of d, which can be taken as a constant for a given wave. When wave front of a surface wave reaches a distance r from the source, initial energy (E_s) is distributed over a circular cylindrical surface with area $2\pi rd$. At a distance r from its source, the intensity of the surface wave is given as (Lowrie, 2007);

$I_s = E_s/2\pi rd$ ……………………………………………………………………… (17)

From equations (16) and (17) it is clear that the body waves attenuated more rapidly than the surface waves.

Intrinsic attenuation is caused by the imperfect elastic behavior of the earth materials. The energy is absorbed by the medium by being transferred into neat by the friction of individual particles moving against each other as the wave passes through the medium. The attenuation in a homogeneous material is explained by;

$A/A_o = r_o/ r \exp \{-\alpha(r-r_o)\}$ ………………………………………………………..… (18)

Where, A and A_o are the amplitudes at a distance r and r_o from the source respectively. α is the attenuation coefficient which is related to the velocity (V) of elastic waves and their frequency (f) by;

$\alpha = \pi f/QV$ ………………………………………………………………………….. (19)

$Q^{-1} = 2\alpha\lambda$ ……………………………………………………………………….. (20)

Where, Q is the quality factor and λ is the wavelength.

Scattering of incident energy is evident as an apparent attenuation takes place by reflection, refraction of seismic waves. There are three levels of scattering can be described in terms of the wave numbers ($k = 2\pi f/V$) and scale of the heterogeneity (a). Material is quasi-homogeneous when ka $\ll$ 00.1 i.e. very large seismic wavelengths as compared to the heterogeneities and the scatters are too small to be seen by the seismic waves. For ka $<$ 0.1, the material is heterogeneous displaying Rayleigh scattering which produces an apparent attenuation. This situation is the most common. And, for ka 0.1-10, the material is highly heterogeneous, where variation in velocity is rapid and significant scattering occurs and the energy dissipation is known as Mie scattering.

3.2.4 Refraction Principle

The seismic refraction principle is based on Snell's law or law of refraction (equation 21). Laws of refraction and reflection can derived from Huygen's principle.

$Sin\ \theta_1/\ V_1 = Sin\ \theta_2/V_2$ ………………………………………………………..……. (21)

Where, θ_1 and θ_2 are angle of incident (equals angle of reflection) and angle of refraction respectively. V_1 and V_2 are velocity of upper and lower layers.

The method of seismic refraction can be understood by applying Huygens' Principle to the critical refraction at the interface between two layers. The seismic disturbance travels immediately below the interface with higher velocity of the lower medium. It is called head waves (Fig. 3.5).
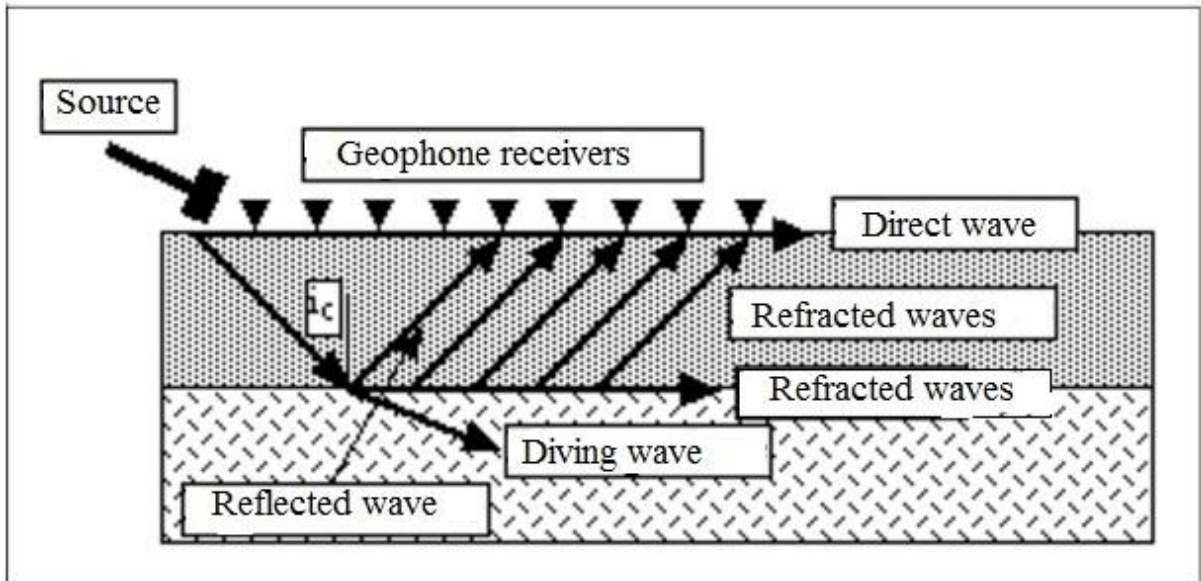
Fig. 3.5: Direct wave, head wave, refracted wave and reflected wave. I_c = angle of incident.

Certain distance off the source (shot point), called crossover distance, the refracted waves arrives prior to reflected waves and hence are the first arrivals to be recorded in seismograph. The method of seismic refraction for the horizontal interface is illustrated in Fig. 3.6.

First arrivals are picked and plotted as a time-distance curve (Fig. 3.6). Then, velocities of the layers, the depth to the interface, and crossover distance can be calculated by following formulas (for notation, see Fig. 3.6);

$V_1 = 1/m_1$ .... (22)

$V_2 = 1/m_2$ .... (23)

$d = 1/2 t_i \{(V_1 V_2)/\sqrt{(V_2^2 - V_1^2)}\}$ .... (24)

$d = \frac{1}{2} X_{cr} \sqrt{(V_2 - V_1)/V_2 + V_1)}$ .... (25)
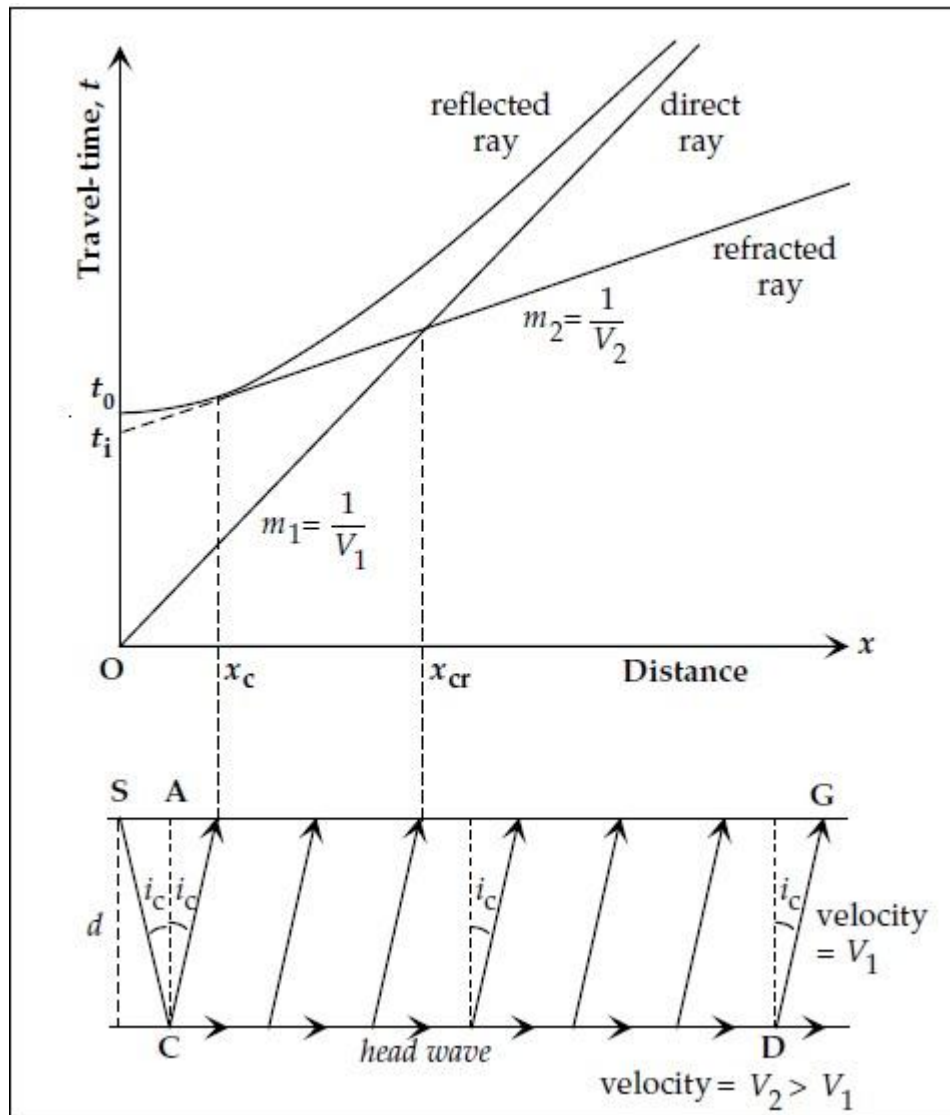
Fig. 3.6: Travel-time versus distance curves for the direct ray and the reflected and refracted rays at a horizontal interface between two layers with seismic velocities V_1 and V_2 ($V_1 < V_2$). S = source, G = geophone, i_c = angle of incident, X_c = critical distance, X_{cr} = crossover distance, d = depth to the interface, m_1 and m_2 are slopes of direct and refracted rays, and t_o is the echo time at t = 0 (source: Lowrie, 2007).

$$X_{cr} = 2d \sqrt{\{(V_2+V_1)/V_2-V_1)\}} \quad \dots\dots\dots\dots\dots\dots\dots\dots\dots\dots\dots\dots\dots\dots\dots\dots\dots\dots\dots\dots \quad (26)$$

In case of inclined refractor the apparent up-dip and down-dip velocities are calculated from the time-distance graph (Fig. 3.7). In this case the forward and reverse shoot is required at both ends of the profile line. Later, those apparent velocities are used to calculate velocities of layers, inclination of refractor and depth to the refractor at both ends (shoot points) of the profile. Working formulas are given below (for notation, see Fig. 3.7);

$$\theta = 1/2\{\sin^{-1}(V_1/V_d) - \sin^{-1}(V_1/V_u)\} \quad \dots\dots\dots\dots\dots\dots\dots\dots\dots\dots\dots\dots\dots\dots\dots\dots\dots \quad (27)$$

$$i_c = 1/2\{\sin^{-1}(V_1/V_d) + \sin^{-1}(V_1/V_u)\} \quad \dots\dots\dots\dots\dots\dots\dots\dots\dots\dots\dots\dots\dots\dots\dots\dots\dots \quad (28)$$

$$t_{id} = 2d_A \cos i_c/V_1 \quad \dots\dots\dots\dots\dots\dots\dots\dots\dots\dots\dots\dots\dots\dots\dots\dots\dots\dots\dots\dots\dots\dots\dots\dots \quad (29)$$

$$t_{ud} = 2d_B \cos i_c/V_2 \quad \dots\dots\dots\dots\dots\dots\dots\dots\dots\dots\dots\dots\dots\dots\dots\dots\dots\dots\dots\dots\dots\dots\dots \quad (30)$$

$$1/V_d + 1/V_u = 2\cos\theta/V_2 \quad \dots\dots\dots\dots\dots\dots\dots\dots\dots\dots\dots\dots\dots\dots\dots\dots\dots\dots\dots\dots\dots \quad (31)$$

3.2.5 Elevation Correction

Dobrin and Savit (1988) suggest that the most usual computational procedure is to put both the shot and the detector on the same imaginary datum plane by subtracting the times that would be required for the wave to travel from the datum to the respective shot or detector locations if they are higher than the datum or by adding the times that would required if they are lower.

Fig. 3.8 demonstrates how this transformation is accomplished. Assume that both the shot and the detector are above the datum plane. Shot point P has to be lowered on the datum plane directly below the shot hole and the detector at Q on the datum plane below E. The hypothetical ray path after the correction is shown by the dotted line. The difference between the time from A to D along the actual path and that from P to D along the hypothetical path is;

$$AB/V_0 - CD/V_1 = AB/V_0 - PB/V_1 = D_s$$
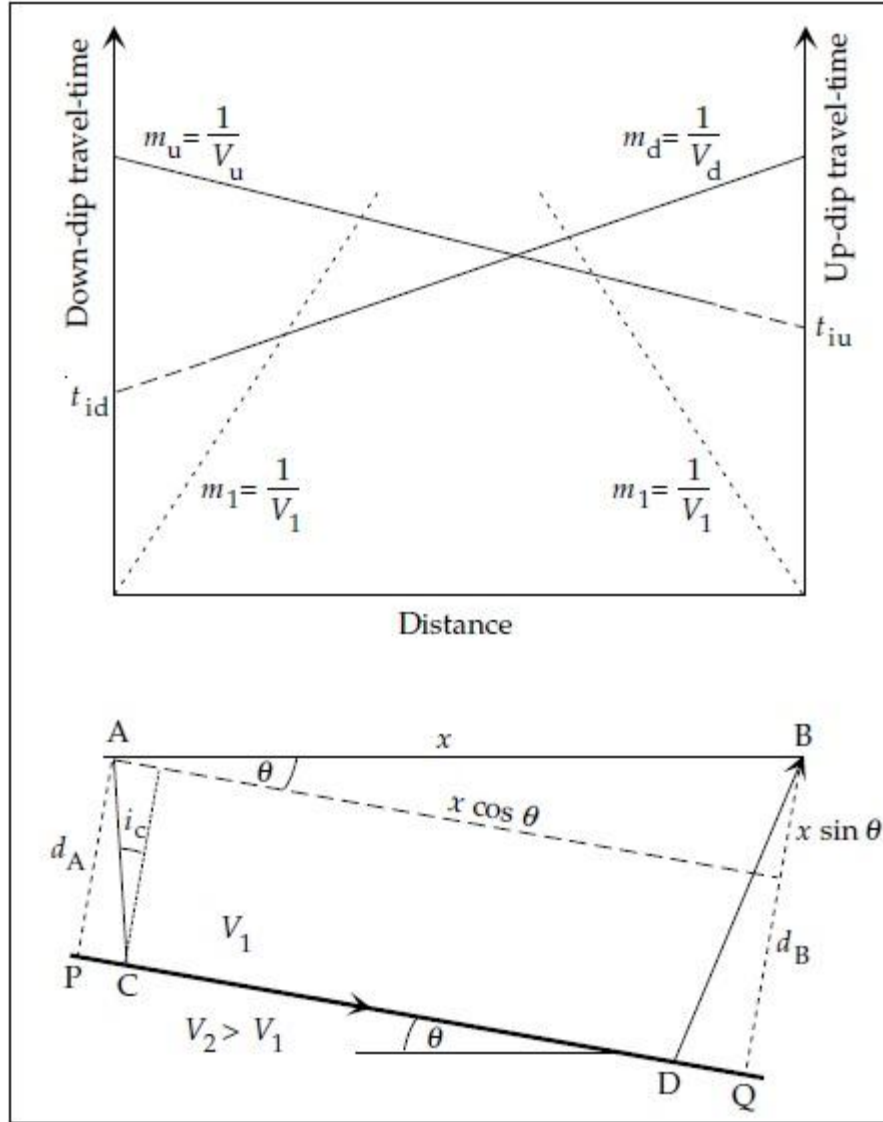
Fig. 3.7: Travel-time versus distance curves of direct and refracted rays for up-dip and down-dip profiles when the refracting boundary dips at θ. A and B are source and geophone locations respectively, V_1 and V_2 are velocities of layers ($V_2 > V_1$), x is distance from source to geophone, θ is the dip of interface, i_c is incident angle, d_A and d_B are depth to refractor at A and B, t_{id} and t_{iu} are down-dip and up-dip time intercepts respectively, m_u and m_d are slopes of up-dip and down-dip refracted waves respectively, m_1 is the slope of direct wave, and V_u and V_d are up-dip and down-dip velocities respectively (source: Lowrie, 2007).

which is, by definition, the delay time associated with the layer between the bottom of the shot at elevation 'e-h' and the datum plane at elevation 'd'. This material constitutes a horizontal slab of thickness 'e-h-d', in this case the delay time is;

31
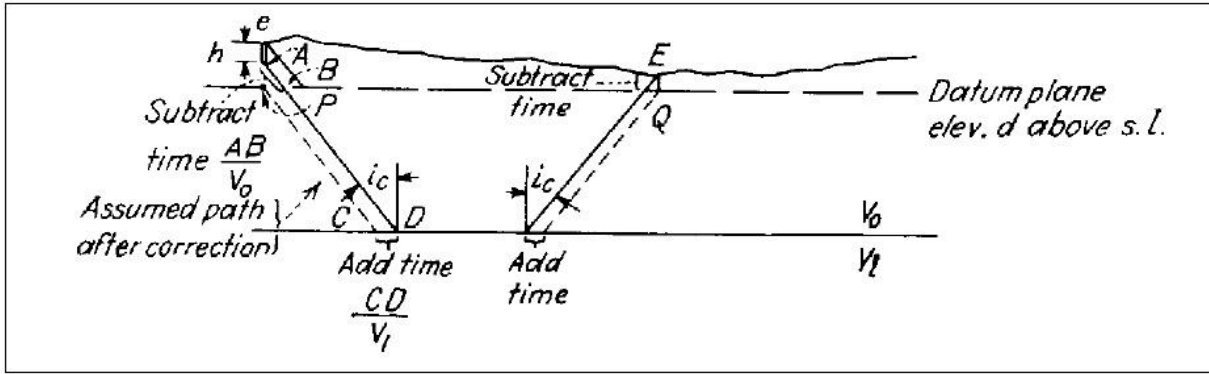
Fig. 3.8: Elevation correction for two-layer case. e is shot elevation, 'E' the detector elevation above sea level (source: Dobrin and Savit, 1988).

$D_s = \{(e-h-d)\cos i_c\}/V_0 = \{(e-h-d)\sqrt{(V_1^2-V_0^2)}\}/V_1V_0$

Similarly, at the detector end where the elevation is 'E', the delay time associated with the path from the surface to the datum is;

$D_d = (E-d)\sqrt{(V_1^2 - V_2^2)}/V_1V_0$

The sum of these corrections in delay time should be subtracted from the observed intercept time in order to place both shot and detector effectively in the datum plane. The elevation of the shot is actually the surface elevation at the top of the shot hole 'e' minus the depth of the charge in the hole 'h', so that the final elevation correction to be applied to the intercept time is;

Elevation correction = $(e-h+E-2d)\sqrt{(V_1^2-V_0^2)}/V_1V_0$ ……………...……………….....…… (32)

3.2.6 Hidden Layer Problem

A hidden layer or blind zone occurs when a layer that is present is not detected by seismic refraction. According to Reynolds (1997) there are four cases of this problem: velocity inversion; lack of velocity contrast; the presence of thin bed; and inappropriate spacing of geophones (Fig. 3.9). In the situation where a layer with lower velocity underlies one with a higher velocity, then the lower-lying layer may not be detected using seismic refraction methods. No critical refraction can occur in such a situation and this no head waves from the

interface are produced. If there is little velocity contrast; then it may be extremely difficult to identify the arrivals of head waves from the top of this zone. In addition, in the case where velocities increases with depth, but the thickness of a layer is less than one wavelength of the incident wave, then the thin bed would not be evident on the corresponding time-distance graph and would therefore effectively be hidden. The hidden layer problem precludes seismic refraction surveys from being undertaken where there is known to be a velocity inversion, such as where there is a layer of strongly cemented material in less consolidated material at shallow depth, such as hard-pan or duricrust. The only way seismic refraction can be undertaken in such circumstances is for each shot and geophone to be located below this hard, higher-velocity layer. This solution can lead to considerable logistical problems and reduced production rates, with a corresponding increase in cost (Reynolds, 1997).
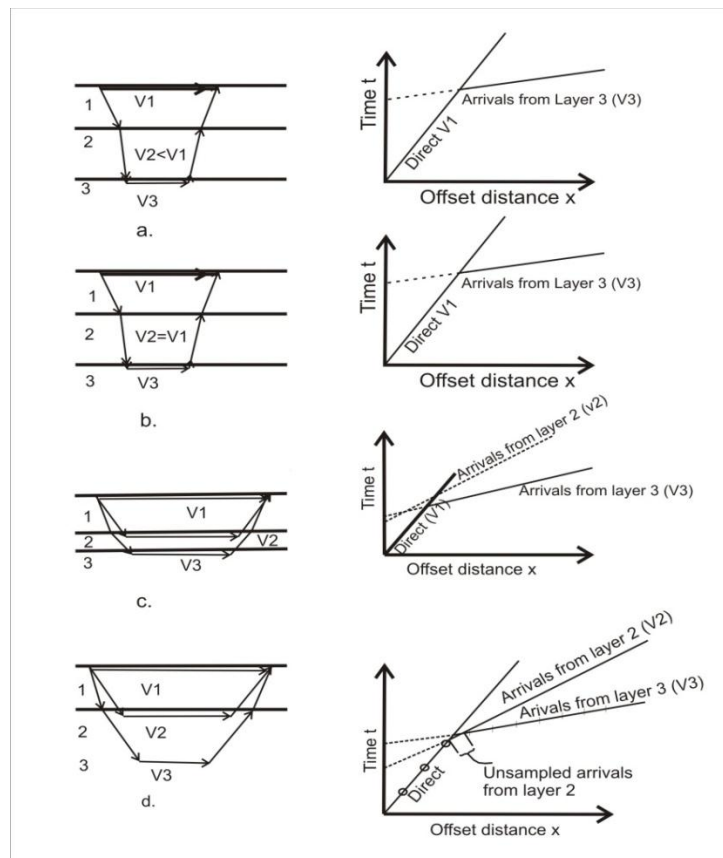
Fig. 3.9: Depiction of the 'hidden layer' problem due to: (a) velocity inversion ($V_2 < V_1$); (b) lack of velocity contrast ($V_2 \approx V_1$) and (c) a thin layer (layer 2) sandwiched between layers 1 and 3. In (d) the distance between geophones is too large to permit the identification of layer 2 (source: Reynolds, 1997).

3.3 Seismic Refraction Survey

3.3.1 Instrument Used for Seismic Refraction Survey

A 24 channel seismograph namely McSEIS 170f from OYO Corporation (Fig. 3.10), Japan was used for data acquisition. One (vertical) component geophones with frequency range between 0.1 and 100 Hz from the same company was used. A 10 Kg hammer was manually impacted to generate the signal.

Fig. 3.10: McSEIS 170f used in seismic refraction survey.

3.3.2 Data Acquisition

Two way inline shooting was deployed for data acquisition. During this study, seismic refraction was carried out along 17 profiles. In inline shooting geophones are spread along a straight line (Fig. 3.11) regarded as profile line hereinafter. Signals are generated at the two

ends of the profile. The seismic energy penetrates the ground and reaches to the geophones. The waveform at each geophone is then transmitted to the seismograph which records the waveform as seismogram. Fig. 3.12 shows the seismic refraction survey carried in this study. Thus, in two way inline shooting, two records of waveforms (seismograms) are obtained as the raw data.

The data acquisition was carried out with sampling frequency of 1000 micro-second. To remove the ambient noise due to many factors like traffic, micro tremor, wind etc. the data was filtered within a narrow band between 30 and 62 Hz. Since the amplitude of the waveform decreases inversely with respect to the distance of the source the gain of the geophone far away from the source was high with respect to the geophone near to source. The range of the gain was between 20 and 50 dB. Further, to homogenize the data for visual inspection all seismograms were normalized. The normalization was carried out by dividing each data of individual waveform by the maximum amplitude.

Fig. 3.11: Installing geophones along a seismic refraction survey line.

3.3.3 Data Processing and Analysis

Data processing includes the picking of travel time from seismograms and preparation of travel time curve. Time spent by seismic signals to reach each geophone was manually picked from the seismogram and was plotted to obtain the travel time curve. Thus, obtained curve was used to estimate the velocities of different layers in the subsurface, depth to the interfaces and the geometry of the interfaces. Elevation corrections were made where needed as described in section 3.2.5.

Fig. 3.12: Conducting seismic refraction survey in field.

3.4 Calculation of PGA

Frequency domain potentials at a point P (Fig. 3.13) due to a finite fault source can be estimated from the following equations (Honda and Yomogida, 2003b);

$$\phi_{\pm} = \sum_{n_y=-N}^{N} \sum_{n_x=-N}^{N} \frac{A_x \pm}{2\mu k_\beta^2 L_x L_y} \exp\left(ik_x(x-x_o) + ik_y(y-y_0) \mp iv(z-z_0)\right)$$

.... (33)

$$\psi_{x\pm} = \sum_{n_y=-N}^{N} \sum_{n_x=-N}^{N} \frac{B_x \pm}{2\mu k_\beta^2 L_x L_y} \exp\left(ik_x(x-x_o) + ik_y(y-y_0) \mp i\gamma(z-z_0)\right)$$

.... (34)

$$\psi_{y\pm} = \sum_{n_y=-N}^{N} \sum_{n_x=-N}^{N} \frac{B_y \pm}{2\mu k_\beta^2 L_x L_y} \exp\left(ik_x(x-x_o) + ik_y(y-y_0) \mp i\gamma(z-z_0)\right)$$

.... (35)

$$\psi_{z\pm} = \sum_{n_y=-N}^{N} \sum_{n_x=-N}^{N} \frac{B_z \pm}{2\mu k_\beta^2 L_x L_y} \exp\left(ik_x(x-x_o) + ik_y(y-y_0) \mp i\gamma(z-z_0)\right)$$

.... (36)

Where, ϕ_+ and ϕ_- represent up-going and down-going P-waves, and ψ_+ and ψ_- for up-going and down-going S-waves, respectively. $k_x = (2\pi/L_x)n_x$ and $k_y = (2\pi/L_y)n_y$ are wavenumbers with the maximum wavenumber of $n_x = n_y = N$. L_x and L_y corresponding to periodic source intervals introduced by the discretization of wavenumbers in x- and y-directions, respectively. Similarly, $v^2 = k_\alpha^2 - k_x^2 - k_y^2$ and $\gamma^2 = k_\beta^2 - k_x^2 - k_y^2$.

$k_\alpha = \omega/\alpha$ and $k_\beta = \omega/\beta$ corresponding to wavenumbers for P-wave and S-wave.

Indeed, ϕ being a scalar potential and $\psi = (\psi_x, \psi_y, \psi_z)$ being a vector potential which are decomposed from a displacement vector U in a Cartesian coordinate system with positive z-axis downward (Honda and Yomogida, 2003b).

Now, source related coefficients $A_\pm$, $B_{x\pm}$, $B_{y\pm}$ and $B_{z\pm}$ are given by

$$A_\pm = -\frac{ik_x^2}{\nu}M_{xx} - \frac{ik_y^2}{\nu}M_{yy} - i\nu M_{zz} - \frac{2ik_xk_y}{\nu}M_{yx} \pm 2ik_xM_{xz} \pm 2ik_yM_{yz}$$

....……..…………….. (37)

$$B_{x\pm} = \pm ik_xM_{yx} \pm ik_yM_{yy} + \frac{i(k_y^2 - \gamma^2)}{\gamma}M_{yz} + \frac{ik_xk_y}{\gamma}M_{zx} \mp ik_yM_{zz}$$

....……..………. (38)

$$B_{y\pm} = \mp ik_xM_{xx} \mp ik_yM_{xy} - \frac{i(k_x^2\gamma^2)}{\gamma}M_{xz} - \frac{ik_xk_y}{\gamma}M_{zy} \pm ik_xM_{zz}$$

....…..……… (39)

$$B_{z\pm} = -\frac{ik_xk_y}{\gamma}M_{xx} + \frac{i(k_x^2 - k_y^2)}{\gamma}M_{xy} \pm ik_yM_{xz} + \frac{ik_xk_y}{\gamma}M_{yy} \mp ik_xM_{yz}$$

....……..... (40)

with moment tensors related to fault parameters ϕ_s, δ and λ (Aki and Richards, 1980 and Fig. 3.13) as;

$M_{xx} = -M_o$ (sin δ cos λ sin $2\phi_s$ + sin 2δ sin λ sin$^2\phi_s$)

$M_{xy} = M_o$ (sin δ cos λ cos $2\phi_s$ +1/2 sin 2δ sin λ sin $2\phi_s$) = M_{yx}

$M_{xz} = -M_o$ (cos δ cos λ cos ϕ_s + cos 2δ sin λ sin ϕ_s) = M_{zx} …………………..…..... (41)

$M_{yy} = M_o$ (sin δ cos λ sin $2\phi_s$ − sin 2δ sin λ cos^2 ϕ_s)

$M_{yz} = -M_o$ (cos δ cos λ sin ϕ_s − cos 2δ sin λ cos ϕ_s) = M_{zy} …………………….……(42)

$M_{zz} = M_o$ (sin 2δ sin λ) ………………………………………………………..(43)
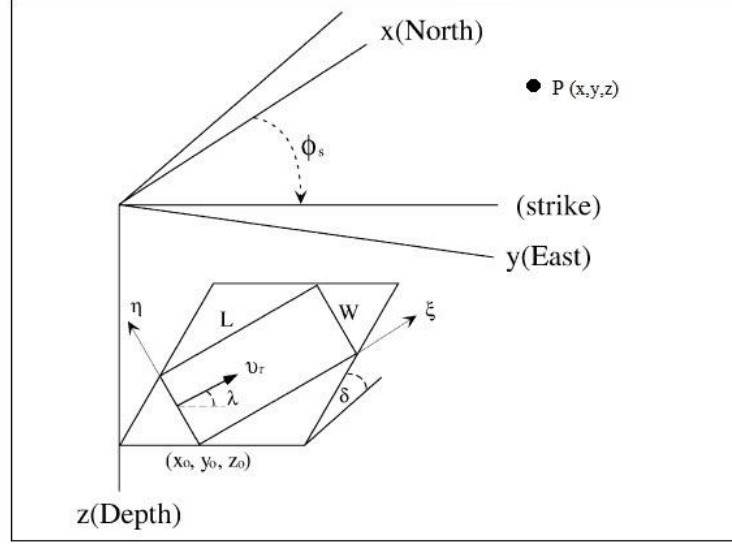
Fig. 3.13: Fault geometry. L, W, ϕ_s, δ and λ are length, width, strike, dip and rake of the fault, respectively, whose definitions are after Aki and Richards, 1980). ξ is the direction of rupture propagation and η is the other direction on the fault plane. Similarly, (x_o, y_o, z_o) is the source location.

With the introduction of finite fault source, and considering $M_o = \mu DS$ with the slip D on a fault area S and decomposing S-wave potentials into SV and SH waves, expressions of potentials radiated from a finite fault (Honda and Yomogida, 1999) are;

$$\Phi_\pm = \sum_{n_x=-N}^{N} \sum_{n_y=-N}^{N} \frac{iD}{2L_x L_y k_\beta^2} \frac{A_\pm}{M_0} \exp i(k_x(x-x_0) + k_y(y-y_0) \mp \nu(z-z_0))$$

$$\times \frac{\{\exp i(W(-C_{11}k_x - C_{21}k_y \pm C_{31}\nu) - 1\}}{(-C_{11}k_x - C_{21}k_y \pm C_{31}\nu)i}$$

$$\times \frac{\{\exp iL\left(\frac{\omega}{\nu_r} - C_{12}k_x - C_{22}k_y \pm C_{32}\nu\right) - 1\}}{\left(\frac{\omega}{\nu_r} - C_{12}k_x - C_{22}k_y \pm C_{32}\nu\right)i}$$

$$= \sum_{n_x=-N}^{N} \sum_{n_y=-N}^{N} C_p \pm \exp(\mp i\nu z)$$

$$\dots\dots\dots\dots\dots\dots\dots\dots\dots\dots\dots\dots\dots\dots\dots\dots\dots\dots\dots \quad (44)$$

$$\psi_{SV\pm} = \sum_{n_x=-N}^{N} \sum_{n_y=-N}^{N} \frac{iD}{2L_xL_yk_\beta^2} \frac{B_{SV\pm}}{M_0} \exp i(k_x(x-x_0) + k_y(y-y_0) \mp \gamma(z-z_0))$$

$$\times \frac{\{\exp i(W(-C_{11}k_x - C_{21}k_y \pm C_{31}\gamma) - 1\}}{(-C_{11}k_x - C_{21}k_y \pm C_{31}\gamma)i}$$

$$\times \frac{\{\exp iL\left(\frac{\omega}{v_r} - C_{12}k_x - C_{22}k_y \pm C_{32}\gamma\right) - 1\}}{\left(\frac{\omega}{v_r} - C_{12}k_x - C_{22}k_y \pm C_{32}\gamma\right)i}$$

$$= \sum_{n_x=-N}^{N} \sum_{n_y=-N}^{N} C_{SV} \pm \exp(\mp i\gamma z)$$

……………………………………………………………………...…………. (45)

$$\psi_{SH\pm} = \sum_{n_x=-N}^{N} \sum_{n_y=-N}^{N} \frac{iD}{2L_xL_yk_\beta^2} \frac{B_{SH\pm}}{M_0} \exp i(k_x(x-x_0) + k_y(y-y_0) \mp \gamma(z-z_0))$$

$$\times \frac{\{\exp i(W(-C_{11}k_x - C_{21}k_y \pm C_{31}\gamma) - 1\}}{(-C_{11}k_x - C_{21}k_y \pm C_{31}\gamma)i}$$

$$\times \frac{\{\exp iL\left(\frac{\omega}{v_r} - C_{12}k_x - C_{22}k_y \pm C_{32}\gamma\right) - 1\}}{\left(\frac{\omega}{v_r} - C_{12}k_x - C_{22}k_y \pm C_{32}\gamma\right)i}$$

$$= \sum_{n_x=-N}^{N} \sum_{n_y=-N}^{N} C_{SH} \pm \exp(\mp i\gamma z)$$

……………………………………………………………………..... (46)

$\psi SH\pm$ and $\psi SV\pm$ are potentials for SH and SV waves with the following coefficients.

$$B_{SV\pm} = \pm\frac{k_x^2}{k}M_{xx} \pm \frac{2k_xk_y}{k}M_{xy} + \frac{k_x(k_\beta^2 - 2k^2)}{\gamma k}M_{xz} \pm \frac{k_y^2}{k}M_{yy} + \frac{k_y(k_\beta^2 - 2k^2)}{\gamma k}M_{yz}$$
$$\mp kM_{zz}$$

$$\dotfill (47)$$

$$B_{SH\pm} = \pm\frac{k_xk_y}{k}M_{xx} \pm \frac{k_x^2 - k_y^2}{\gamma}M_{xy} \pm k_yM_{xz} + \frac{k_xk_y}{\gamma}M_{yy} \pm k_xM_{yz}$$

$$\dotfill (48)$$

Where, C_{11}, C_{12}, ..., C_{33} are defined by the following rotation matrix;

$$\begin{pmatrix} C11 & C12 & C13 \\ C21 & C22 & C23 \\ C31 & C32 & C33 \end{pmatrix}$$
$$= \begin{pmatrix} sin\phi s\ cos\delta cos\lambda - cos\phi s\ sin\lambda & sin\phi s\ cos\delta sin\lambda + cos\phi s\ cos\lambda & sin\phi s\ sin\delta \\ -cos\phi s\ cos\delta cos\lambda - sin\lambda\ sin\phi s & -cos\phi s\ cos\delta sin\lambda + sin\phi s\ cos\lambda & -cos\phi s\ sin\delta \\ -sin\delta cos\lambda & sin\delta sin\lambda & cos\delta \end{pmatrix}$$

$$\dotfill (49)$$

To remove singularities such as surface wave poles from the integration path over k_x and k_y, a complex frequency with a small positive imaginary part ω_i was introduced by Honda and Yomogida (2003b). Hence, it is not necessary to change formulations mentioned above, even in the calculation of static component.

Moreover, displacements are affected by truncation number of wavenumbers. Reuired truncation horizontal wavenumver k_{max} can be estimated by following flow chart (Fig. 3.14) given by Honda and Yomogida (2003b).

Now, displacement can be calculated using the following formula described by Honda and Yogodisa (2003a);

$$Ur' = \frac{\partial\phi\pm}{\partial r'} - \frac{\partial\psi sv\pm}{\partial z} \dotfill (50)$$

$$W = \frac{\partial\phi\pm}{\partial z} + \frac{\partial\psi sv\pm}{\partial r'} \dotfill (51)$$

Where, Ur and r' component (direction of the wave propagation) of surface displacement and W is the vertical. The surface displacement by SH-waves, which is horizontal and perpendicular to $U_{r'}$ is given by;

$$V_\theta = - \partial \, \psi_{SH\pm} / \partial \, r' \dots\dots\dots\dots\dots\dots\dots..\dots\dots\dots\dots\dots\dots\dots\dots..\dots\dots\dots\dots (52)$$
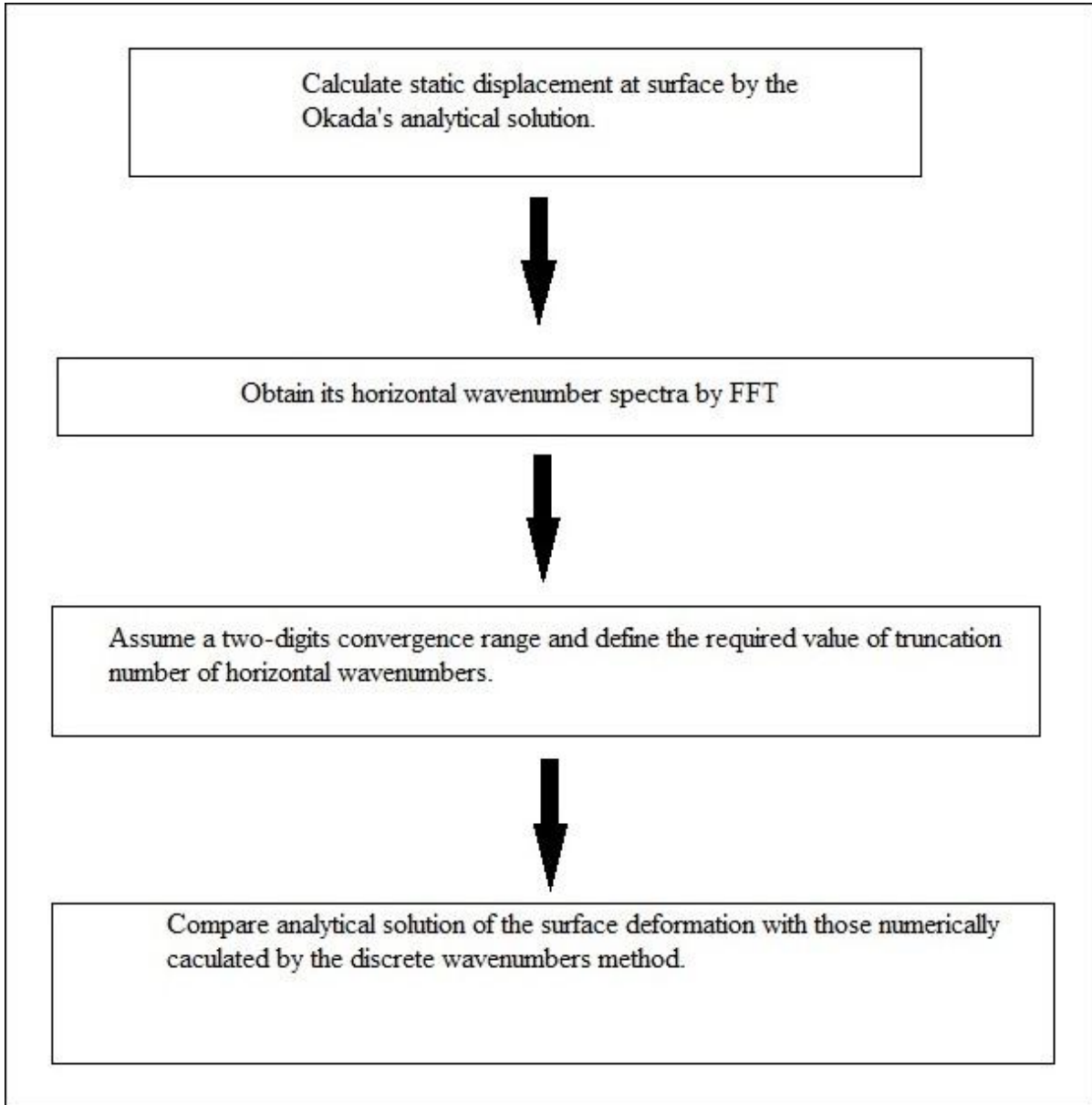
Fig. 3.14: Flow chart to estimate a required truncation horizontal wavenumber K_{max} (source: Honda and Yomogida, 2003b)

Based on these theories double differentiating equations (50), (51) and (52) with respect to time the acceleration can be obtained. These equations were used in the program (C+ program) written by Honda (2003). This program was used to estimate the PGA in this study.

PGA calculation was done in the area with a grid of 10mx10m. The velocity model (Fig. 3.15) of the source was taken as suggested by Ghimire and Kasahara (2007). We use 1934 Taplejung earthquake, 1988 Udayapur earthquake (Fig. 3.16) and two hypothetical earthquakes located (Fig. 3.17) 50 km northeast and 50 km northwest of study area to calculate PGA. Mechanisms of earthquakes are tabulated below (Table 3.3).

Table 3.3: Parameters used to simulate the earthquakes.

Earthquake	Location	M_w	Depth (km)	Mechanism	Dip $\phi°$	$\delta°$	τ (s)
1934 Taplejung	27°17'26'' N 87°32'46'' E	8.4	15	T	0	12	130
1988 Udayapur	26.75° N 86.62° E	6.7	45	S	325	54	38
H1	28°9'58''N 85°10'13''E	6.0	10	T	0	20	18
H2	27°46'15''N 85°43'13''E	6.0	10	T	0	20	18

*Mw=Moment Magnitude, T=Thrust event, S=Strike-slip event, ϕ=dip-direction of the fault plane, δ=dip-amount of the fault plane, τ=duration of the earthquake.
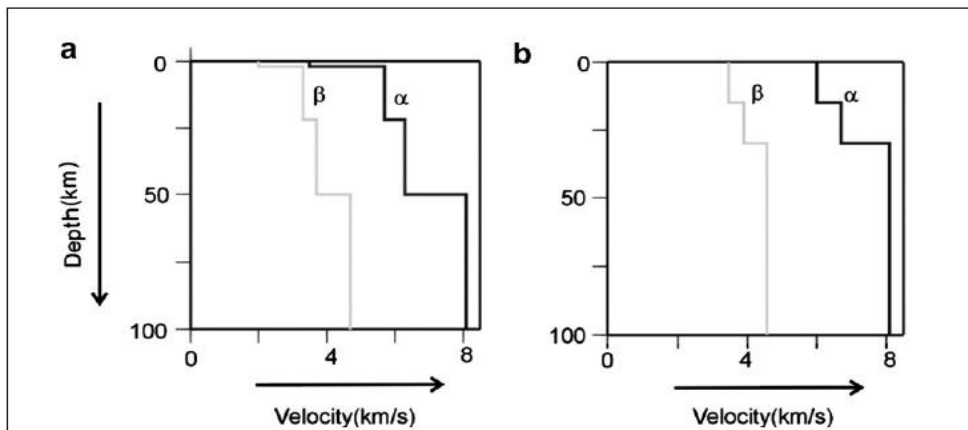
Fig. 3.15: Velocity model for the (a) source region and (b) station site (source: Ghimire and Kasahara, 2003).
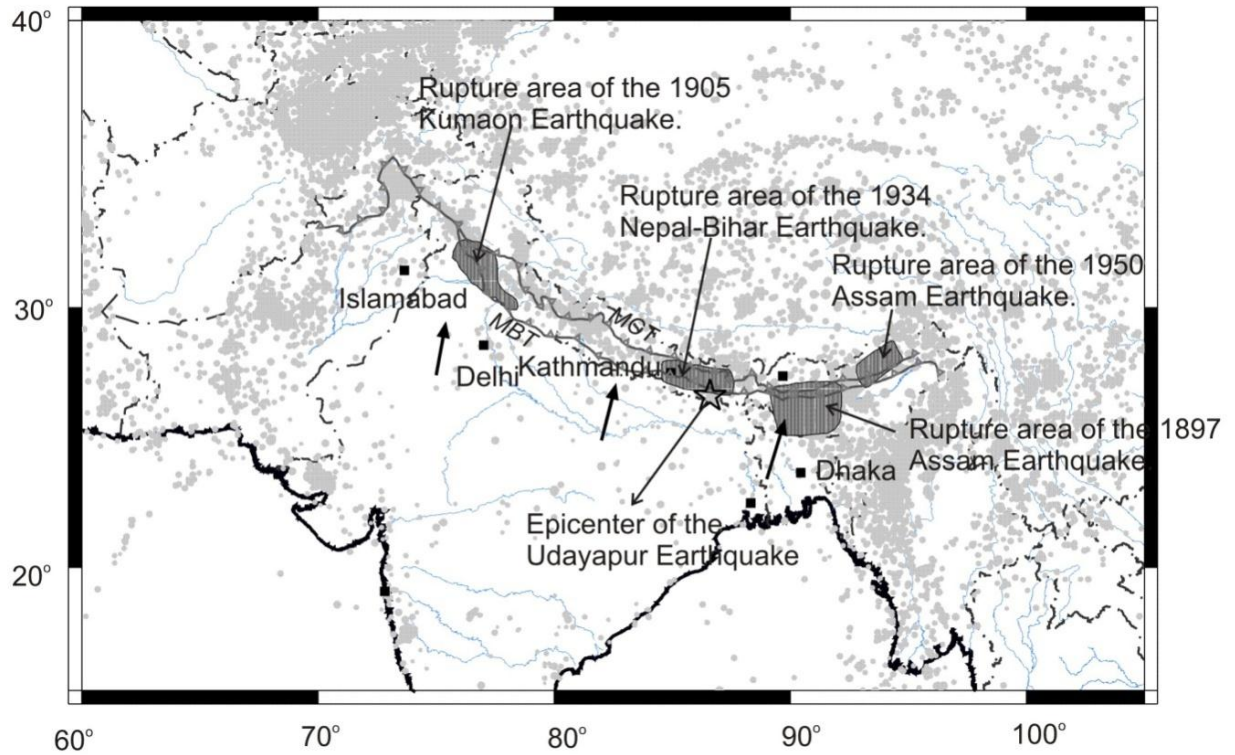
Fig. 3.16: Regional seismicity in and around Himalaya. Rupture areas of the great Himalayan earthquakes are shown as shaded regions. Background seismicity between 1973 and 2012 (from USGS catalog) is shown as grey colored solid circles. The MBT and MCT are plotted as solid lines where the saw-teeth represent the dip direction of these thrust-faults. Major cities in the vicinity of the Himalaya are plotted as solid squares (source: Ghimire and Kasahara, 2003).
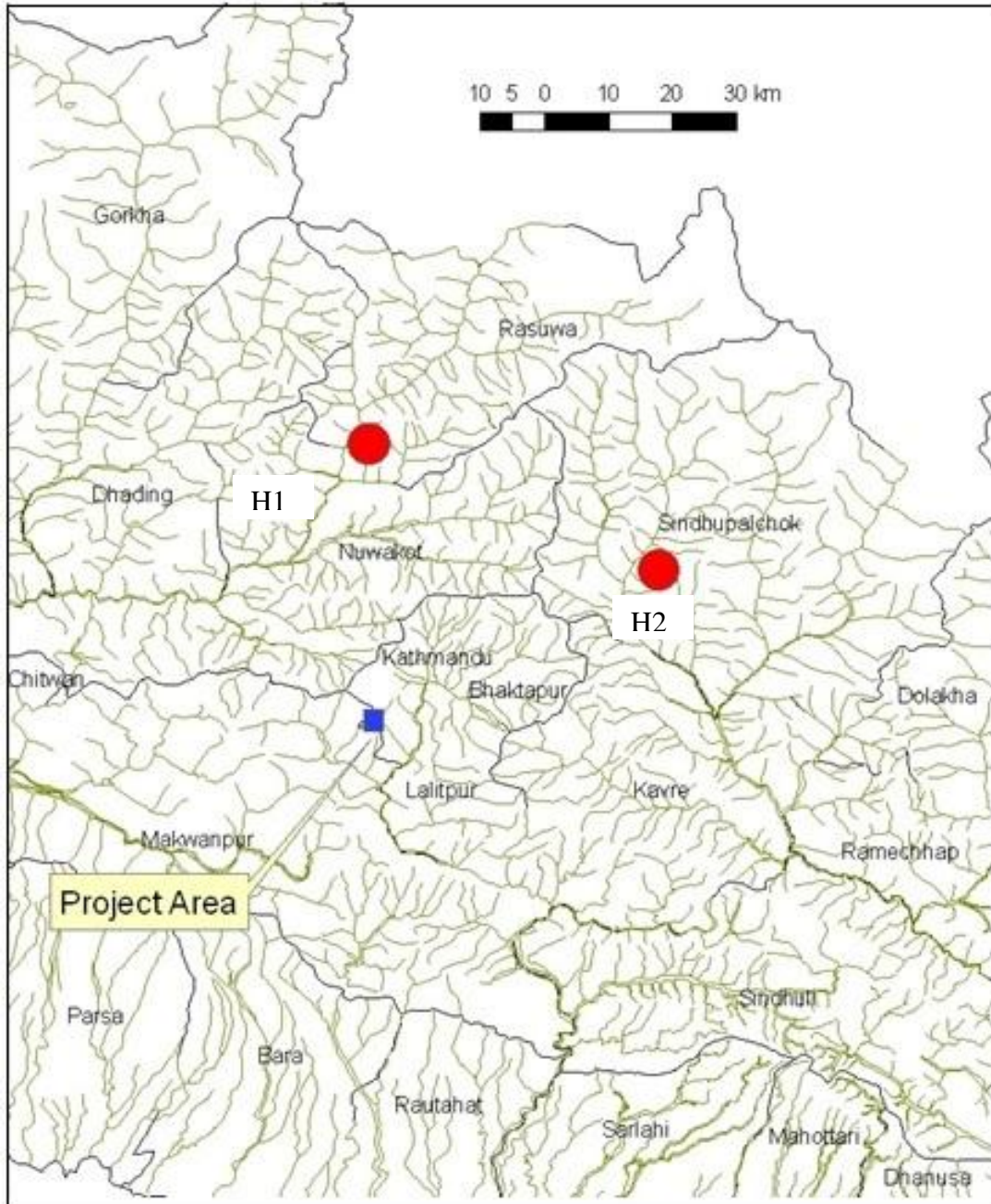
Fig. 3.17: Map showing the locations of hypothetical earthquakes (solid dots labeled as H1 and H2) used to calculate peak horizontal ground acceleration in the study area.

3.5 Correlation as a Statistical Tool

Correlation is a statistical tool which studies the relationship between two variables under study. Two variables are said to be correlated if the change in one variable results in a corresponding change in the other variable. If the values of the two variables deviate in the same direction i.e., if an increase in the values of one variable results, on an average, in a corresponding increase in the values of the other variable or if a decrease in the values of one variable results, on an average, in a corresponding decrease in the values of the other variable, correlation is said to be positive or direct. On the other hand, correlation is said to be negative or inverse if the variables deviate in the opposite direction i.e., if an increase (or decrease) in the values of one variable results, on the average, in a corresponding decrease (or increase) in the values of the other variable. The correlation coefficient (r) lies between -1 and +1. If r is +1 then the correlation is said to be perfect and positive. Similarly, if r is -1 then the correlation is said to be perfect and negative. Correlation coefficient between two variables X and Y, usually denoted by r_{xy} or r is given by;

$$r = \frac{\sum(X - \overline{X})(Y - \overline{Y})}{\sqrt{\sum(X - \overline{X})^2}\sqrt{\sum(Y - \overline{Y})^2}}$$

………………….... (53)

Where, $\overline{X}$ is the mean of X values and $\overline{Y}$ is the mean of Y values.

In this study the correlation coefficient is frequently used in order to study the relation between P-wave velocity and other geotechnical parameters.

RESULTS

4.1 Geotechnical Studies

4.1 In-situ Direct Cone Penetration Test

Direct Cone Penetration Tests was conducted in seven different pits at 2m below the surface. DCP strength was calculated and was used in calculation of California Bearing Ratio (CBR), Unconfined Compressive Strength (UCS) and Bearing Capacity. Three or four DCP tests were conducted in every pit holes. The Table 4.1 shows the average of all three or four tests. Summary of the test, i.e. penetration versus blows plots for seven pits, are shown in Fig. 4.1. For the sample format of test and detailed calculations, refer ANNEX A.

Table 4.1: CBR, UCS, and bearing capacities from DCP test at seven pit locations (for pit locations see Fig. 1.2 in chapter 1).

	Pit numbers						
	1	2	3	4	5	6	8
CBR	32.8	7.5	6.4	20.7	12.2	10.2	7.4
UCS (KPa)	321.3	87.5	76.7	213.1	134.9	114.9	87.0
Bearing ca. (KPa)	261.2	98.6	89.4	189.8	136.6	120.9	97.5

4.2 Soil Profiles

Soil profiles of all seven pits were prepared. The depths of soil logs were limited to 2m depth. (See ANNEX B). Description of soil logs of all seven pits are described below in Table 4.2. Soil profiles of all seven pits show only little variations. The general pattern is top (organic clay) soil layer followed by clayey colluvium. Profile 3 and 8 show boulder in third and second layer respectively, otherwise the soil is gravel rich clay.
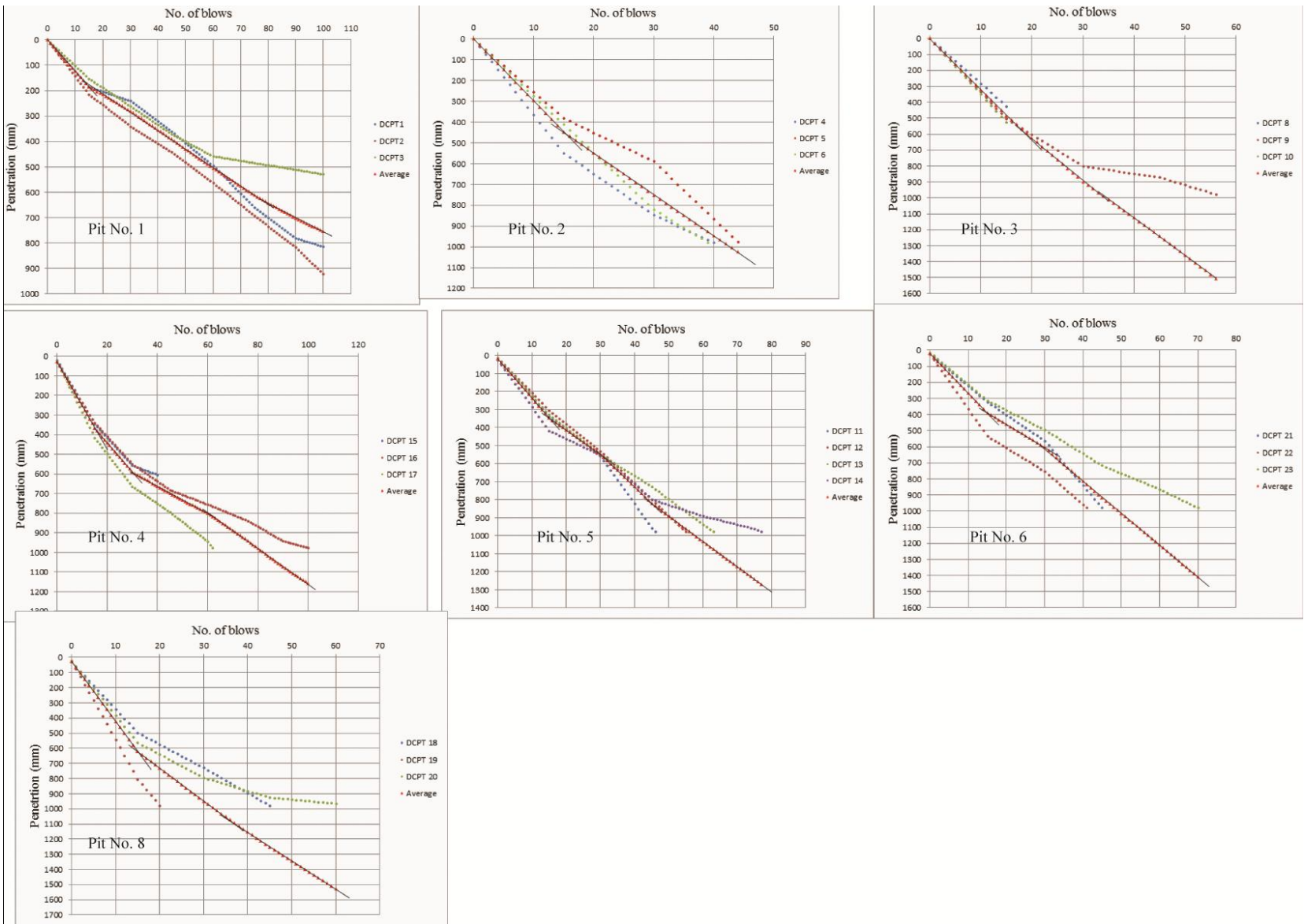
Fig. 4.1: Summary of DCP test (penetration in mm versus no. of blow plot)

Table 4.2: Summary of soil profiles of seven pits (for figures see ANNEX B).

Pit No.	Layer 1	Layer 2	Layer 3	Layer 4	Layer 5
1.	50cm thick, top soil, black to dark, humous (organic clay)	60cm thick, brown, few nodules of pebbles, highly weathered, clay rich soil (colluvium)	90cm thick, brown, angular gravels (>layer2) of fine grain sandstone, clay rich gravelly soil (colluvium)		
2.	60cm thick, top soil, black to dark brown, humous with few pebbles (organic clay)	90cm thick, brown to dark brown, with few pebbles and gravels, highly weathered, clay rich soil (colluvium)	50cm thick brown to dark brown, angular gravels and pebbles with their proportion greater than second layer, clay rich soil (colluvium)		
3.	30cm thick, top soil, black to dark brown, humous with few pebbles (organic clay)	60cm thick, brown, with few gravels, highly weathered, clay rich soil (colluvium)	110cm thick, brown, with a large boulder (2-3m) and gravels(>layer2), clay rich soil (colluvium)		
4.	40cm thick, top soil, black to dark brown, humous soil with gravels (organic clay)	70cm thick, light reddish brown, gravels (<5%), few cobbles, silty clayey soil	90cm, reddish brown, gravels (>10%), silty clayey soil with couple of thin (2-3 cm) gravelly clay layers		
5.	35cm thick, top soil, black to dark brown, humous soil (organic clay)	70cm thick, light brown, angular gravel rich clayey soil	25cm thick, light brown to reddish brown, gravel (~5%), clayey soil	20cm thick light brown, angular ravel rich clayey soil	50cm thick, light brown to reddish brown, gravel (>5%), clayey soil
6.	30cm thick, top soil, black to dark brown in color with few (<8%) gravels (organic clay)	170cm thick, reddish brown to light brown, few (~10%) gravelly silty clay			
8.	20 cm thick, black, top soil with gravels (organic clay)	180cm thick, very light brown, to yellowish brown, cobble and boulder rich gravelly clayey soil (colluvium)			

4.3 Laboratory Test

To study geotechnical parameters, laboratory studies included classification of sampled soils, moisture content determination Atterberg limit test, specific gravity test and direct shear test.

Table 4.3: Laboratory test of geotechnical parameters of samples.

Pit No.	Soil classification	Moisture content (%)	Atterber limits			Specific gravity	Direct shear test	
			LL	PL	PI		(c) Kpa	φ (degree)
1.	Reddish brown clayey silt with gravel and sand	18.2	38.30	33.38	4.92	2.5	4	24
2.	Brownish grey sandy silt with clay and traces of gravel	24.7	33.50	25.48	8.02	2.574	12	17
3.	Brownish red sandy silt with clay and traces of gravel	27.4	16.70	NP	NP	2.577	6	19
4.	Brownish grey sandy silt with clay and traces of gravel	23.7	32.80	26.99	5.81	2.439	6	17
5.	Brownish grey sandy clayey silt with traces of gravel	25.4	28.30	24.61	3.69	2.522	16	16
6.	Brownish grey clayey sandy silt with traces of gravel	19.5	25.00	22.12	2.88	2.485	11	21
8.	Brownish grey sandy silt with clay and traces of gravel	32.8	35.50	27.43	8.07	2.621	13	16

Sieve analysis and hydrometer test were performed for the soil classification. Distribution of particle sizes larger than 75 μm (retained in No. 200 sieve) was determined by sieving, while the distribution of particles smaller than 75 μm was determined by a sedimentation process, using a hydrometer. Cumulative curves were prepared for all seven pit holes and the soil was classified (Table 4.3). Moisture contents of samples taken from all seven test pits were

determined by ASTM D22169-98 procedure. Results are shown in Table 4.3. To characterize the fine-grained fractions of soil Atterberg limit tests were conducted. This included the liquid limit test, plastic limit test and plasticity index calculation (Table 4.3) according to the standard procedure of ASTM D4318-10. Similarly, specific gravity of samples was also determined and are presented in Table 4.3. Shear strength parameters were calculated by direct shear test. This included the determination of cohesion (c) and angle of internal friction (ϕ). Results are presented in Table 4.3.

For the sample format of detailed calculations made for and after individual laboratory test of samples, refer ANNEX C.

4.4 Description of Results from Geotechnical Studies

Pit no. 1 lay on colluvial terrain (washed out soil) consisting of rock fragments of limestone, slates and quartzites. The soil is reddish brown clayey silt with gravel and sand with gravel 18%, sand 17%, silt 38% and clay 27%. DCP result shows the bearing capacity at 2m depth of 261.2 KN/m^2. Plasticity index, moisture content, cohesion and friction angles are 4.92, 18.2%, 4KPa and 24° respectively. Thickness of soil at this pit hole is estimated to be 10m from seismic refraction survey (Fig. 4.2).

Pit no. 2 also consist colluvium (washed out deposit) with fragments of limestone, slates and quartzites. The thickness of colluvium deposit is approximated between 12.5 m to 15 m (Fig. 4.2). The soil is poorly graded with gravel 2.8%, sand 24%, silt 47.9% and clay 25%. The bearing capacity from DCP test is 98.6 KN/m^2. Similarly, plasticity index, moisture content, cohesion and friction angles are 8.02, 24.7%, 12 KPa and 17° respectively.

Colluvium deposits of pit no. 3 consist of fragments of metasandstone and phyllitic slates, and the thickness ranges from 7.5 m to 10 m (Fig. 4.2). The boulders of 2-3 m diameter are found (as indicated in soil profile Table 4.2). The soil is well graded with gravel 8.9%, sand 25.6%, silt 46.5% and clay 19%. Bearing capacity, moisture content, cohesion and friction angles are 89.4 KN/m^2, 27.4%, 6 KPa and 19°respectively. Meanwhile, the soil is found to be non plastic (Table 4.3).

Colluvium with fragments of limestone, quartzite and slates are dominant in pit no. 4 and the thickness of the colluvium ranges from 10 m to 12.5 m (Fig. 4.2). The soil is brownish grey sandy silt with clay and traces of gravels. Similarly, soil is humus and poorly graded with gravel 2.6%, sand 16.2%, silt 66.2% and clay 15%. Bearing capacity, moisture content, plasticity index, cohesion and friction angles are 189.8 KN/m^2, 23.7%, 5.81, 6 KPa, 17° respectively.

Similarly, the pit no. 5 consists of colluvium with limestone, slate and quartzite fragments. The thickness is about 10 m (Fig. 4.2) and consists of mixture of gravel and brown grey sandy clayey silt. This clayey soil is poorly graded with gravel 1.9%, sand 22.1%, silt 55.0% and clay 21%. The bearing capacity, moisture content, cohesion and friction angles are 136.6 KN/m^2, 25.4 %, 16 KPa and 16° respectively.

The coluvium of pit no. 6 consist of brownish grey clayey sandy silt with traces of gravels in which gravels are of slate, limestone and quartzites. Seismic refraction survey concluded the soil depth to be of 10 to 12.5 m. Soil is well graded with gravel 7.1%, sand 11.7%, silt 65.2% and clay 16%. The bearing capacity at 2 m depth is 120.9 KN/m^2. Similarly, water content, cohesion, friction angle are 19.5%, 11 KPa and 21° respectively.

Pit no. 8 is made up of brownish grey sandy silt with clay and traces of gravels and the thickness ranges from 7.5 m to 10m (Fig. 4.2). Similarly, the soil consist boulders of 1-2 m diameter. The soil is poorly graded with gravel 1.5%, sand 9.8%, silt 58.7% and clay 30%. The bearing capacity obtained from DCP is 97.5 KN/m^2. Similarly, moisture content, cohesion and friction angles are 32.8%, 13 KPa, 16° respectively.

4.5 Seismic Refraction Survey

During this study, seismic refraction was carried out along 17 profiles and the geophone spacing was 5m. Signals were generated at the two ends of the profile. Time spent by seismic signals to reach each geophone was manually picked from the seismogram and was plotted to obtain the travel time curve. Thus, obtained curve was used to estimate the velocities of different layers in the subsurface, depth to the interfaces and the geometry of the interfaces (Table 4.4). Refer ANNEX D for sample format of travel time curves preparation and raw data obtained in this study.

In this study the seismic velocity of soil ranges between 200 and 1300 m/s. The P-wave velocity of rocks is dependent on porosity, water content and compactness and degree of weathering of the rock. Generally sedimentary rocks like shale, mudstone etc. have low seismic velocity comparable with the compact soils. The seismic velocity of rocks like limestone, dolomite is very high up to 6 km/s. Metamorphic rocks like quartzite, gneiss have very high seismic velocity. In this study, the velocity of the rocks is generally more than 2000 m/s. The layers with different velocities are correlated with the lithology based on surface observations and geological observations. Based on the results from the seismic refraction along all profiles a map of soil depth is compiled and is presented in Fig. 4.2.

The location of seismic refraction profiles are provided in Table 4.4 with location of first geophone and last geophone. Different velocity layers and apparent dip angles of interfaces unveiled by seismic refraction survey are presented also in Table 4.4. Velocities of topmost and second layers are also provided together with up-dip and down-dip depth to the refracting interface.

All seismic profiles are of 115m in length with geophone spacing of 5m. The topmost layer unveiled by all seismic profiles are interpreted as loose soil due to low velocity except for profile Sr4 (Table 4.4) where the velocity is comparatively high and surface geological observations favors it as compact soil. Second layers in all profiles have velocity comparable to weathered rock. However, in profiles Sr1, Sr3, Sr12 and Sr15 the second layers are interpreted as highly compact soils or weathered rock. Furthermore, profile Sr2 shows no refracted pulse and direct wave velocity unveils the top layer is loose soil of thickness >25m. (refer ANNEX D for travel time curve of Sr2).

Table 4.4: Location of the seismic profiles and the results (Note: Sr2 showed no refracted pulse).

Profiles	UTM Location of the profile (end points)				Velocity of the topmost layer (m/s)	Velocity of the second layer (m/s)	Inclination of the interface (º)	Up-dip depth to the interface (m)	Down-dip depth to the interface (m)
	Geophone 1		Geophone 24						
	Easting	Northing	Easting	Northing					
Sr1	619997	3063748	620046	3063652	467.73	1125.59	1.79	3.6528	3.0611
Sr2	620036	3063775	620085	3063675	391.67	-	-	-	-
Sr3	620098	3063777	620029	3063700	657.02	995.70	3.51	6.2199	5.9132
Sr4	619982	3063606	620029	3063700	726.85	1223.14	2.42	9.9951	8.0503
Sr5	619982	3063606	619954	3063506	590.75	996.32	7.79	11.6250	11.1067
Sr6	619903	3063551	620000	3063506	484.11	1605.00	2.96	16.3206	10.4228
Sr7	619971	3063657	620040	3063575	669.06	1387.22	4.12	11.8689	10.3375
Sr8	619177	3061564	619130	3061468	439.24	1114.86	1.90	14.5837	14.3447
Sr9	619100	3061526	619201	3061491	246.83	1003.49	3.12	6.5988	3.6724
Sr10	619301	3061350	619196	3061328	345.39	1353.97	2.07	7.9709	6.5233
Sr11	619196	3061328	619111	3061260	522.89	1503.31	4.70	11.3597	7.7224
Sr12	619616	3061264	619538	3061338	366.14	884.50	5.20	5.0485	7.3
Sr13	619616	3061264	619674	3061172	386.02	1256.00	2.22	10.1084	5.8458
Sr14	619674	3061172	619727	3061079	325.89	1468.21	1.98	13.5942	6.6884
Sr15	619619	3061358	619579	3061259	248.29	575.11	2.26	8.0500	3.8000
Sr16	619959	3063491	619912	3063394	372.76	1788.72	4.65	8.8905	6.2712
SR17	619894	3063473	619986	3063428	375.24	860.26	9.44	5.3686	12.0000
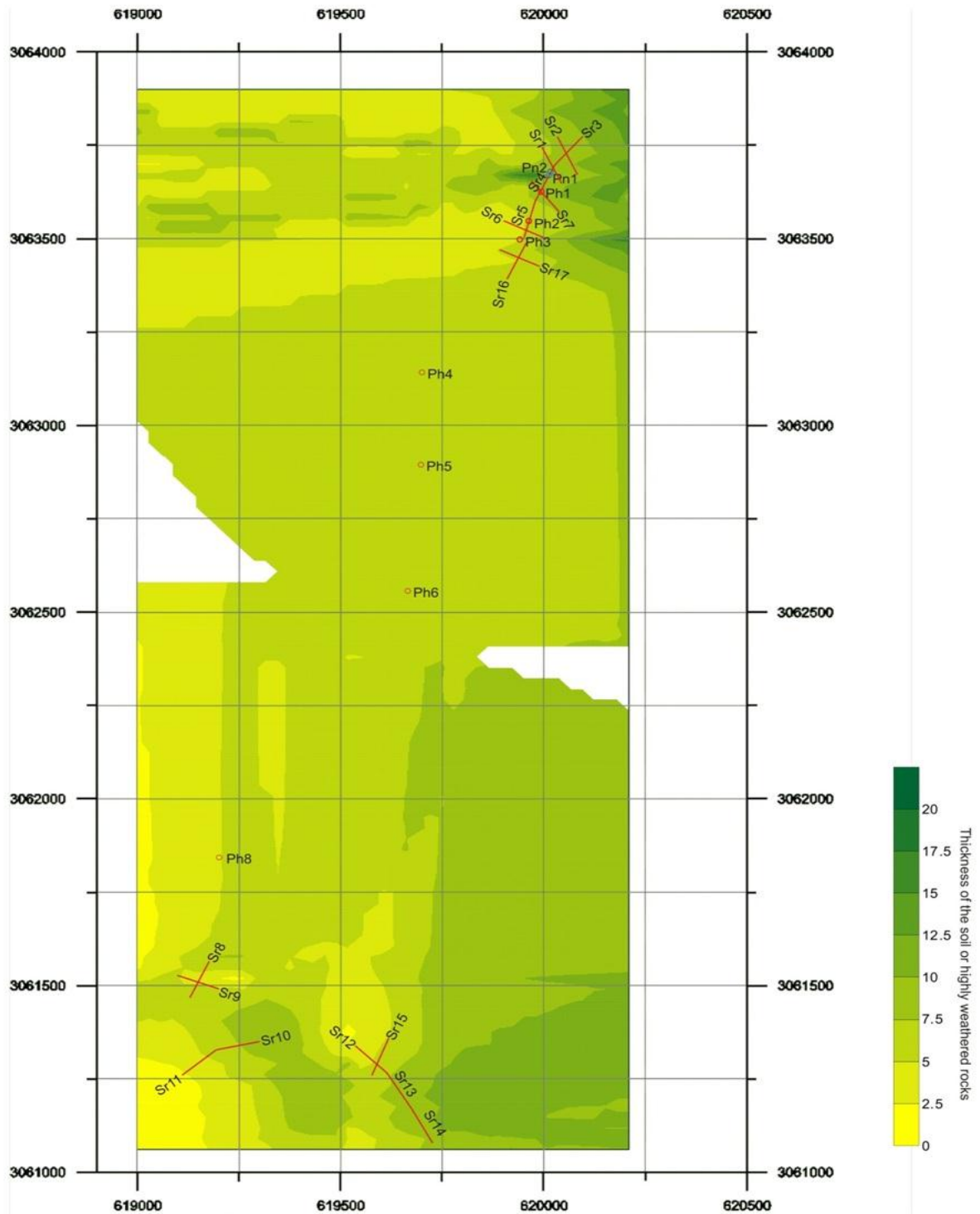
Fig. 4.2: Soil (or highly weathered rocks) depth map prepared from the results of seismic refraction survey. The lithology with P-wave velocity ≤ 1000 m/s has been categorized as soil or highly weathered rocks. The red open circles labeled as Ph1, Ph2 etc. represent the pit holes dug for geotechnical investigation. The solid red lines labeled as Sr1, Sr2 etc. represent the seismic profile lines along which seismic refraction survey was carried out.

4.6 Peak Ground Acceleration (PGA) Calculation

Based on the finite fault source and synthetic horizontal peak ground acceleration for different scenario earthquakes has been deployed to access the PGA map of the study area. The soil depth map (Fig. 4.2) is one of the most important parameter to estimate PGA. From seismic refraction survey the layers with P-wave velocity less than 1000 m/s are interpreted as soil. The parameters used to simulate earthquakes are presented in Table 3.3. The project area was divided into a mesh of size 10mx10m and the maximum horizontal acceleration at each square grid was searched. The peak ground acceleration is then contoured to prepare the PGA map. PGA map due to 1943 Taplejung earthquake, 1988 Udayapur earthquake and two hypothetical earthquakes are presented in Fig. 4.3, 4.4, 4.5 and 4.6 respectively. The length and width of the fault of the Taplejung earthquake are 150 km and 75 km and those of Udayapur earthquake are 39 km and 21 km (Ghimire and Kasahara, 2007). A synthetic accelerogram obtained by simulating 1934 Taplejung earthquake in this study is shown in Annex E (as a sample).

The maximum PGA of more than 150 gal (cm/s^2) due to the Taplejung earthquake is observed in the northeastern corner of the project area. To the south and southwestern part PGA progressively decreases below 40 gal.

The maximum PGA of more than 1.0 gal due to the Udayapur earthquake is observed in the northeastern corner of the project area. To the south and southwestern part PGA progressively decreases below 0.25 gal.

The maximum PGA due to two hypothetical earthquakes exceeds 10 gal in the northeastern corner of the project area. However, the pattern of PGA distribution is different for these two earthquakes. For H1, which is located in the northwest direction of project area, Ph1 to Ph3 are characterized by PGA more than 9.0 gal. In the case of H2, the PGA is different for these pit holes.
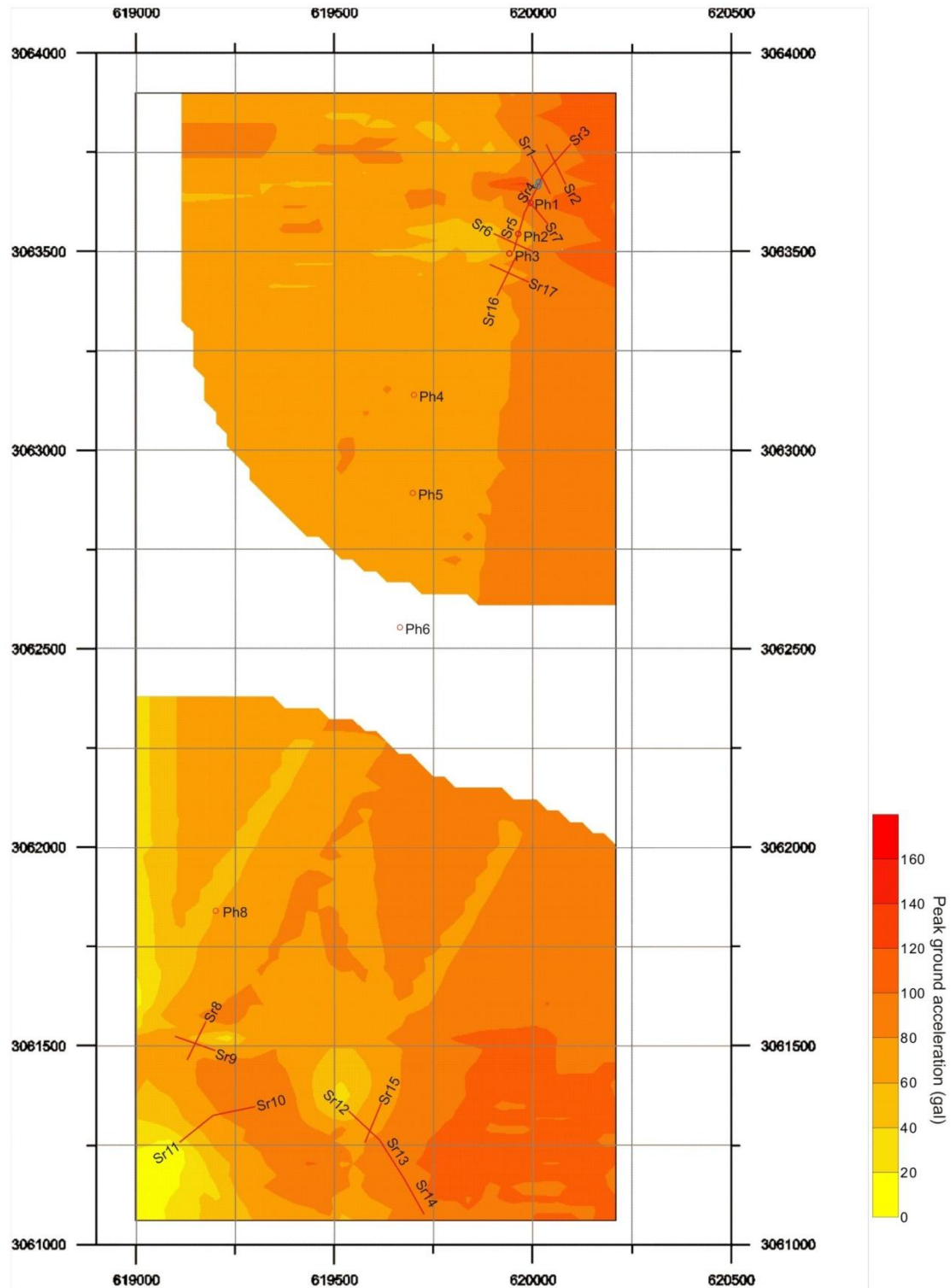
Fig. 4.3: Map showing the distribution of peak ground acceleration in the study area due to the 1934 Taplejung Earthquake (Mw=8.4). Open red circles labeled Ph1, Ph2 etc. represent the pit holes dug for geotechnical investigation. Solid red lines labeled Sr1, Sr2 etc. represent seismic profile lines.
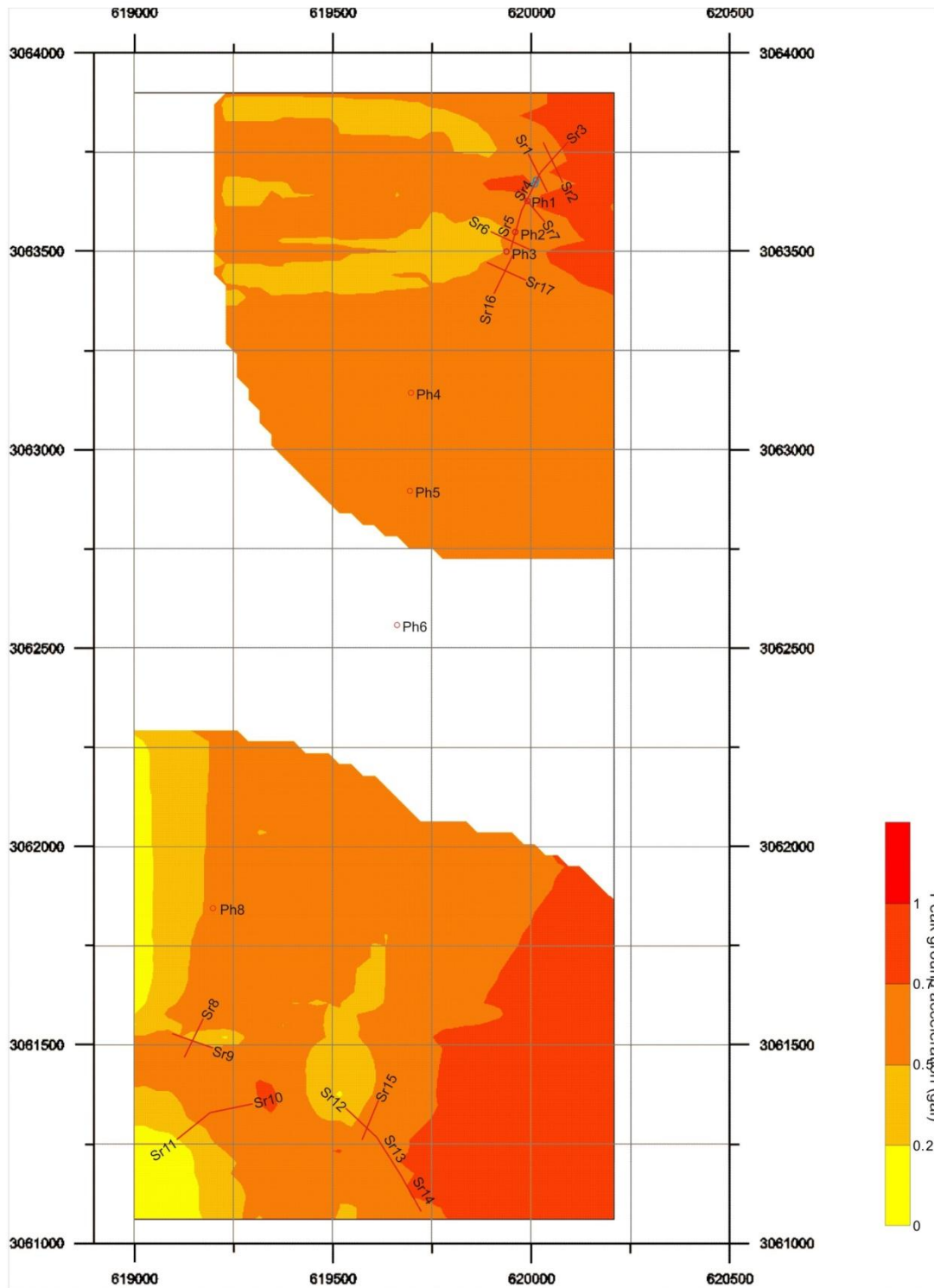
Fig. 4.4: Map showing the distribution of peak ground acceleration in the study area due to the 1988 Udayapur Earthquake (Mw=6.7). Open red circles labeled Ph1, Ph2 etc. represent the pit holes dug for geotechnical investigation. Solid red lines labeled Sr1, Sr2 etc. represent seismic profile lines.
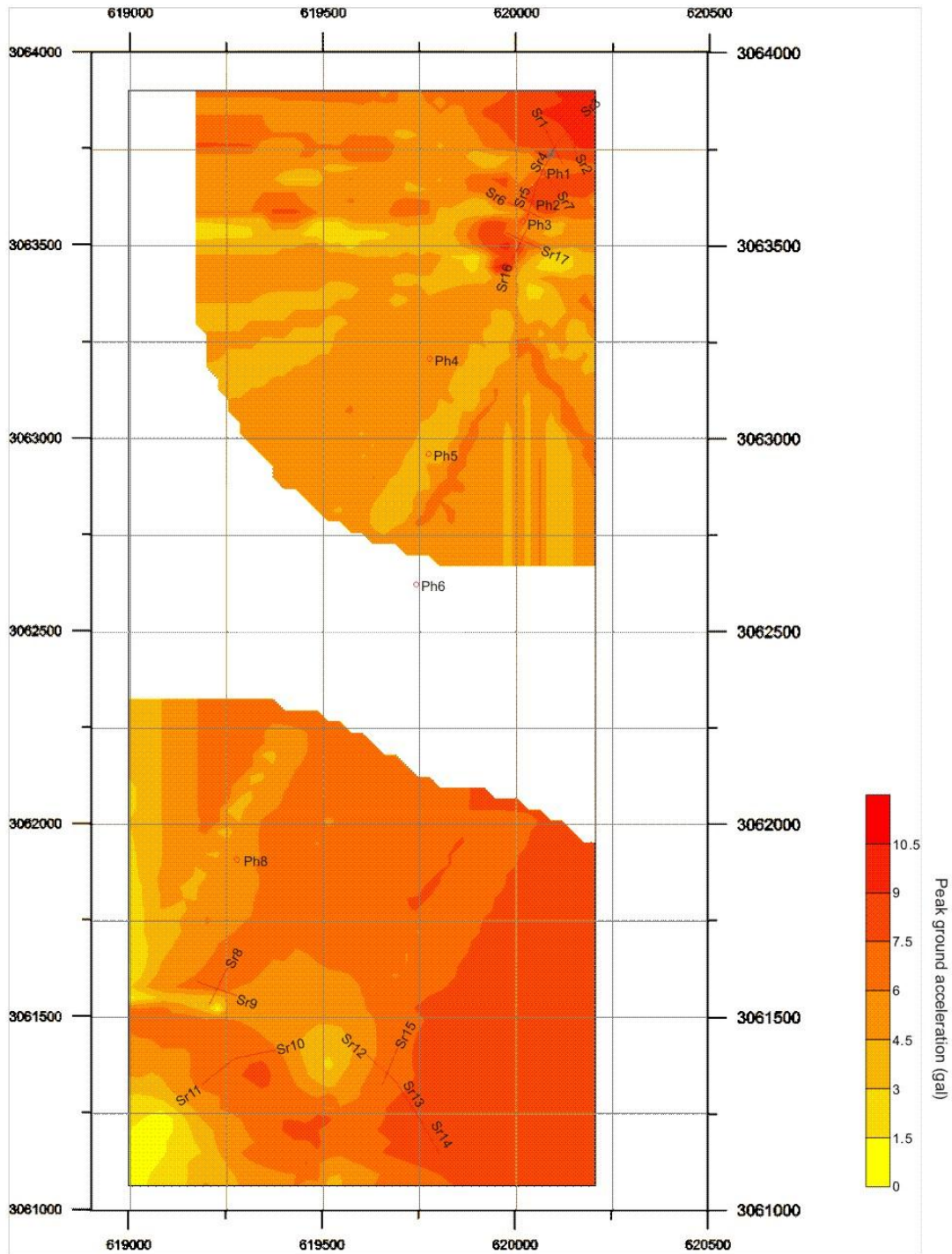
Fig. 4.5:Map showing the distribution of peak ground acceleration in the study area due to the Hypothetical Earthquake H1 (Mw=6.0), at 50 km northwest of the project area. Open red circles labeled Ph1, Ph2 etc. represent the pit holes dug for geotechnical investigation. Solid red lines labeled Sr1, Sr2 etc. represent seismic profile lines.
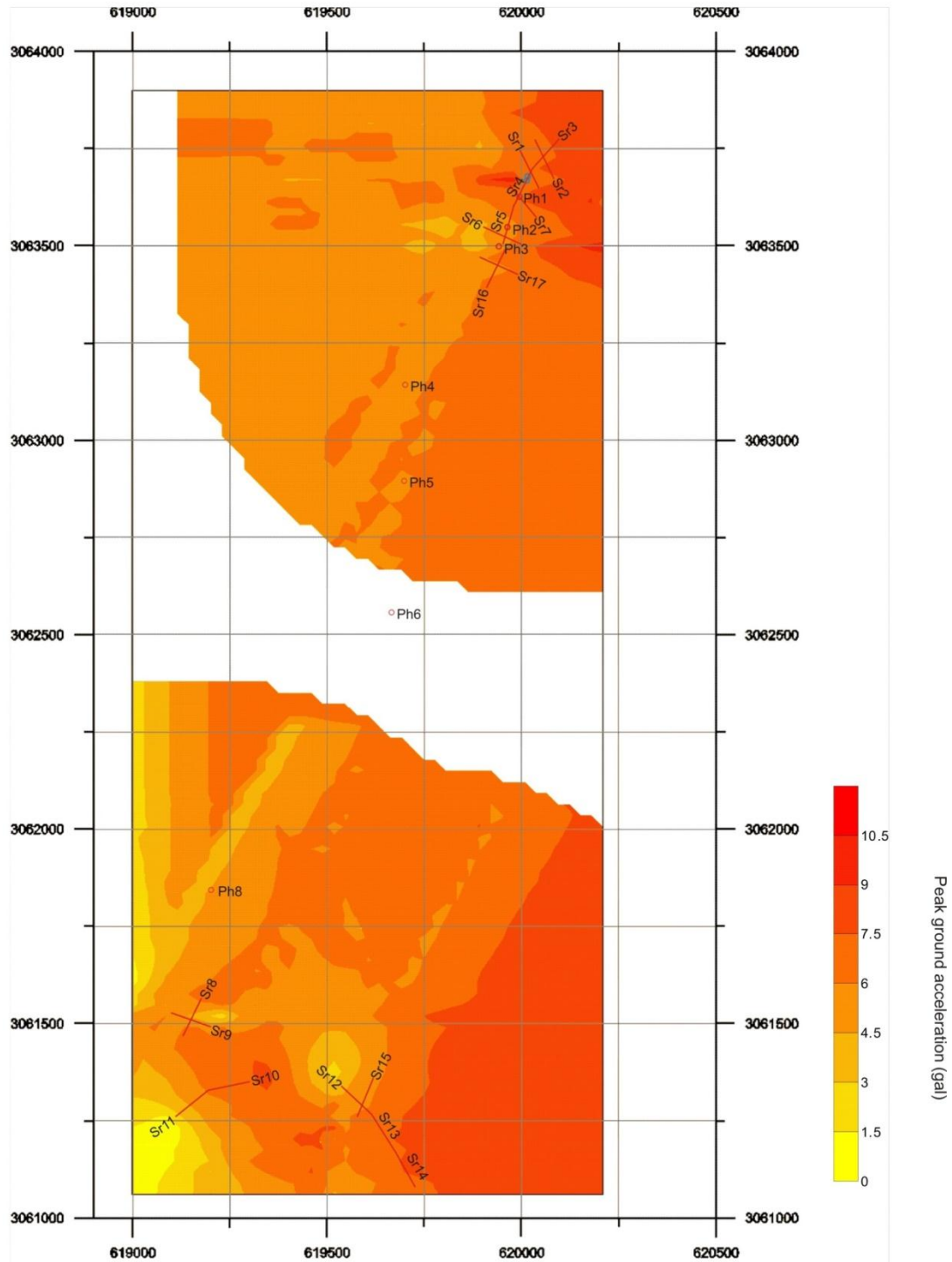
Fig. 4.6: Map showing the distribution of peak ground acceleration in the study area due to the Hypothetical Earthquake H2 (Mw=6.0), at 50 km northeast of the project area. Open red circles labeled Ph1, Ph2 etc. represent the pit holes dug for geotechnical investigation. Solid red lines labeled Sr1, Sr2 etc. represent seismic profile lines.

CHAPTER V

DISCUSSION

The soil profiles and the soil classification show the washout colluvium of the study area comprises of clay rich soil. Moreover, the percentage of coarser particles (particularly gravel) shows an increasing trend with the depth. This signifies that the study area is under continuous weathering and the high degree of weathering is confined to near surface conditions only, with no other significant disturbances. Relatively high amount of clay results in low stiffness of the soil which is reflected in the bearing capacities of the soil. Similarly, the high clay content in the colluvium also shows the effect on unconfined compressive strength, cohesion (c) and friction angle. With such low bearing capacity, cohesion and friction angle the bearing capacity factors are also small (Terzaghi, 1943). Which ultimately describes the soil in the study area cannot tolerate high pressures. High amount of fine content cannot easily drain the moisture content. The colluvial soil of the study area shows variation in moisture content and the excess pore pressure is not likely to be dissipated from the soil. This high amount of moisture and fine contents may have reduced the bearing capacity of the soil in the study area. Such low values of bearing capacities will finally affect the stability of soil in terms of bearing failure. In the case of foundation on non-homogeneous deposit Lee (1983) suggests that the strength of the saturated clay increases with depth. But unavailability of instrument for sampling at greater depth has posed problem to find the suitable depth of reasonable bearing values in the study area. In order to estimate geotechnical parameters, at some depth where sampling is difficult, this research work tempted to establish some correlation with P-wave velocities.

Kurtulus, et al. (2009), suggested that there exists a good correlation between P-wave velocity and plastic limit and liquid limit in clay rich soils (Fig. 5.1). However, in the study area Atterberg limits of the clay rich colluvium soil fluctuates from one pit to another (Fig. 5.2). Fewer amounts of observed data are noteworthy and that may have affected the further correlation. Nevertheless, a reasonably good correlation between P-wave velocity and other geotechnical parameters was found which will be discussed successively.
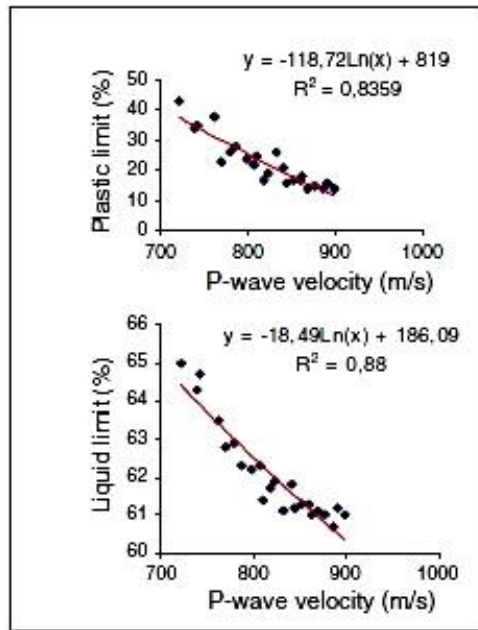
Fig. 5.1: Correlation of P-wave velocity with plastic limit and limit (source: Kurtulus, et al., 2009).
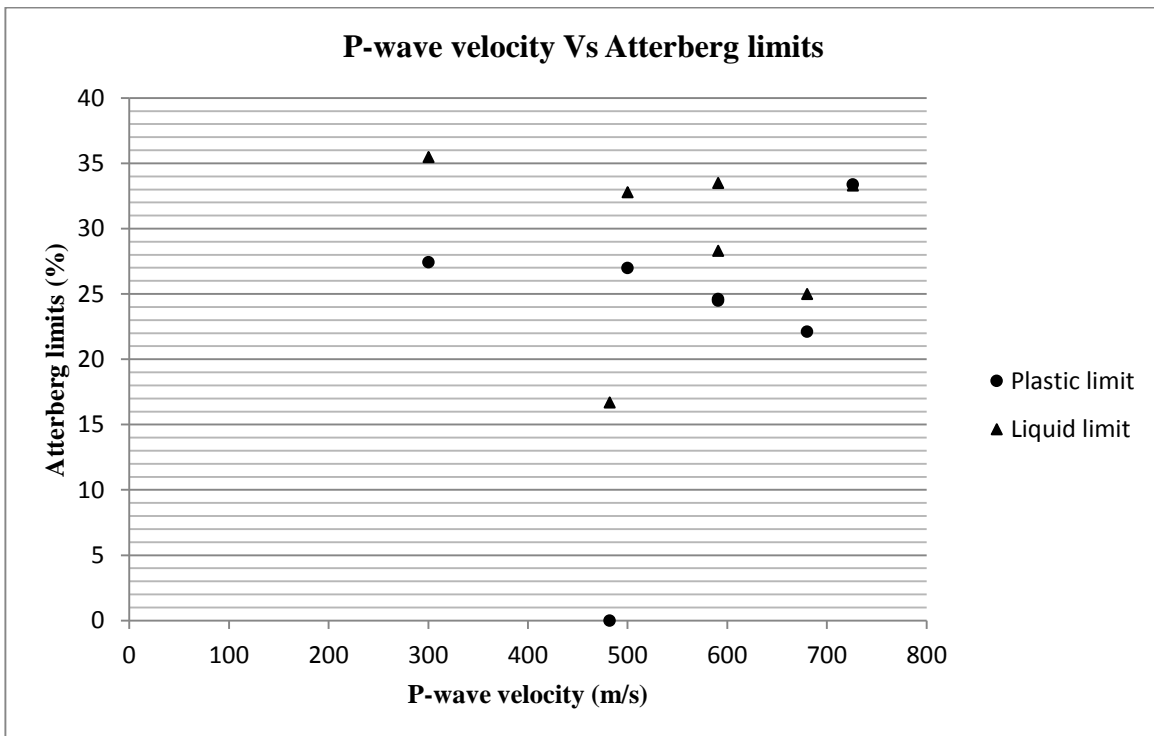
Fig. 5.2: Relation between P-wave velocity and Atterberg limits in the study area.

The seismic velocity of a particular material depends on its elastic properties like rigidity, Young's modulus, porosity, moisture content and degree of weathering of rocks. The velocity increases as the soil becomes more compact and dry. Hence, there exists a significant correlation between friction angle and P-wave velocity. In this study correlation between P-wave velocity and geotechnical parameters were studied. If there would have been large amount of data then the statistical correlation will be much more precise, hence, the little disperses of data can be attributed to this limitations. Similarly, sample tested in laboratory is disturbed one that may have affected the test results. Fig. 5.3 shows the correlation between moisture content and P-wave velocity. The correlation co-efficient is -0.94 which shows data are highly correlated and as the moisture content decreases the P-wave velocity increases. This signifies that increasing moisture content (and increasing pore water pressure) in the study area, softens the elastic mineral frame by opening cracks and flaws, trending to low velocity. Decrease in velocity with increasing clay content is also noteworthy; this is the result of low stiffness of water-clay aggregates or sediments.
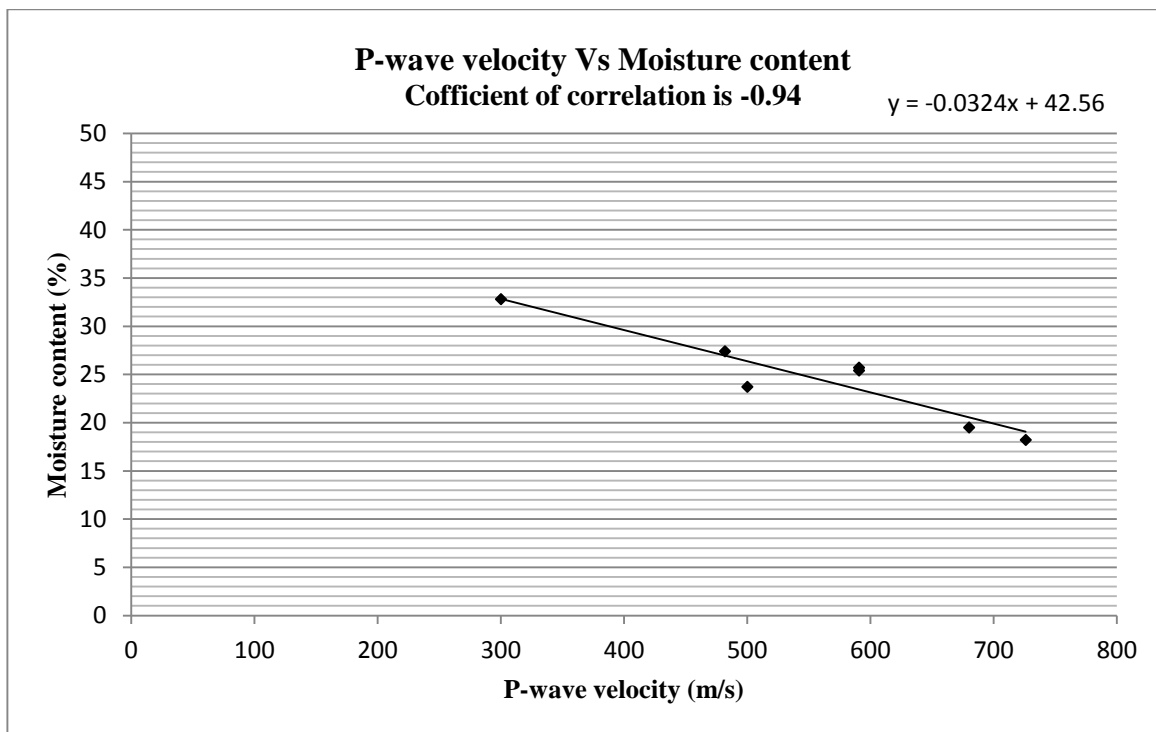
Fig. 5.3: Correlation between P-wave velocity and moisture content.

Similarly, unconfined compressive strength (UCS) obtained from in-situ direct cone penetration test was correlated with P-wave velocity (Fig. 5.4). There has been much work done in correlating UCS with P-wave velocity for different works (Bery and Saad, 2012 and Sheraz, et al., 2014). However, in soil it is still not well constrained. This study showed that the correlation coefficient (0.74) such that there exist a significantly good correlation between UCS and P-wave velocity. As the strength of colluvium increases the P-wave velocity also increases.
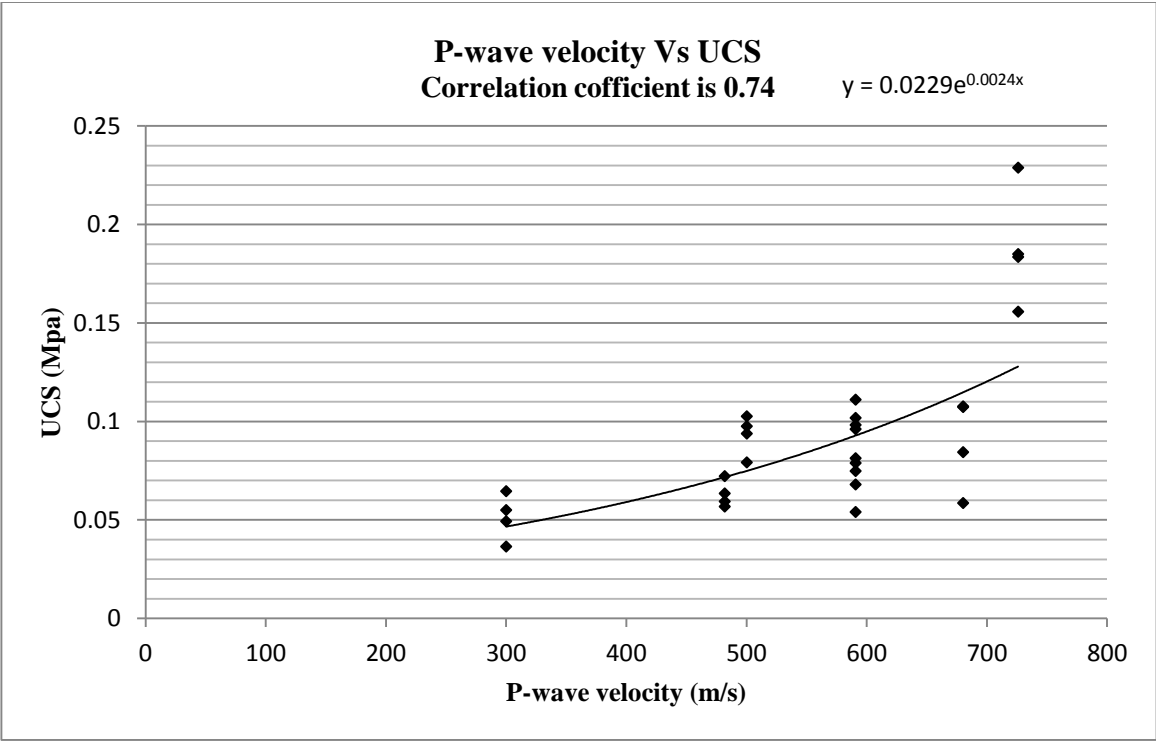
Fig. 5.4: Correlation between P-wave velocity and UCS.

Likewise, there have been relatively few attempts to find relationship between friction angle (ϕ) and geophysical log measurement because of the fact that even weak rocks have relatively high ϕ, and there are complex relationships (Chang et al., 2006). Nonetheless, some experimental evidences shows that materials with higher Young's modulus generally tend to possess a higher ϕ (Chang et al., 2006). Fig. 5.5 shows the correlation between P-wave

velocity and friction angle in the study area with correlation coefficient 0.70, which shows the data are reasonably fairly correlated. As the friction angle increases the P-wave velocity also increases.

To relate porosity with P-wave velocity, equation 14 is modeled for different material velocity (V_m) keeping fluid velocity (V_f) fixed to 1450 m/s. All together five models are prepared with values of V_m = 1545, 1550, 1560, 1570 and 1575 m/s. Porosity is calculated for different P-wave velocities ranging between 300 and 1400 m/s. An exponential relation is observed for the synthetic data (Fig. 5.6). All these lines converge for high P-wave velocity indicating porosity does not change significantly after a particular P-wave velocity (~1400 m/s). However, the observations were few the data fits significantly well with the modeled with V_m 1560 m/s. In this study the soil is assumed to be fully saturated however, field observations and laboratory data indicates soil is not saturated. The misfit between observed data and the model can be attributed to this limitation.

Fig. 5.5: Correlation between P-wave velocity and Friction angle.

P-wave Velocity Vs Porosity

$y = 132.58e^{-0.003x}$
$R^2 = 0.9917$
at V_m 1560 m/s
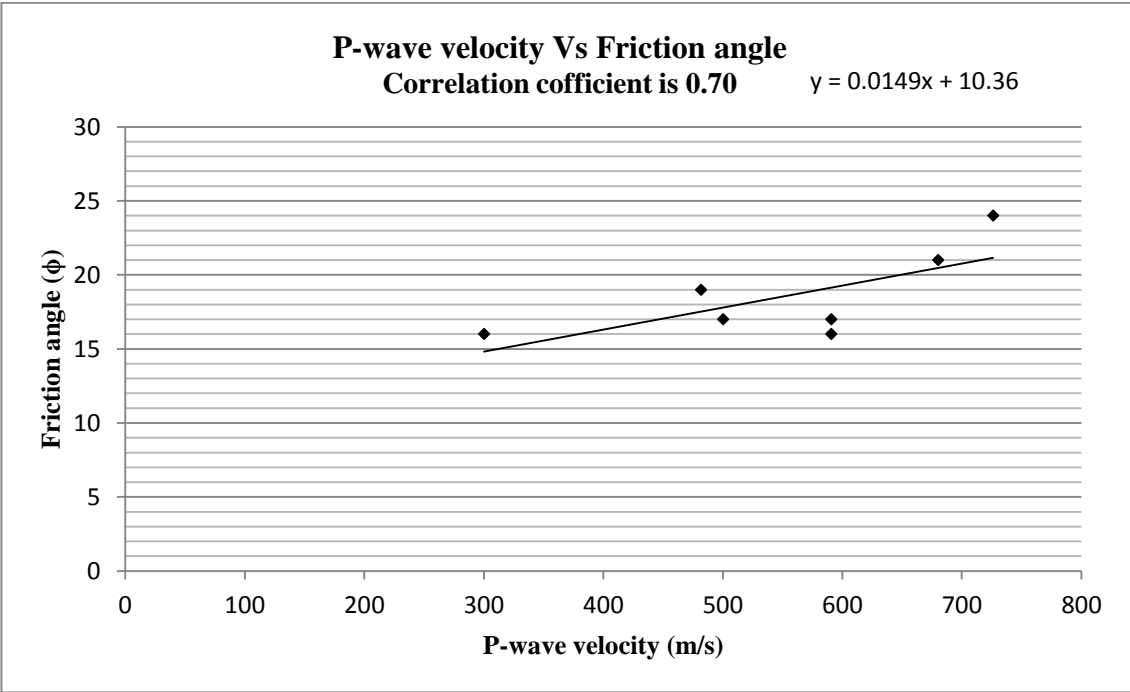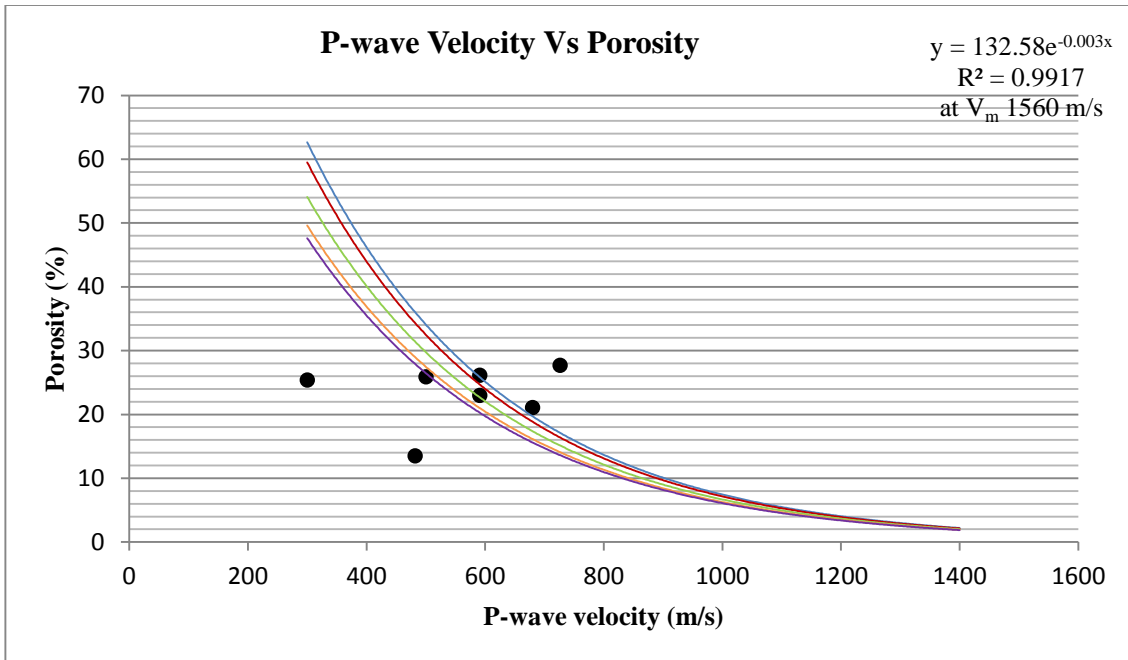
Fig. 5.6: Relation between P-wave velocity and porosity. Solid lines blue, red, green, orange and purple are modeled curves for material velocity (V_m) 1545, 1550, 1560, 1570 and 1575 m/s respectively. Solid circular dots represent observed data.

There exist significant correlation between velocity and porosity for unconsolidated sediments (Schon, 1983). But much of the works are confined to continental terrace/shelf and slope and permafrost areas. Hamilton et al. (1982) derived the second order polynomial in order to relate the P-wave velocity with porosity for continental terrace/shelf and slope sediments. This study shows an exponential relation is the best correlation between P-wave velocity and porosity. This variation may be attributed to the difference in soil type from different landform.

This research work tempted to attempt the level of peak ground acceleration (PGA) in the study area taking 1934 Taplejung earthquake, 1988 Udayapur earthquake, and two hypothetical earthquakes. The former two were used because these are the major earthquakes that caused huge damage wrecking havoc in Nepal (Bhattarai et al, 2011). The PGA distributions due to scenario earthquakes show that the PGA reaches maximum at northeastern corner of the study area whereas to the south and southwestern part PGA progressively decreases. This difference in PGA distribution can be attributed to varying soil depth of the

study area where northeastern corner consist greater soil thickness as compared to south and southwestern part. As compared to the earlier work in regional scale by Bhattarai et al. (2011) the computed values of PGA in this study are lower. This difference may be attributed to number of sources considered for computation and scale of the study.

The difference in spatial distribution of PGA in the study area due to the earthquakes of same magnitude, epicentral distance, and depth (two hypothetical earthquakes) is attributed to the directivity of seismic waves and damping effect of the sediments in the Kathmandu basin. Since, the seismic waves propagate towards southwest from H2 and encounter overwhelming sediment deposit, the real input motion at the project site must have significantly changed with respect to the waves from H1 (Fig. 3.17). On the other hand, seismic energy from H1 travels southeast and reaches the project site before penetrating the valley sediments. Peak Ground Acceleration (PGA) due to scenario earthquakes suggests that for mega quakes the area is prone to high seismic hazard. The PGA in case of M>8.0 earthquake may exceed 150 gal (~0.15 g) in the area with an epicentral distance more than 100 km. For small but strong events the PGA hardly reach 15 gal (0.015 g). The simulation of PGA shows that the seismic hazard in the area is high for the earthquakes located to the northeast relative to that in northwest.

Ground response is estimated using linear approach with a single layer of soil assuming the maximum thickness (including top soil and highly weathered rocks) of 60 m and 30 m in the northern and southern part respectively in the project area. Based on the velocity structure obtained from seismic refraction survey, an average S-wave velocity of 650 m/s is considered while computing the ground response. The results (Fig. 5.7) show the maximum amplifications of 13 and 12 with 5% damping in the northern and southern part respectively. The amplification factor decreases with the higher value of damping factor. The fundamental frequencies associated with the maximum amplification factor in the northern and southern part of the profile are 9.7 and 4.8 Hz respectively (Fig. 5.7).
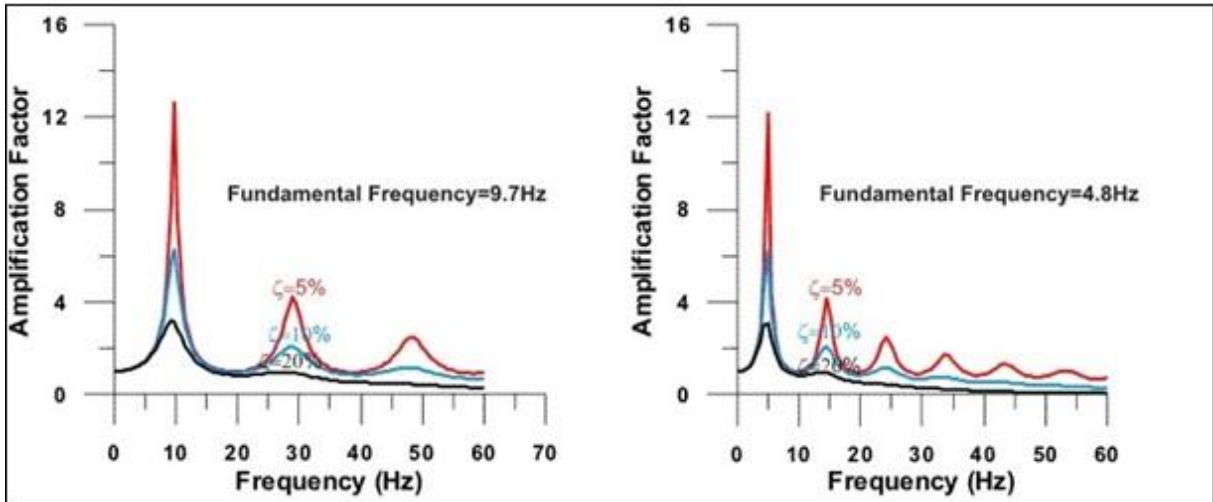
Fig. 5.7: Ground response function (GRF), for a unit input motion, of soil in the project area. The left panel represents GRF in the northern part while the right panel represents GRF in the southern part of the project area. ζ represents the damping factor of soil. Red, blue and black curves represent amplification factor for $\zeta = 5\%$, 10%, and 20% respectively.

CHAPTER VI

CONCLUSION

Based on the present study focused in the geotechnical and geophysical investigations with PGA estimation of the Kathmandu Fun Park Project, Thankot, Kathmandu following conclusions are made.

The study area lies on the washout colluvium deposit with high amount of moisture and fine content suggesting low bearing capacities. Hence, the soil is weak.

Depth to the bedrock, geometry of the subsurface interface and velocity distribution in the subsurface was determined by seismic refraction survey. Thickness of soil was used in PGA calculations. Similarly, the P-wave velocity and geotechnical parameters exhibit good correlation. The results of the present study with further correlation between P-wave velocity and geotechnical parameters at different locations of such colluvium soil (in Nepal Himalaya) serves the best model equation for determination of such geotechnical parameters from P-wave velocities (for the area where soil sampling is difficult to conduct). The present study shows the following relation between P-wave velocity (V_p) and moisture content (w), unconfined compressive strength (UCS) and friction angle (ϕ).

$w = -0.0324V_p + 42.56$

$UCS = 0.0229e^{0.0024V_p}$

$\phi = 0.0149V_p + 10.36$

Modeled relation between P-wave velocity and porosity (Φ) from this study is found to be $\Phi = 132.58e^{-0.003V_p}$ at fluid velocity 1450m/s. The modeled relation shows the material (colluvium) velocity in the study area is 1560m/s.

The simulation of PGA shows that the seismic hazard in the area is high for the earthquakes located to the northeast relative to that in northwest which might be assigned to soil thickness and basin effects of Kathmandu valley. Large earthquakes (M>8) may generate PGA up to150 gal in the area. With 5% damping the amplification of ~13 was found in the frequency range between 9.7 and 4.8 Hz.

REFERENCES

Acharya, K. K. and Dhital, M. R., 2006. Geology and structure of Raniban-Chapadevi area, Kathmandu valley, Central Nepal. Journal of Nepal Geological Society, vol. 33, pp. 1-10.

Aki, K., and Richards, P. G., 1980. Quantitative Seismology: Theory and Methods. Freeman, San Francisco.

Amatya, K. M., and Jnawali, B. M., 1994. Geological map of Nepal. Department of Mines and Geology, ICIMOD.

Anon, 1981. Code of Practice on site investigation, BS5930, British Standards Institution, London. In: Bell, F.G., 2011 (reprint). Fundamentals of engineering geology. BS Publication (Indian reprint), Hyderabad, India.

Arora, K. R., 2000. Soil mechanics and foundation engineering. Standard Publishers Distributors, New Delhi, India. 860p.

ASTM D2216-98, 1998. Standard test method for laboratory determination of water (moisture) content of soil and rock by mass., ASTM International, USA.

ASTM D2487-06, 2006 (current edition). Standard practice for soil classifications of soils for engineering purposes (Unified Soil Classification System). ASTM International, USA.

ASTM D3080-98, 1998. Standard test method for direct shear test of soils under consolidated drained conditions. ASTM International, USA.

ASTM D422-63, 2007 (revised). Standard test methods for particle-size analysis of soils. ASTM International, USA.

ASTM D4318-10, 2010. Standard test methods for liquid limit, plastic limit, and plasticity index of soils. ASTM International, USA.

ASTM D5777-00, 2011 (reapproved). Standard guide for using the seismic refraction method for subsurface investigation. ASTM International, USA.

ASTM D6951-03, 2003. Standard test method for use of the dynamic cone penetrometer test in shallow pavement application. ASTM International, USA.

ASTM D854-10, 2010. Standard test methods for specific gravity of soil solids by water Pycnometer. ASTM International, USA.

Bery, A. A. and Saad, R., 2012. Correlation of seismic P-wave velocities with engineering parameters (N value and rock quality) for tropical environmental studies, International Journal of geosciences, vol. 3, pp. 749-757.

Bhattarai, G. K., Chamlagain, D., and Rajaure, S., 2011. Seismic hazard assessment for eastern Nepal using 1934 and 1988 earthquakes, Journal of Nepal Geological Society, vol. 42, pp. 85-93.

Chang, C., Zoback, M. D., and Khaksar, A., 2006. Emperical relations between rock strength and physical properties in sedimentary rocks, Journal of Petroleum Science and Engineering, vol. 51, pp. 223-237.

Dobrin, M. B. and Savit, C. H., 1988. Introduction to geophysical prospecting. McGraw-Hill Book Co., USA, 867p.

Gansser, A., 1964. Geology of the Himalayas. Interscience, London, 289 p.

Ghimire, S. and Kasahara, M., 2007. Source process of the M_s = 6.6, Udayapur earthquale of Nepal-India border and its tectonic implication. Journal of Asian Earth Science, vol. 31, pp. 128-138.

Hamilton, E. L., Bachman, R. T., Berger, W. H., Johnson, T. C., and Mayere, L. A., 1982. Acoustic and related properties of calcareous deep-sea sediments, Journ. Sediment. Pet., vol. 52, pp. 733-753.

Honda, R., 2003. Calculation of synthetic waveforms using discrete wavenumber method. Ph.D. Thesis, unpub., submitted to Hokkaido University, Sapporo, Japan.

Honda, R. and Yomogida, K., 1999. Synthetic seismograms near a finite fault system. Geophysics, vol. 1.11(3), pp. 611-623.

Honda, R. and Yomogida, K., 2003a. Contribution of vertically travelling plane S-waves to dynamic and static displacements near a finite fault. Geophysics Journal Int., vol. 152, pp 443-454.

Honda, R. and Yomogida, K., 2003b. Static and dynamic displacement near a fault with the discrete wavenumber method. Phys. Earth Planet. Inter., vol. 137, pp 107-127.

Honda, R. and Yomogida, K., 2003c. Effect of complex fault geometry and slip style on near-fault strong motions and static displacement. Earth Planet Space, vol. 55, pp. 515-530.

Jackson, M., and Bilham, R., 1994. Constraints on Himalayan deformation inferred from vertical velocity fields in Nepal and Tibet. In: Upreti, B. N., 1999. An overview of the stratigraphy and tectonics of the Nepal Himalaya. Journal of Asian Earth Science, vol. 17, pp. 577-606.

Klimentos, T., 1991. The effects of porosity-permeability-clay content on the velocity of compressional waves. Geophysics, vol. 56 (12), pp. 1930-1939.

Klyen, E. and Van Heerden, M.J., 1983. Using DCP soundings to optimize pavement rehabilitation. The Haul Transportatio .IP, Convention Showgrounds, Johannesburg, S. Africa, Vol.3.

Kurtulus, C. Sertcelik, F., Canbay, M. M., and Sertcelik, I., 2009. Estimation of Atterberg limits and bulk mass density of an expansive soil from P-wave velocity measurements. Bulleten of Eng. Geo. and Environ., DOI 10.1007/s10064-009-0237-7.

Lee, I. K., White, W. and Ingles, O. G., 1983. Geotechnical Engineering, Pitman Publishing Inc., Massachusetts, USA, 409p.

Lowrie, W., 2007. Fundamentals of Geophysics (second edition). Cambridge University Press, New York, USA. 381p.

Okada, Y., 1985. Surface deformation due to shear and tensile faults in a half space. Bulletin of Seis. Sci., Am., Vol. 75, pp. 1135-1154.

Pandey, M. R., Tandukar, R. P., Avouac, J. P., Lavé, J., Massot, J. P., 1995. Interseismic strain accumulation on the Himalayan crustal ramp (Nepal). In: Upreti, B. N., 1999. An overview of the stratigraphy and tectonics of the Nepal Himalaya. Journal of Asian Earth Science, vol. 17, pp. 577-606.

PCA, Design of concrete airport pavement, Portland Cement Association, 1995. In: Zacny, K. Wilson, J., Craft, J., Asnani, V., Oravece, H., Creager, C., Johnson, J., Fong, T., 2010. Robotic Lunar Geotechnical Tool. ASCE Earth and Space, Honolulu, HI.

Reynolds, J. M., 1997. An Introduction to applied and environmental Geophysics. John Willey and Sons Ltd, 209-414p.

Sah, R. B., 1999. Current understandings and existing problems on stratigraphy of Nepal Himalaya. Journal of Stratigraphic Association of Nepal (SAN), vol. 1, pp. 1-29.

Sakai[*], H., Sakai, H., Yahagi, W., Fujii, R., Hayashi, T., Upreti, B. N., 2006. Pleistocene rapid uplift of the Himalaya frontal ranges recorded in the Kathmandu and Siwalik basins. Palaeogeography, Palaeoclimatology, Palaeoecology (Elsevier/Palaeo), vol. 241, pp. 16-27.

Schon, J. H., 1983. Physical properties of rocks: Fundamentals and principles of petrophysics. Seismic Exploration, Second Edition, Elsevier Science Ltd, Oxford, Ox 5 1GB, UK, vol. 18, 583p.

Seeber, L. and Armbruster, J. G., 1981. Great detachment earthquakes along the Himalayan arc and long term forecasting. In: Upreti, B. N., 1999. An overview of the stratigraphy and tectonics of the Nepal Himalaya. Journal of Asian Earth Science, vol. 17, pp. 577-606.

Sheraz, A. M., Emad, M. Z., Shahzad, M. and Arshad, S. M., 2014. Relation between uniaxial compressive strength, point load index and sonic wave velocity for dolerite, Pakistan Journal of Science, vol. 66, pp. 60-66.

Sheriff, R. E., and Geldart, L. P., 1982 (first published). Exploration Seismology. Cambridge University Press, New York, USA. Pp. 230-300.

Stöcklin, J. and Bhattarai, K. D., 1977. Geology of the Kathmandu area and central Mahabharat range, Nepal Himalaya. Report of Department of Mines and Geology/UNDP (unpub.), 86p.

Telford, W. M., Geldart, L. P., Sheriff, R. E., Keys, D. A., 1981 (reprinted). Applied Geophysics, Cambridge University Press, New York, NY 10022, USA. 821p.

Terzaghi, K., 1943. Theoretical soil mechanics. John Wiley and Sons, New York. In: Lee, I. K., White, W. and Ingles, O. G., 1983. Geotechnical Engineering, Pitman Publishing Inc., Massachusetts, USA, 409p.

Upreti, B. N., 1999. An overview of the stratigraphy and tectonics of the Nepal Himalaya, Journal of Asian Earth Science, vol 17, pp. 577-606.

Wyllie, M. R., Gregory, A. R., and ardner, G. H. F., 1958. An experimental investigation of factors affecting elastic wave velocity in porous media. Geophysics, vol. 23 (3), pp. 459-493.

ANNEX A: In-situ DCP Tests.

(ANNEX A includes only sample format)

DYNAMIC CONE PENETRATION TEST (DCPT) – Pit No.1

Project: Kathmandu Fun Park	Date: July 5, 2013
Location: E00619996, N03063632	Start Layer: 2 meter down from surface
Test No.: DCPT 1, 2, 3 **Pit No.: 1**	Zero Error (mm): 0
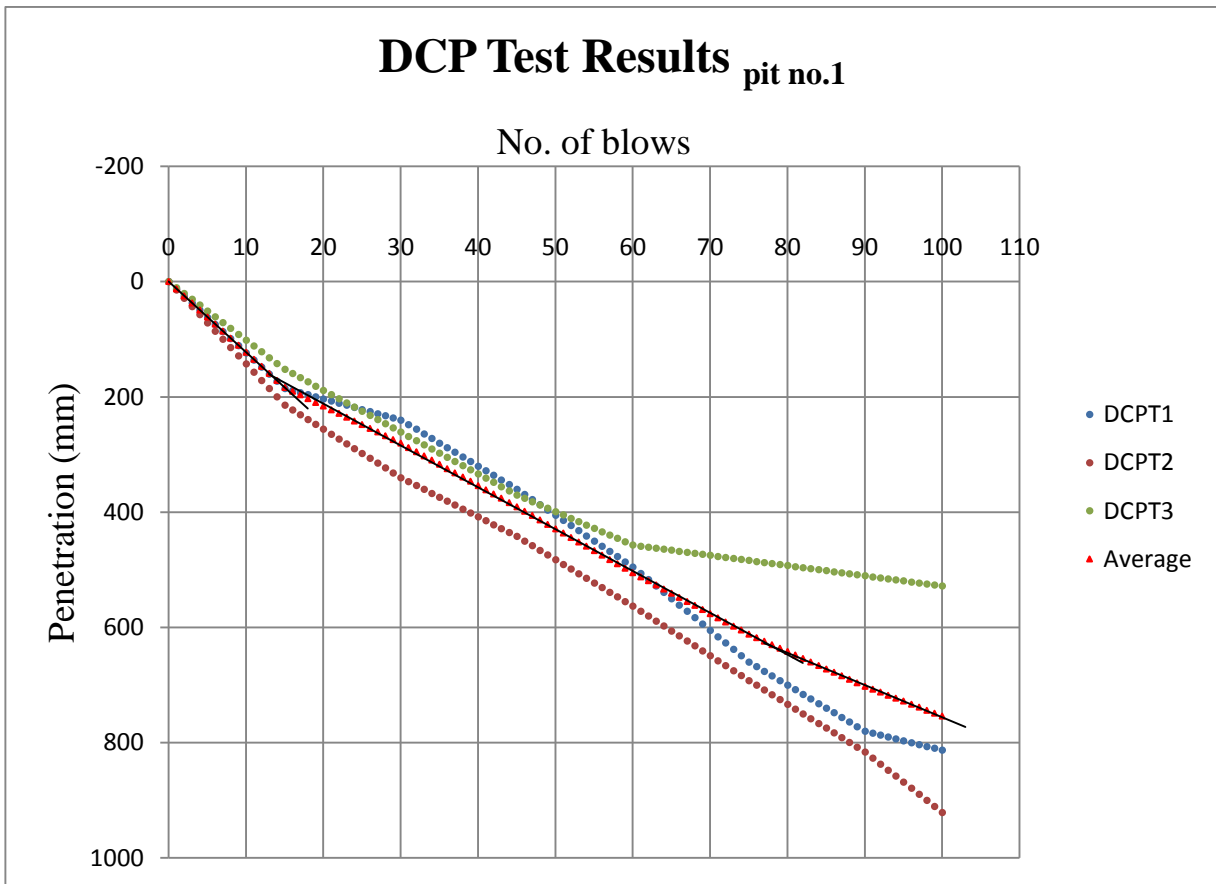
Figure IS 1.1: DCPT Results of Pit No.01

Details of DCPT 1	Soil Layers						Average
	1	2	3	4	5	6	
Layer Bottom depth	185	240	495	660	780	813	
Thickness (mm)	185	55	255	165	120	33	
Strength(mm/blow)	12	4	9	11	8	3	
CBR BY TRL R.N.31	21.2	76.6	31.4	23.9	33.5	85.5	45.4
CBR BY KLEYN & VAN	17.2	81.4	27.6	19.9	29.9	93.0	44.8
UCS (DCP Strength), Kpa	187.6	705.0	280.5	212.5	300.6	789.3	412.6
UCS (TRL R.N.31), Kpa	220.7	682.9	311.0	245.4	330.0	752.0	423.6
UCS (KLEYN & VAN), Kpa	183.4	720.4	277.9	208.6	298.5	809.5	416.4
BEARING CAPACITY*	198.9	466.5	257.7	215.5	269.5	501.7	318.3
BEARING CAPACITY**	173.0	485.7	236.7	190.6	249.9	530.4	311.1

Details of DCPT 2	Soil Layers						Average
	1	2	3	4	5	6	
Layer Bottom depth	214	340	442	816	921		
Thickness (mm)	214	126	102	374	105		
Strength(mm/blow)	14	8	7	8	11		
CBR BY TRL R.N.31	18.2	31.8	39.8	31.9	25.2		29.4
CBR BY KLEYN & VAN	14.3	28.1	36.8	28.2	21.1		25.7
UCS (DCP Strength), Kpa	160.1	285.1	358.9	285.9	223.5		262.7
UCS (TRL R.N.31), Kpa	192.7	315.3	383.8	316.1	256.2		292.8
UCS (KLEYN & VAN), Kpa	155.7	282.6	358.5	283.4	219.8		260.0
BEARING CAPACITY*	179.6	260.4	302.0	260.9	222.7		245.1
BEARING CAPACITY**	152.9	239.7	286.9	240.3	198.3		223.6

Details of DCPT 3	Soil Layers						Average
	1	2	3	4	5	6	
Layer Bottom depth	152	370	457	473			
Thickness (mm)	152	218	87	16			
Strength(mm/blow)	10	7	6	2			
CBR BY TRL R.N.31	26.1	37.1	47.1	164.5			68.7
CBR BY KLEYN & VAN	22.1	33.8	45.2	205.3			76.6
UCS (DCP Strength), Kpa	232.4	333.9	426.8	1549.7			635.7
UCS (TRL R.N.31), Kpa	264.9	360.9	445.0	1337.3			602.0
UCS (KLEYN & VAN), Kpa	228.8	332.7	428.9	1625.6			654.0
BEARING CAPACITY*	228.3	288.3	337.7	774.7			407.3
BEARING CAPACITY**	204.5	271.2	328.4	897.6			425.4

Details of average of pit no.01	Soil Layers						Average
	1	2	3	4	5	6	
Layer Bottom depth	159	624	754				
Thickness (mm)	159	465	130				
Strength(mm/blow)	12	7	6				
CBR BY TRL R.N.31	21.4	37.2	48.9				35.8
CBR BY KLEYN & VAN	17.4	33.9	47.2				32.8
UCS (DCP Strength), Kpa	189.1	334.2	443.2				322.2
UCS (TRL R.N.31), Kpa	222.2	361.2	459.6				347.6
UCS (KLEYN & VAN), Kpa	184.9	333.1	445.9				321.3
BEARING CAPACITY*	199.9	288.5	346.0				278.1
BEARING CAPACITY**	174.1	271.4	338.2				261.2
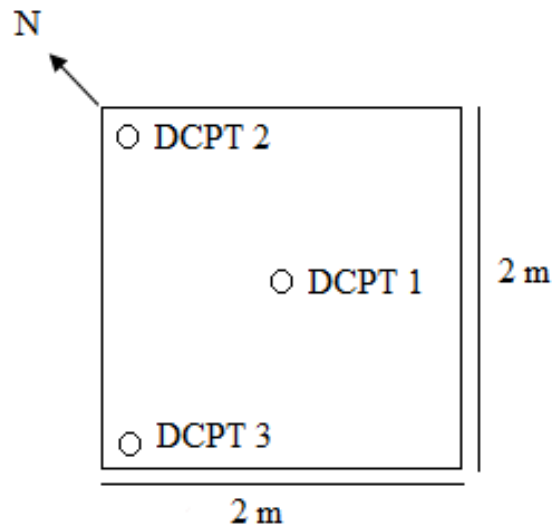
Figure IS 1.2: Sketch of Pit No.01

TRL R.N. 31 equation- $\log_{10}(CBR) = 2.48-1.057*\log_{10}(Strength)$
Kleyn equation- $\log_{10}(CBR) = 2.632-1.28*\log_{10}(Strength)$
UCS (From DCP Strength) = $2900*(Strength)^{-1.09}$
UCS (From TRL R.N. 31) = $15*CBR^{0.88}$
UCS (From KLEYN & VAN) = $15*CBR^{0.88}$
Bearing Capacity* = $26.16*(CBR)^{0.66}$ in Kpa   [CBR by TRL R.N. 31]
Bearing Capacity** = $26.16*(CBR)^{0.66}$ in Kpa   [CBR by KLEYN & VAN]

ANNEX B: Soil Profiles.

SOIL LOG OF KATHMANDU FUN PARK PROJECT

Project : Geotechnical Investigation
Pit No..: 01
UTM Easting: E00619996
UTM Northing: N03063632

Sample no.	Depth (cm)	Soil Legend	Soil Description
Pit 01/01	0.00 – 50.00		Top soil, black to dark brown in color, humous (ORGANIC CLAY)
Pit 01/02	50.00 – 110.00		Brown in color, with few nodules of pebbles, highly weathered, clay rich soil (COLLUVIUM)
Pit 01/02	110.00 – 200.00		Brown in color, angular gravels of fine grained sandstone, clay rich gravelly soil (COLLUVIUM)

Fig. SP1 (a)

Fig. SP1 (b)

SOIL LOG OF KATHMANDU FUN PARK PROJECT

Project : Geotechnical Investigation
Pit No.: 03
UTM Easting: E00619946
UTM Northing: N03063499

Sample no.	Depth (cm)	Soil Legend	Soil Description
Pit 03/01	0.00–30.00		Top soil, black to dark brown in color, humous, with few pebbles(ORGANIC CLAY)
Pit 03/02	30.00–90.00		Brown in color, with few gravels, highly weathered, clay rich soil (COLLUVIUM)
Pit 03/03	90.00–200.00		brown in color with a large boulder and gravels, clay rich soil (COLLUVIUM)

Fig. SP1 (c)

SOIL LOG OF KATHMANDU FUN PARK PROJECT

Project : Geotechnical Investigation
Pit No.: 04
UTM Easting: E00619801
UTM Northing: N03063145

	Sample no.	Depth (cm)	Soil Legend	Soil Description
	Pit 04/01	0.00–40.00		Top soil, black to dark brown in color, humous soil, with gravels (ORGANIC CLAY)
	Pit 04/02	40.00–110.00		Light reddish brown in color, gravels (<5%), few cobble, silty rich clayey soil
	Pit 04/03	110.00–200.00		Reddish brown in color, gravels (<3%), silt rich claey soil on the left left side of the face. Where as in right face couple of thin (2cm-3 cm) layers of gravelly clay

Fig. SP1 (d)

SOIL LOG OF KATHMANDU FUN PARK PROJECT

Project : Geotechnical Investigation
Pit No.: 05
UTM Easting: E00619697
UTM Northing: N03062900

Sample no.	Depth (cm)	Soil Legend	Soil Description
Pit 05/01	0.00 – 30.00		Top soil, black to dark brown in color, humous soil(ORGANIC CLAY)
Pit 05/02	40.00 – 100.00		Light brown in color, angular gravel rich clayey soil in the left part of the face. While in the right part gravel is <5%
Pit 05/03	110.00 – 130.00		Light brown in color, gravel (<5%), clay rich soil in the right part. While in the left part the color of soil is reddish brown
Pit 05/02	140.00 – 150.00		Light brown in color, angular gravel rich clayey soil in the left part of the face. While in the right part gravel is <5%
Pit 05/03	160.00 – 200.00		Light brown in color, gravel (<5%), clay rich soil in the right part. While in the left part the color of soil is reddish brown

Fig. SP1 (e)

X

SOIL LOG OF KATHMANDU FUN PARK PROJECT

Project : Geotechnical Investigation
Pit No.: 06
UTM Easting: E00619659
UTM Northing: N03062571

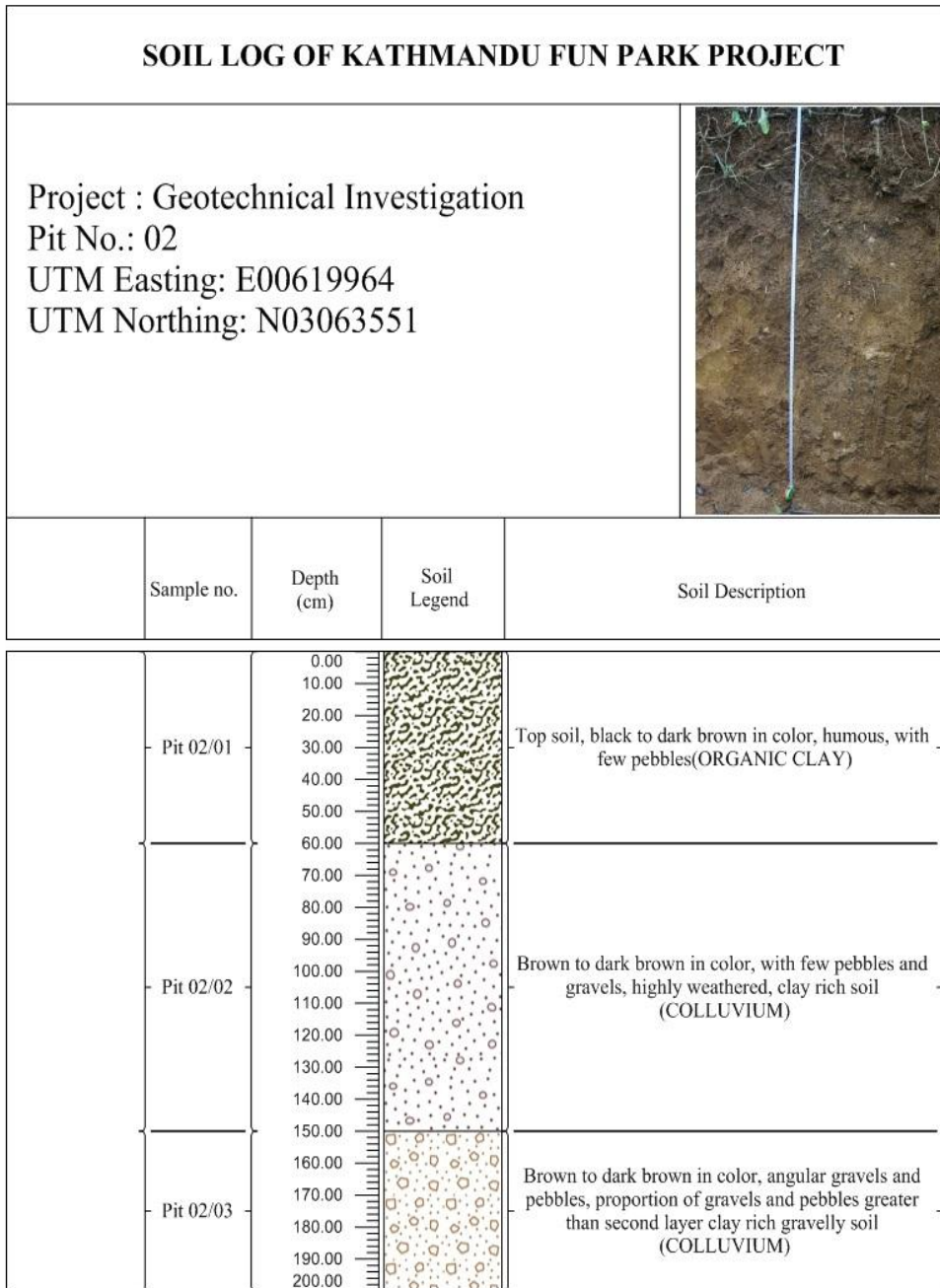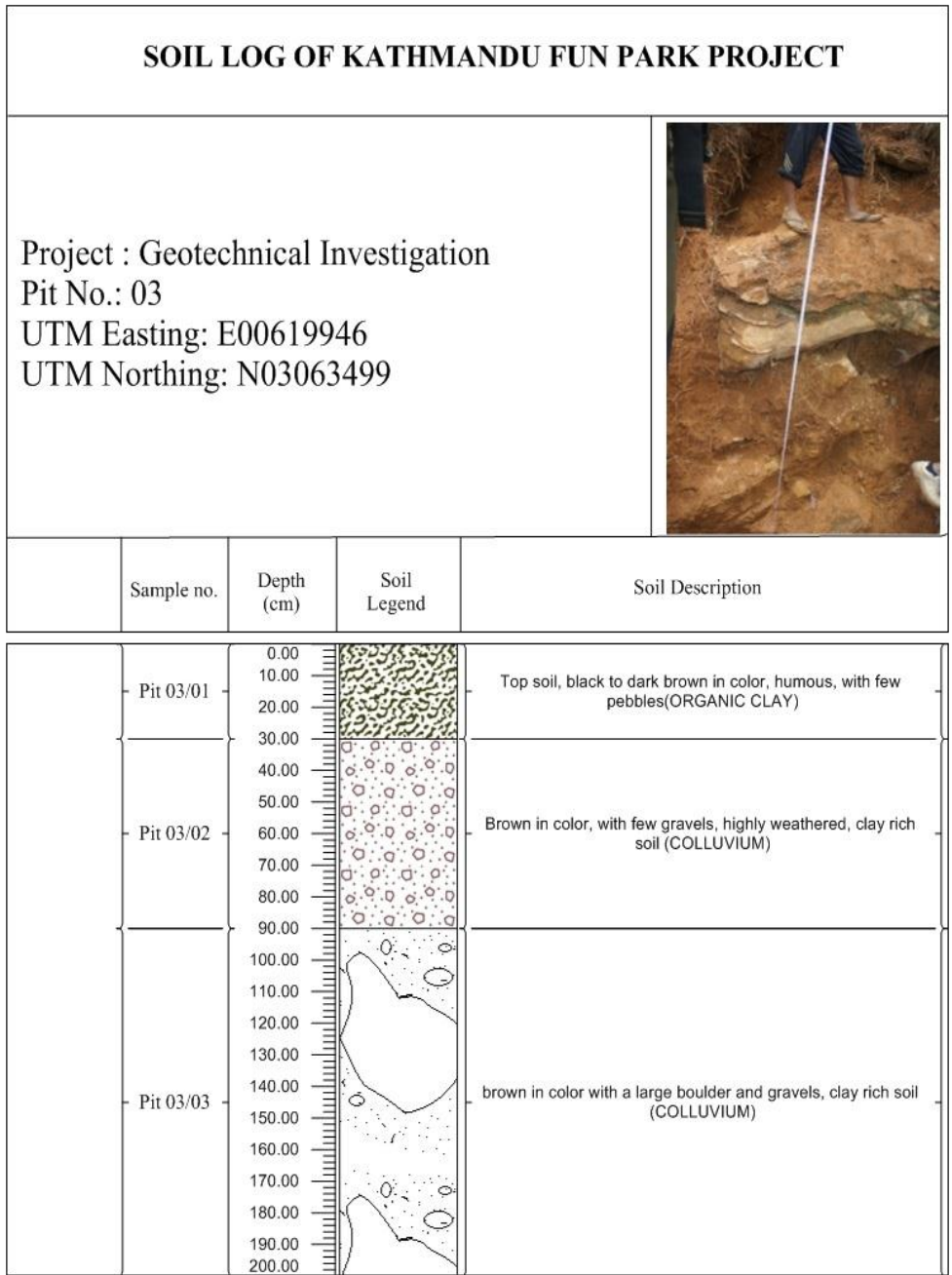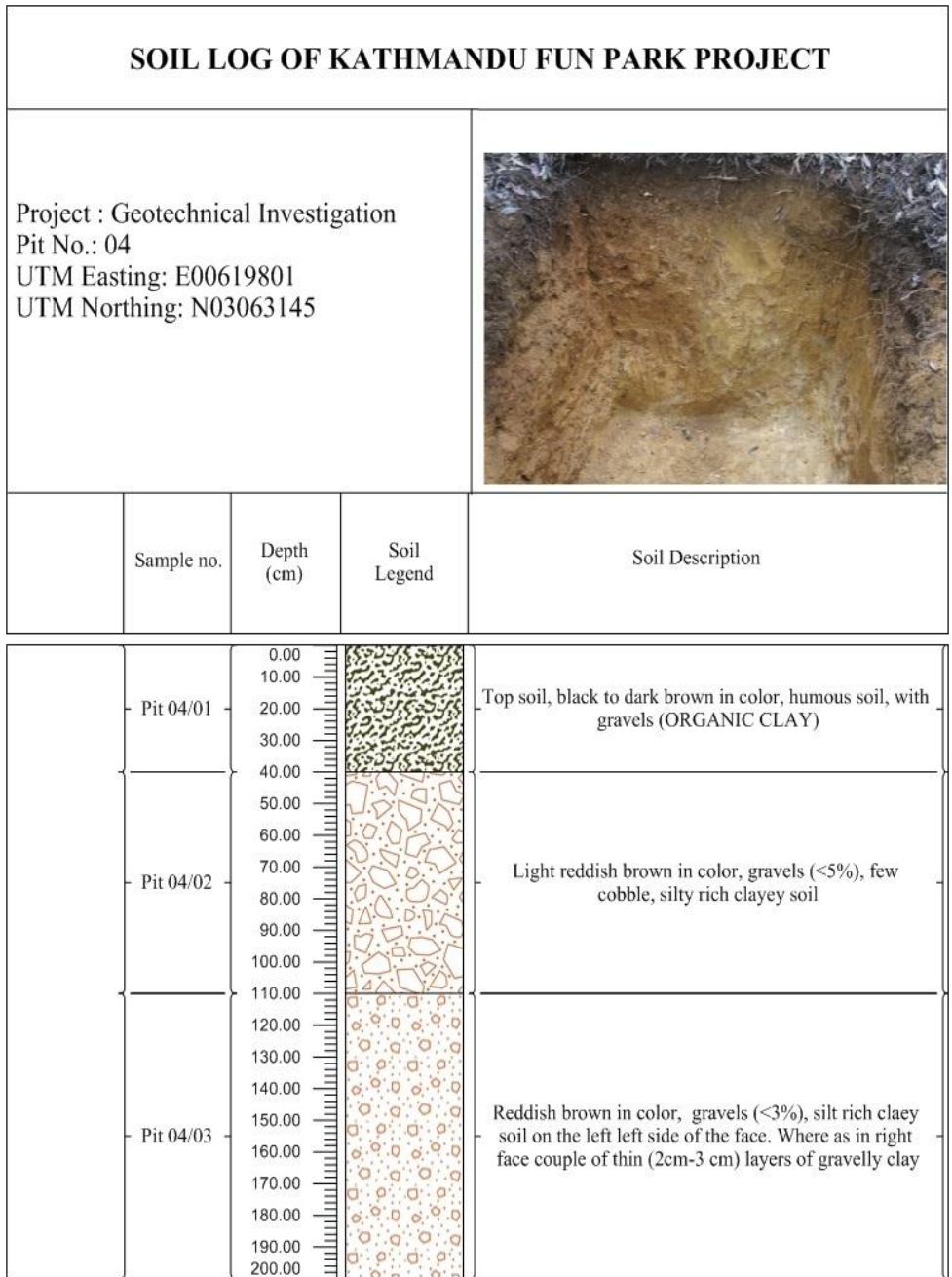|	Sample no.	Depth (cm)	Soil Legend	Soil Description
	Pit 06/01	0.00–30.00		Top soil, black to dark brown in color with few (<8%) gravels (ORGANIC CLAY)
	Pit 06/02	30.00–200.00		Reddish brown to light brown in color, few (<5%) gravels, silty clay

Fig. SP1 (f)

SOIL LOG OF KATHMANDU FUN PARK PROJECT

Project : Geotechnical Investigation
Pit No.: 08
UTM Easting: E00619200
UTM Northing: N03061845

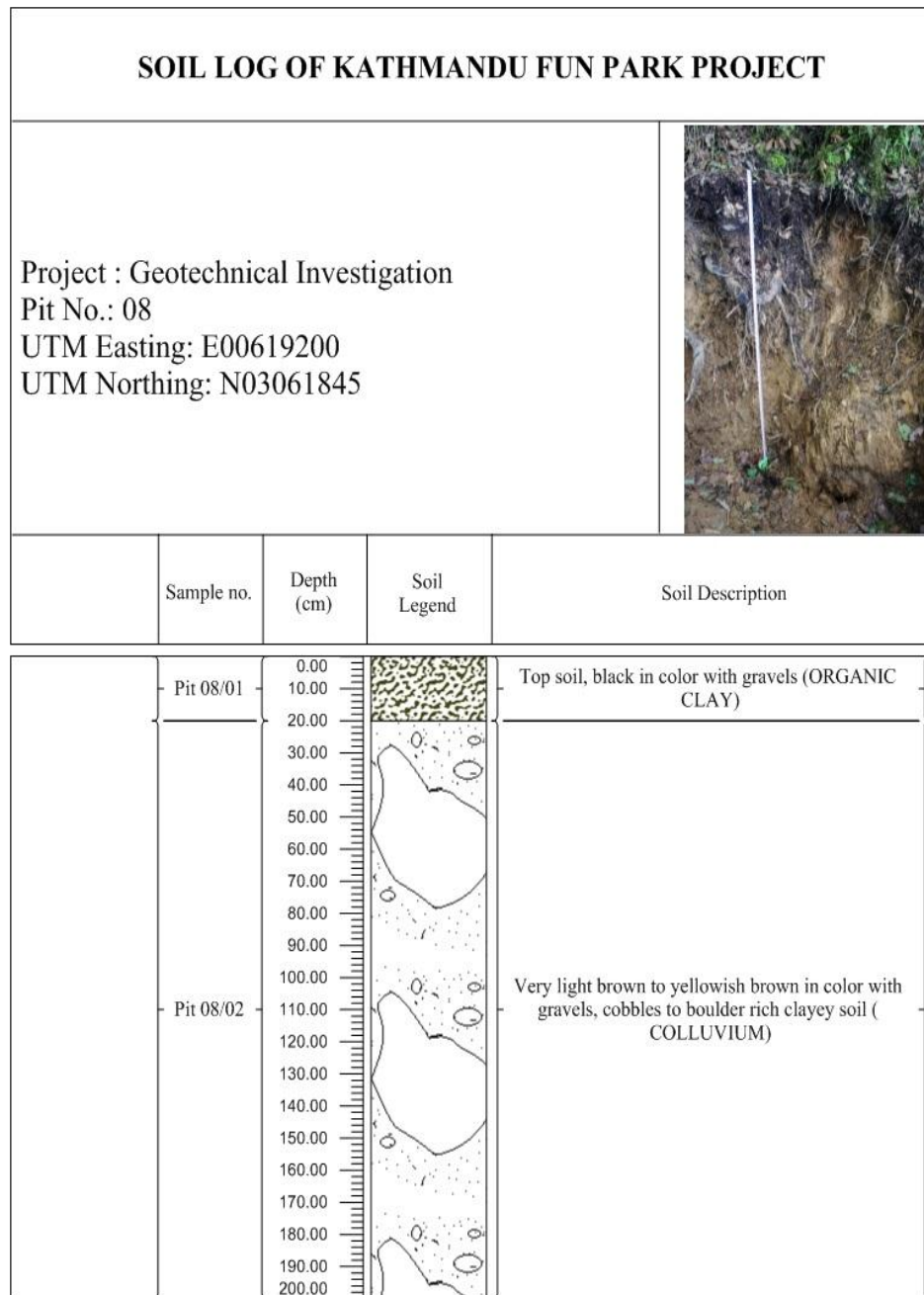|	Sample no.	Depth (cm)	Soil Legend	Soil Description
	Pit 08/01	0.00 10.00 20.00		Top soil, black in color with gravels (ORGANIC CLAY)
	Pit 08/02	30.00 40.00 50.00 60.00 70.00 80.00 90.00 100.00 110.00 120.00 130.00 140.00 150.00 160.00 170.00 180.00 190.00 200.00		Very light brown to yellowish brown in color with gravels, cobbles to boulder rich clayey soil (COLLUVIUM)

Fig. SP1 (g)

Fig. SP1: Soil Profiles of different pit holes (a to g represents profiles of 7 pits).

ANNEX C: Laboratory Tests of Samples.

       - Moisture content Determination

       - Soil Classification (sieve and hydrometer analysis)

       - Atterberg Limit test

       - Specific gravity test

(ANNEX C includes only sample format)

ERMC GEO-TECH SERVICES P.LTD.

MOISTURE CONTENT

Project   **Geotechnical Soil Investigation of Kathmandu Fun Park**

Sample Description   -   Date of Sampled   **07-11-13**

Location   Thankot, Chandragiri, Kathmandu   Date of Testing   **22/7/2013**

Test No.   **GSI-KFP-1**

Pit No -->		1	2	3	4	5	6	8
Container No.	No	B-33	B-18	B-33	B-24	B-27	B-30	B-26
Wt. of Container + Wt. of Wet Soil	gm	732.0	804.0	786.0	550.0	678.0	744.0	651.0
Wt. of Container + Wt. of Dry Soil	gm	631.0	660.0	634.0	458.0	556.0	635.0	508.0
Wt. of Water, W_w	gm	101.0	144.0	152.0	92.0	122.0	109.0	143.0
Wt. of Empty Container	gm	77.0	77.0	80.1	69.7	76.0	76.6	72.0
Wt. of Dry Soil, W_d	gm	554.0	583.0	553.9	388.3	480.0	558.4	436.0
Moisture Content	%	**18.2**	**24.7**	**27.4**	**23.7**	**25.4**	**19.5**	**32.8**

Comments:

Tested By: Checked By:

<u>Krishna Gurung</u>   <u>Tara P. Bhattarai</u>

Sr. Lab.Technician   **Geological Engineer**

ERMC GEO-TECH SERVICES P.LTD.

SIEVE ANALYSIS

Project : **Geotechnical Soil Investigation of Kathmandu Fun Park**   Sample Depth: **Below 2m**

Location: **Thankot, Chandaragiri, Kathmandu**   Pit No.: **# 1**

Description of Soil : **Reddish brown clayey Silt with gravel and sand**   Date of Testing : **25-07-2013**

Location/Chainage: **Thankot Chandragiri ktm**   Date of Sampled   **11-07-2013**

Test No.:   **1**

Soil Sample Size (ASTM D1140-54)

Nominal Diameter of Largest Particle	Approximate Minimum Wt. of Sample, $_g$
No. 10 sieve	200
No. 4 sieve	500
3/4 in.	1500

Wt. of dry sample + container, $_{(g)}$	605.0
Wt. of container, $_{(g)}$	77
Wt. of dry sample, Ws $_{(g)}$	528.0

Sieve Analysis and Grain Shape

Sieve No.	Diam. (mm)	Wt. retained	% retained	% passing
	25	0	0.0	100.0
	20	0	0.0	100.0
	12.5	16	3.0	97.0
	9.5	55	10.4	86.6
	4.75	24	4.5	82.0
	2.36	37	7.0	75.0
	1.180	5	0.9	74.1
	0.6	13	2.5	71.6
	0.425	15	2.8	68.8
	0.300	7	1.3	67.4
	0.150	12	2.3	65.2
	0.075	1	0.2	65.0
PAN		343	65.0	
	Total	528		

Results:

Gravel %	18.0
Sand %	17.0
Silt%	38.0
Clay%	27.0

Tested by	Checked by
Krishna Gurung Sr.Lab.Technician	Tara P. Bhattarai Geological Engineer

ERMC GEO-TECH SERVICES P.LTD.
HYDROMETER ANALYSIS

Project : **Geotechnical Soil Investigation of Kathmandu Fun Park** Sample Depth: **Below 2m**
Description of Soil : **Reddish brown clayey Silt with gravel and sand** Date of Test: **25-07-13**
Location/Chainage : **Thankot Chandragiri ktm** Tested By : **K Gurung**
Test No.: **1** Checked By: **Tara P. Bhattarai**
Pit No.: **# 1**

G_s = **2.500**
y_w = **0.9965**
m = **8.55**
y_c = **0.9965**

SOIL SAMPLE WEIGHT

	Tested Sample	Poured off

Hydrometer No : **1** Container No. **B-24**
Dispersing Agent : **Sodium HM 4%** Weight of Container + Dry Soil g **123.5**
Amount : **5 g per 125 cc** Weight of Container   g **69.71**
Meniscus correction x 1,000= **0.50** Weight of Dry Soil, Ws   g **53.79**
Total Weight Dry Soil   g **53.79**
Fraction Finer No. 200 Sieve= **64.962**

Date	Time	Hyd. Reading	Elapsed Time, t min	$R = $ 1000 (r-1)	$R_w = $ 1000$(y_w$-1)	Temp. ^{0}c	R-R_w	N= K_1(R-R_w) %	R_c	Z_r cm.	$\sqrt{\dfrac{Z_r (cm)}{t (min)}}$	$D = K_2\sqrt{\dfrac{Z_r}{t}}$	N' %
24/7		1.03050	0.25	30.50	-0.90	27	31.40	96.95	31.00	8.71	5.901	0.0778	63.0
		1.03000	0.50	30.00	-0.90	27	30.90	95.41	30.50	8.88	4.213	0.0556	62.0
		1.02850	1.00	28.50	-0.90	27	29.40	90.78	29.00	9.38	3.063	0.0404	59.0
		1.02750	2.00	27.50	-0.90	27	28.40	87.69	28.00	9.72	2.205	0.0291	57.0
		1.02650	2.00	26.50	-0.90	27	27.40	84.60	27.00	6.95	1.864	0.0246	55.0
		1.02450	5.00	24.50	-0.90	27	25.40	78.43	25.00	7.63	1.235	0.0163	50.9
		1.01800	8.00	18.00	-0.90	27	18.90	58.36	18.50	9.83	1.108	0.0146	37.9
		1.01650	15.00	16.50	-0.90	27	17.40	53.72	17.00	10.34	0.830	0.0109	34.9
		1.01500	30.00	15.00	-0.90	27	15.90	49.09	15.50	10.84	0.601	0.0079	31.9
		1.01350	60.00	13.50	-0.90	27	14.40	44.46	14.00	11.35	0.435	0.0057	28.9
		1.01150	120.00	11.50	-0.90	27	12.40	38.29	12.00	12.03	0.317	0.0042	24.9
		1.00700	240.00	7.00	-0.90	27	7.90	24.39	7.50	13.55	0.238	0.0031	15.8
25/7		1.00650	1200.00	6.50	-0.90	27	7.40	22.85	7.00	13.72	0.107	0.0014	14.8

$$K_1 = \frac{y_c \times G_s \times 100}{(G_s - 1) W_s} = 3.087624713$$

y_c = Unit Wt. of water at the temp.of hydrometer calibration, g/cm^3
G_s = Specific gravity of solids
W_s = Wt. Of dry soil, g

$$K_2 = 5.531 \times 10^{-3} \sqrt{\frac{m =}{y_s - y_w}} = 0.013187318$$

m = Viscosity of water at the temp. of the test, millipoises
y_s = Unit Wt. of soil grains, g/cm^3
y_w = Unit Wt. of water at the temp.of the test, g/cm^3

ERMC GEO-TECH SERVICES P.LTD.
PARTICLE SIZE DISTRIBUTION CHART

Project : **Geotechnical Soil Investigation of Kathmandu Fun Park**
Description of soil : **Reddish brown clayey Silt with gravel and sand**
Location/Chainage: **Thankot Chandragiri ktm**
Test No.: **2**

Sample Depth: **Below 2m**
Date of Testing : **25-07-13**
Tested By: **K Gurung**
Checked By : **Tara P. Bhattarai**
Pit No.: **# 1**

Unified Soil Classification System	COBBLES		GRAVEL		SAND			SILT or CLAY		
			Coarse	Fine	Coarse	Medium	Fine			
A A S H T O Classification	BOULDERS		GRAVEL		SAND			SILT		
							Fine			
ASTM Classification			GRAVEL		SAND			SILT		
					Coarse		Fine			
B S Classification	BOULDERS	COBBLE	GRAVEL			SAND			SILT		CLAY
			Coarse	Medium	Fine	Coarse	Medium	Fine	Coarse	Medium	Fine
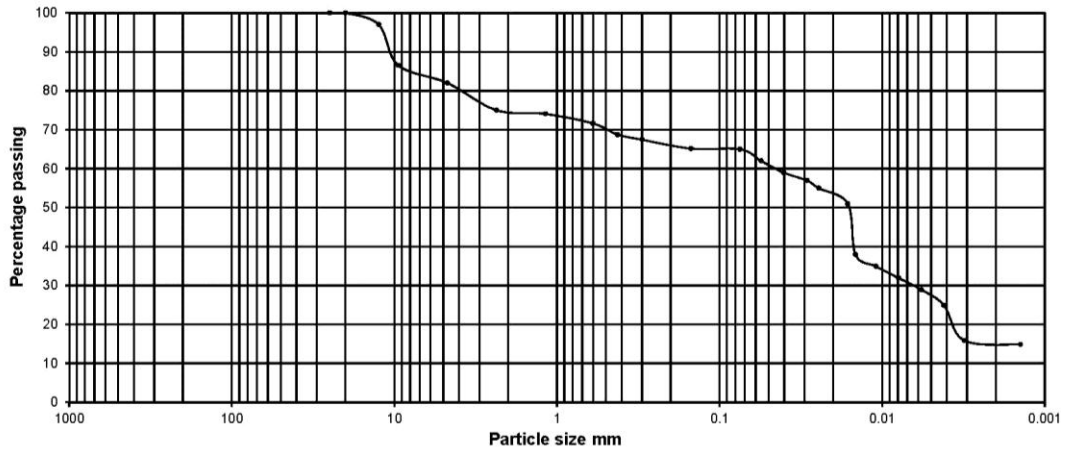
ERMC GEO-TECH SERVICES P.LTD.

ATTERBERG LIMITS TEST

Location	**Thankot Chandragiri ktm**		Pit #	1	
Date: of Sampled	11-7-2013		Date of test	**25/07/2013**	
Project	Geotech.Investigation				
Sample Description:					
Sample No:	5				

PLASTIC LIMIT NATURAL WATER CONTENT

Container No.	A-7	A-9		Analysis Data	Result
Weight of Wet Soil + Container,g	16.72	15.99		% passing 0.425mm	
Weight of Dry Soil + Container,g	14.76	14.14		% Passing 2mm	
Weight of Water, g	1.96	1.85		% Passing 0.075mm	64.9
Weight of container, g	8.98	8.51		Palsticity Index	4.92
Weight of Dry Soil, g	5.78	5.63		Plasticity Modules	0.0
Water Content, W %	33.91	32.86		Liquid Limit, W_L =	38.30
Average %	33.38			Plastic Limit, W_P=	33.38
LIQUID LIMIT				Plasticity Index,PI=	4.92
Number of Blows	**38**	**29**	**19**		
Container No	A-12	A-19	A-5		
Weight of Wet Soil + Container,g	25.29	26.38	30.42		
Weight of Dry Soil + Container,g	21.00	21.73	23.94		
Weight of Water, g	4.29	4.65	6.48		
Weight of Container, g	8.91	9.24	7.94		
Weight of Dry soil, g	12.09	12.49	16.00		
Water Content, W %	**35.48**	**37.23**	**40.50**		
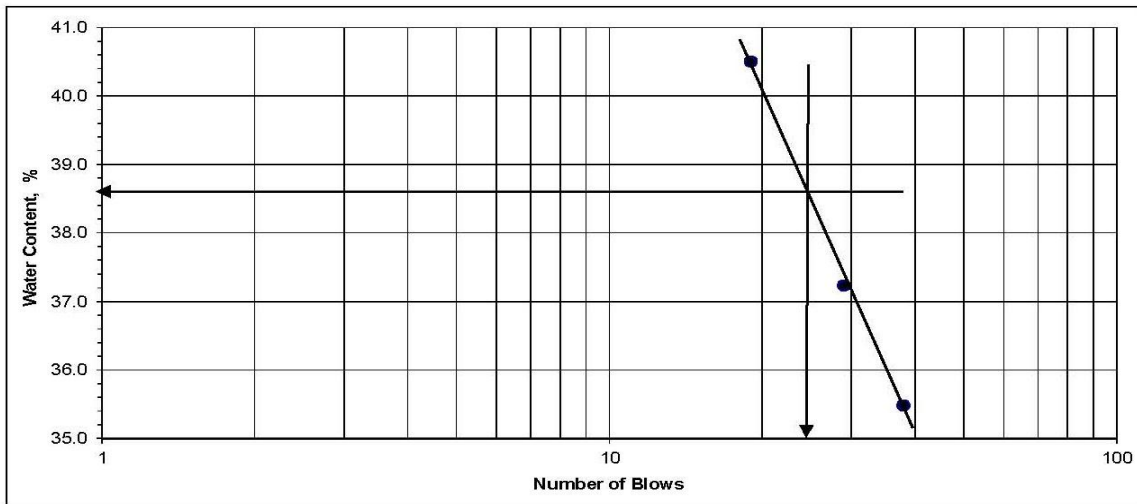
Tested By:	Checked By:
_____	_____
Krishna Gurung	Tara P. Bhattarai
Sr.Lab.Technician	Geological Engineer

Aterberg limit

ERMC GEO-TECH SERVICES P.LTD.

SPECIFIC GRAVITY AND ABSORPTION OF SOIL

Project: Geotechnical Soil Investigation of Kathmandu Fun Park
Location/Chainage Thankot Chandragiri , Kathmandu   Pit No.:   **#1**
Desciption: Redish brown clayey Silt with gravel and sand   Sample No:
Sampled Date 11-07-2013   Date fo Test: 26/07/2013

Description	1	2	Average
7. Weight of saturated surface dry sample (gm)	106.9	106.9	
8. Weight of Oven dry sample (gm)	100.0	100.0	
9. Weight of bottle filled with water (gm)	357.6	357.1	
10. Wt. Of bottle with sat.surf.dry sample & water (gm)	417.8	416.9	
11. Absorption = (Line 7 - Line 8)	6.9	6.9	**6.90**
12. % Absorption = Line 11/Line8 * 100	6.9	6.9	**6.90**
13. Specific Gravity:			
(a) Bulk, Oven-dry =Line 8 / (Line 7+Line 9-Line 10)	2.14	2.12	**2.132**
(b) Bulk, sat.surf.dry =Line7 / (Line 7+Line 9 - Line 10)	2.29	2.27	**2.279**
(c) Apparent = Line 8 / (Line 8 + line 9 - Line 10)	2.51	2.49	**2.500**

Project: Geotechnical Soil Investigation of Kathmandu Fun Park
Location/Chainage Thankot Chandragiri , Kathmandu   Pit No.:   **#2**
Desciption: Brownish grey sandy Silt with clay and traces of gravel   Sample No:
Sampled Date 11-07-2013   Date fo Test: 26/07/2013

| Description	1	2	Average
7. Weight of saturated surface dry sample (gm)	108.6	108.6	
8. Weight of Oven dry sample (gm)	100.0	100.0	
9. Weight of bottle filled with water (gm)	354.3	354.2	
10. Wt. Of bottle with sat.surf.dry sample & water (gm)	415.2	415.6	
11. Absorption = (Line 7 - Line 8)	8.6	8.6	**8.60**
12. % Absorption = Line 11/Line8 * 100	8.6	8.6	**8.60**
13. Specific Gravity:			
(a) Bulk, Oven-dry =Line 8 / (Line 7+Line 9-Line 10)	2.10	2.12	**2.108**
(b) Bulk, sat.surf.dry =Line7 / (Line 7+Line 9 - Line 10)	2.28	2.30	**2.289**
(c) Apparent = Line 8 / (Line 8 + line 9 - Line 10)	2.56	2.59	**2.574**

Project: Geotechnical Soil Investigation of Kathmandu Fun Park
Location/Chainage Thankot Chandragiri , Kathmandu   Pit No.:   **#3**
Desciption: Brownish red sandy Silt with clay and traces of gravel   Sample No:
Sampled Date 11-07-2013   Date fo Test: 26/07/2013

Description	1	2	Average
7. Weight of saturated surface dry sample (gm)	108.1	108.1	
8. Weight of Oven dry sample (gm)	100.0	100.0	
9. Weight of bottle filled with water (gm)	351.5	351.8	
10. Wt. Of bottle with sat.surf.dry sample & water (gm)	412.8	412.9	
11. Absorption = (Line 7 - Line 8)	8.1	8.1	**8.10**
12. % Absorption = Line 11/Line8 * 100	8.1	8.1	**8.10**
13. Specific Gravity:			
(a) Bulk, Oven-dry =Line 8 / (Line 7+Line 9-Line 10)	2.14	2.13	**2.132**
(b) Bulk, sat.surf.dry =Line7 / (Line 7+Line 9 - Line 10)	2.31	2.30	**2.305**
(c) Apparent = Line 8 / (Line 8 + line 9 - Line 10)	2.58	2.57	**2.577**

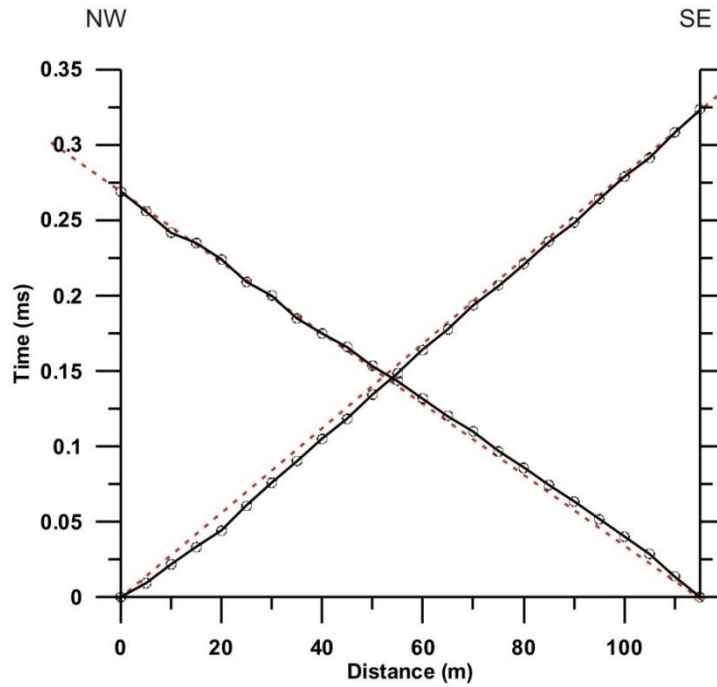| Tested by	Checked by
Krishna Gurung Sr. Lab.Technician	Tara P. Bhatarai Geological Engineer

ANNEX D: Seismic Refraction Waveform Data and Travel-time Curves

(ANNEX D includes only sample format)
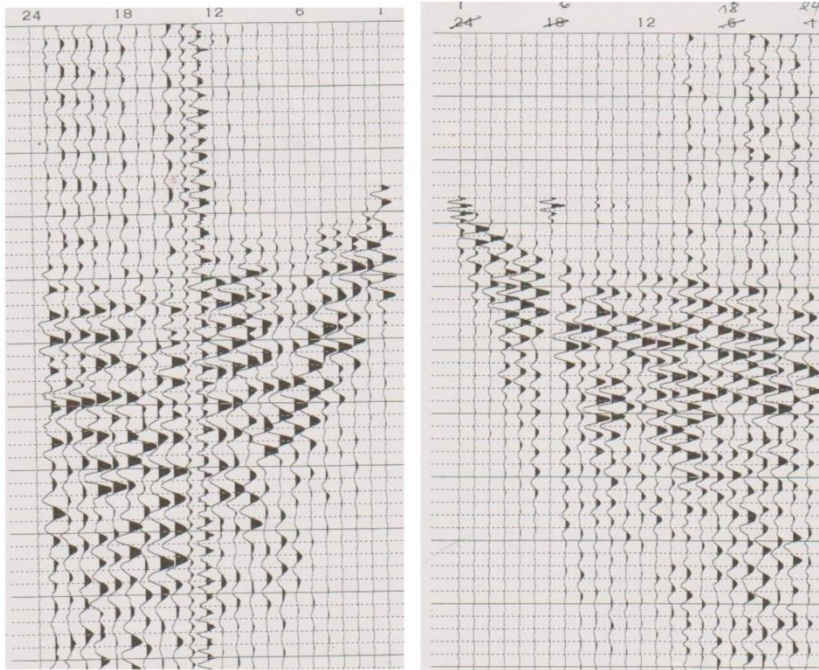
Figure SRD6. Waveform data along profile 6. Left panel represents forward shooting and right panel represents reverse shooting.

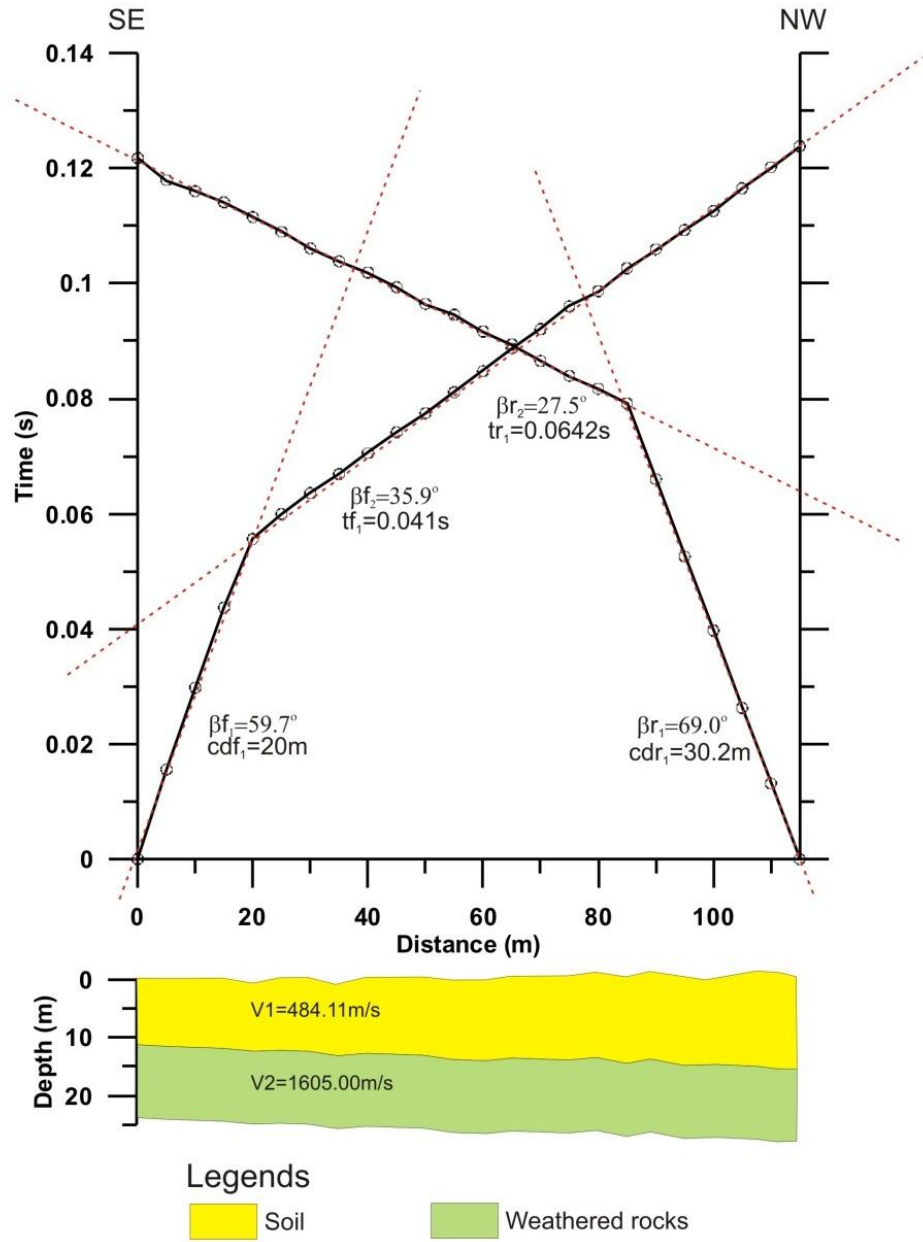Figure TTC2: Travel time curve along profile 2 (Sr2)

Figure TTC6: Interpretation of seismic refraction data along profile 6. The upper panel represents travel-time curve and the bottom panel represents the interpretative cross section.

ANNEX E: A synthetic accelerogram obtained by simulating 1934 Taplejung earthquake
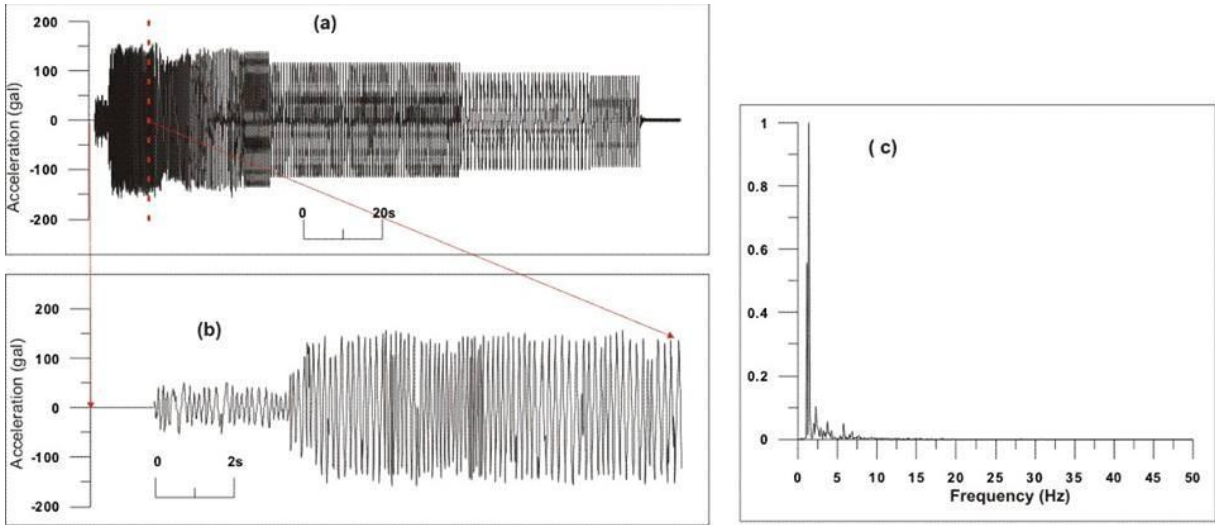
(ANNEX E includes only sample format)

Figure SAT1: (a) Synthetic accelerogram near Thankot obtained by simulating 1934 Nepal Bihar earthquake (Taplejung earthquake) assuming a finite fault of length 150 km and width 75 km. The mechanism is thrust with duration of 140s. (b) Detailed view in a 15s window. (c) Spectral analysis of the seismogram. (Location: near pit no. 1)